School of Applied Science

Monitoring Fire over Indonesia Using MODIS Data

Bowo Eko Cahyono

This thesis is presented for the Degree of
Doctor of Philosophy
of
Curtin University

January 2017

Declaration

This thesis contains no material which has been accepted for the award of any other degree or diploma in any university.

To the best of my knowledge and belief this thesis contains no material previously published by any other person except where due acknowledgement has been made.

Signature: 

Date: 26/1/2017

Abstract

Fire monitoring over Indonesia using MODIS satellite data is analysed using the Indofire and MOD14 algorithms. The analysis studies the relationships between fire occurrence during the decade 2001-2010 with cloud cover, vegetation cover, and climate parameters. The sensitivity of the algorithm to fire detection is also investigated. This understanding is important especially to the forest management authority in Indonesia to support its improved management of the fires and to reduce the negative impacts, particularly on the environment.

The study shows cloud cover, seasons, vegetation cover type, and climate parameters influence the distribution of detected fires. Cloud cover obstructs the satellite view of fire on the earth's surface, therefore the number of observed fire hotspots (FHS) is likely less than the actual number of occurring fires. We have applied a correction to the number of FHS by using proportion of cloud cover relative to land cover. The estimation of FHS number based on monthly cloud cover data is shown to be different to estimations based on yearly cloud cover data. Seasonal data analysis shows the occurrence of fires in the dry season in higher than during the wet season. Vegetation cover is also analysed and the data show that swamp bush areas are the most prone areas to be burned, particularly during the dry season. Finally, the climate parameters precipitation and SOI that indicate the El-Nino and La-Nina phenomenon are shown to be correlated with the temporal patterns of fire occurrence. The El-Nino phenomenon tends to delay the onset of the wet season and therefore the number of fire was detected is higher during the El-Nino than the La-Nina.

There is potential to adjust algorithm threshold coefficients to correct for wet season versus dry season biases. This justification is based on sensitivity analysis of the fire detection algorithm applied to MODIS data over Indonesia. The analysis was conducted using the MOD14 algorithm and shows that the algorithm displays a different response to the MODIS data acquired in the dry and wet seasons. The sensitivity to detecting and monitoring fires is related to the operation of the remote sensing algorithm, in particular the selection of detection threshold values. The

results suggest it may be appropriate to apply threshold values of 317 K for the dry season and 316 K for MODIS data applied in Indonesia.

Acknowledgements

I would like to thank my supervisor Dr. Peter Rhoderick Cochrane Stuart Fearns and my co-supervisor Dr. Brendon McAtee for their support, assistance, and invaluable motivation during my study in the Department of Imaging and Applied Physics of Curtin University. I do not forget also to thank Prof. Mervyn Lynch as a senior in the remote sensing research group for his chatting and some directions while I did the research. All their support and motivations really pushed me in to step of finishing this thesis. Hard job and big sacrifice has been done now and hope this experience will bring me to the next success habits of working hard.

I must also thank my respected parents (Muraji and Sukinem) and my beloved wife “Miftahul Jannah” for all the patience and support so that these studies can be resolved and finished. I would like also say thank you to my children (Barra, Brilli, Fairuz, and Naura) who have inspired me to finish in the noble task of studying.

To all people in Remote Sensing and Satellite research Group (RSSRG), Mark Broomhall, Helen, Lachlan, Mark Grey, Daniel, Rodrigo, Victor, and also people in Landgate WA, Mike Steber, Dave Foster, Agnes Cristina, and Ron Craig, thank you for all your help in either documents, discussions, or other materials supporting to my research. I will remember the good experience in our interactions and gatherings. I apologize for my behaviour during my study which may not please to you all.

Finally I give my thanks to the Directorate General of Higher Education (DIKTI) and Jember University for the scholarship for my study and other materials and support.

Table of Contents

List of Figures

List of Tables

CHAPTER 1

INTRODUCTION

1.1 Background

Rainforests play significant roles in sustaining the balance of global ecosystems, such as keeping air healthy; preventing the occurrence of floods, droughts, soil erosion, and landslides; and mitigating anthropogenic factors affecting climate change (REDD-Indonesia, 2011a). Rainforests provide medicinal plants, food resources, and much biological diversity, as well as providing homes for many kinds of animals (Mongabay, 2010a). Their existence is significant for balancing the ecosystem and reducing emission of greenhouse gases, mostly carbon dioxide (CO_2), into the atmosphere (REDD-Indonesia, 2011b). Additionally, rainforests are considered as lungs of the world due to their function in converting CO_2 to oxygen (O_2) and keeping the air fresh and healthy (Mongabay, 2010c). To keep the world's ecosystems balanced, the existence of rainforests should be maintained (Mongabay, 2010b).

Many environmental conservation researchers (Siegert and Hoffmann, 2000; Page et. al., 2002; Siegert, 2008; Ballhorn et. al., 2009; Jaenicke et. al., 2010) are aware of, and concerned with, the prevention of decreasing and degrading rainforests, especially tropical rainforests, located in the tropical "belt" (within latitudes 23.5 North and 23.5 South). The three countries with the largest tropical rainforests are Brazil, Congo, and Indonesia (Mongabay, 2010b).

Indonesia, geographically located in the tropics region, has a large area of tropical rainforests, representing twenty percent of the world's rainforests (Mongabay, 2010b). Most of the forests are located on three large islands: Sumatra 8.3 Mha, Kalimantan 6.8 Mha, and West Papua 4.6 Mha (Dwiyono and Rachman, 1996; Page and Riley, 2004). However, severe deforestation has destroyed tropical rainforests in Southeast Asia (FAO, 2001), particularly in Kalimantan with various types of forests (Langner, 2009). Langner (2009) reported the annual deforestation

rate in Kalimantan island was 1.7% between 2002 and 2005. The decreasing forest area is mostly caused by humans undertaking activities aiming to make their lives better; however, these activities have often had the opposite impact on the natural environment. For example, over the three decades 1980 to 2010, cutting down or clearing tropical rainforests in Kalimantan has been increasing due to massive transmigration and logging. Moreover, the increase of deforestation has also been caused by Indonesian government policy regarding Indonesia's paddy production as part of the Mega Rice Project. As a result, millions of hectares of tropical rainforest areas in Kalimantan have been degraded (Roach et. al., 2004). As part of the Mega Rice Project, large areas of forest were converted into farmlands and canals. The Indonesian government created more than 4000 km of canals, 12 m wide, for drainage of the rice paddies (Riley, 2006).

Deforestation and forest degradation in non-industrialized countries reduces the balance of O_2 produced by forests as sources and the CO_2 absorbed from the atmosphere (Harris et. al., 2008). Maintaining the existence of rainforests prevents a positive net amount of CO_2 in the atmosphere. CO_2 is a major greenhouse gas, which is absorbed by rainforests, considered as globally significant CO_2 sinks (Levine, 1995). CO_2 causes heat to be trapped as it enters the Earth's atmosphere; this leads to an increase in the global mean temperature (Saharjo, 2004).

The United Nations (UN), as representative of many countries in the world, is concerned with environmental conservation, particularly with respect to rainforests. The UN developed and supported conventions aimed at supporting the sustainability of the world's rainforests. For example, the Kyoto Convention, known as the "Kyoto Protocol", is an agreement to manage the forests to help provide a sink for anthropogenic emissions of CO_2 as greenhouse gases, which impact global warming and climate change (Australian-Government, 2013). The Kyoto protocol initiated the concept of placing a value on the produced oxygen or carbon dioxide by any country in the world. A country that produces O_2 more than CO_2 is considered in positive credit, and the opposite will be considered in negative credit. As a consequence, a country which has negative total credit should pay another country with positive credit; this mechanism was introduced as carbon trading (NOVA, 2010).

In tropical regions, humans often undertake burning activities to manage their plantation fields and effect cultivation shifting activities (Crutzen and Andreae, 1990). Fire or combustion is considered the easiest method in land clearing, and is often used to convert extensive areas of forest into plantations and cultivation land for agriculture (Siegert et. al., 2001). Fire is also employed to prevent spreading of invasive shrubs in grasslands, and in land use changing from primary forest to other uses. To reduce losses caused by fires, the alternative methods such as slash and pile are offered to gain better environmental stability. However, these methods are impractical due to the excessive time required and expenses (Tomich et. al., 1998).

The uncontrolled use of fire has reduced wetland forests in Kalimantan over the last two decades (Siegert and Hoffmann, 2000; Fuller and Fulk, 2001). These activities decrease soil humidity, mostly in peat lands, and so increase the susceptibility to fire (Thoumi, 2009). Every year massive amounts of forest are burnt as a result of human activities (Ruchiat, 2001).

In addition, Hoffmann et al. (1999) reported that rainforests in Kalimantan Indonesia have experienced an increase in severe fires due to a long period of ENSO (El-Nino Southern Oscillation) drought in late 1997. These forest fires had a significant impact on peatland because most of the fires occurred in the peatland area. Page, et al. (2002) utilized Landsat TM (Thematic Mapper) images to study the impact of fire. They reported that there are 5.2 million ha of peatland rainforests in East Kalimantan of Indonesia; 25% of the entire province was affected by fires in 1997.

In the late 1997 forest fire period, the Central Kalimantan province also dealt with numerous fires. This significant event affected most of Southeast Asia, not only in human respiratory disease but also a trans-boundary haze smoke pollution in Singapore, mainland Malaysia, Sumatra and Kalimantan itself (Tacconi, 2003).

In the case of peatland forest fires, increasing carbon dioxide is not only caused by vegetation burning but also by peatlands burning (Jaenicke et. al., 2008). Research by Page et al.(2002) estimated that about 0.81 to 2.57 Giga tonnes of carbon in peatland forest was burned and drove carbon dioxide release into the atmosphere in Indonesia in 1997. The C to CO_2 ratio is 44/12 therefore one would expect 2.97 to 9.42 Giga tonnes of CO_2 released into the atmosphere. This was

equal to 13-40% of global carbon emissions. During that period the burning of peatlands contributed to 60% of smoke production in South-East Asia, and impacted 35 million people (ADB and BAPPENAS, 1999; MWH-Indonesia, 2005).

The rate of increasing global temperature may be controlled by minimizing forest burning which emits a significant amount of CO_2 (Aldhous, 2004). Forest fire in Indonesia will become seriously worse in terms of the frequency of occurrence due to low awareness of people in land clearing management (Langner and Siegert, 1996). The Indonesian government has realized that the fires that have occurred in Indonesia have had a global impact, especially in terms of climate change and global warming (Adiningsih, 2003). Many national and international researchers have been encouraged to conduct environmental research in order to solve this problem (Langner and Siegert, 2006, 2009).

The Indonesian government tasked three agencies, The Ministry of Forestry, LAPAN (Lembaga Penerbangan dan Antariksa Nasional) or translated as the National Institute of Aeronautics and Space, and the Ministry of Environment to take responsibility to manage the forest fires and their impacts. The Ministry of Forestry is responsibe for managing, controlling, and suppressing the forest fire occurrence in Indonesia. LAPAN undertakes research and develops systems to monitor and manage forest fires. The Ministry of Environment is authorized to act upon fire prevention, extinction, and rehabilitation of the environment after the effects of fire. The fire monitoring is carried out both manually and using remote observations from space: remote sensing technology (Lillesand and Keifer, 2004). Remote sensing technology is important when fire monitoring and information collection is aimed at understanding broad fire occurrence, and when gathering information in areas of limited accessibility. Remote sensing also gathers fire information in a consistent manner in terms of acquisition time and methodology, thus there is potential to utilize remote sensing data to understand spatial and temporal patterns.

Remote sensing using satellite data is the main method applied in the research and development of the three agencies. The Forest Planning Agency (BAPLAN which is spelled out from Badan Planologi Kehutanan), as the agency

responsible in Indonesian for forest planning and sustainability, has conducted collaborative research related to fires and existing forest monitoring using Landsat-7 ETM+ with 30 m spatial resolution, MODIS (Moderate Resolution Imaging Spectroradiometer) with spatial resolution 1 km, and SPOT (Satellite Pour l'Observation de la Terre) –Vegetation with spatial resolution 20m (BAPLAN, 2006). LAPAN used NOAA-AVHRR (National Oceanic and Atmospheric Administration's - Advanced Very High Resolution Radiometer) data with spatial resolution 1.1 km for their fire monitoring activities and research (Thoha, 2008). Beside the different data, both BAPLAN and LAPAN also used different methods and algorithms for fire detection which produce different fire detection results (Thoha, 2008). The algorithm utilized by LAPAN applied threshold values of 320 K and 314 K to the NOAA-AVHRR day and night data respectively. Meanwhile, the threshold values applied to the BAPLAN algorithm with MODIS data was 315 K and 310 K for the day and night respectively. Therefore typically LAPAN reports a lower number of detected hotspots compared to BAPLAN (Thoha, 2008).

To manage these issues, the Indonesian government initiated the collaborative project between the Indonesian and Australian governments to create the fire detection and monitoring system called IndoFire. Currently, the main system of fire monitoring in Indonesia is IndoFire. The IndoFire system is based on the fire detection algorithm developed by NASA's land research team for MODIS data application, namely the MOD14 algorithm. However, the system is still in need of adjustment. It requires research and development to meet the accurate, near-real time information required to support monitoring of fire activity in Indonesia, to provide information regarding fire activity and its relationship to fire hazard, and fire mitigation through early warning systems.

Despite the promising potential of remote sensing technology to support "easier" observations for wide areas and in near-real time, the accuracy of detection results are affected by several factors such as cloud cover (Seielstad et. al., 2002), solar radiation (Giglio et. al., 1999), vegetation cover classification (Bucini and Lambin, 2002; Miettinen and Liew, 2003; Tulbure et. al., 2011), and seasonal factors (Schwemlein and Williams, 2006; Dayamba et. al., 2010). The accuracy and

sensitivity of the IndoFire system, which has been developed for Indonesian fire detection, has not yet been assessed (Steber, 2013).

Assessing IndoFire as a fire detection system is important. Assessment results contribute to providing reliable information and an understanding of the performance and accuracy of the system for monitoring the occurrence of active fires, known as fire hot spots (FHS).

1.2 Research Aim and Significance

Research Aim

This research aims to:

1. Analyse the impact of cloud cover on the reported FHS number, and design an approach to predict the actual number of FHS for the whole area of interest.
2. Investigate and analyse the impact of vegetation cover types on the fire activity based on the reported FHS number in various land cover classifications.
3. Determine the sensitivity of the MOD14 algorithm applied to the MODIS data over Indonesia.
4. Analyse the relationship of detected FHS number and the seasonal factors, precipitation and Southern Oscillation Index (SOI), for a decadal time series.

Significance

The results of this research will contribute to science development, and potentially be included in considerations by the Indonesian Government and authorities who have responsibility for fire monitoring and management.

Firstly, the contributions in relation to science are: (1) the development of a new technique for fire mapping which considers cloud cover; (2) a deeper understanding of fire-prone vegetation cover types in Indonesia, which will give focus to fire prevention efforts and avoid associated negative impacts on the environment, health, and other resources; (3) develop an enhanced analysis of fire detection algorithms used in Indonesia based on MODIS data; and (4) conduct further analyses to determine the relationship between FHS characteristics and factors such as cloud coverage, vegetation cover, and climate parameters (precipitation and SOI).

Secondly, the results of this research provide scientific evidence and rational analysis of several factors that potentially impact fire detection using remote sensing data from satellites. The Indonesian authority agency in fire management will have additional reliable information about active fire characteristics and the fire detection method or algorithm. This research also contributes to the further development of an automated burnt area mapping algorithm, to improve the predictability of the impact of fire on infrastructure and environment.

1.3 Thesis Structure

This thesis is written in four chapters: introduction, review of literature, results and analysis of fire detection, and conclusion.

Chapter 1. The Introduction describes general information related to this research including background to the Indonesian forest environment, the role of fire in this environment, and associated problems and issues. The efforts of the Indonesian Government in managing and controlling fire is also introduced in this chapter, followed by research aims, significance, and thesis structure.

Chapter 2. The Review of Literature provides an overview of general understanding and concepts of remote sensing, especially satellite remote sensing, focusing the discussion on fire detection purposes. Descriptions and characteristics of remote sensing satellites are also introduced in this chapter. Also presented is the physical background theory of remote sensing, including how electromagnetic radiation interacts with the atmosphere and the Earth's surface. Finally, a review of research regarding fire detection and principles using satellite remote sensing is explored, including thermal band discussions and the detection algorithms which have been used.

Chapter 3. The Results and Analysis of Fire detection contains research findings and scientific explanations involving parameters which affect the fire detection results. Data and evidence supporting this research is presented. The cloud coverage as an uncontrolled factor is considered in the discussion of estimating the number of FHS. Fire characteristics in the different vegetation cover types are also discussed. Finally, the relationship of climate factors (precipitation and SOI) in the pattern of fire activity during the decade 2001-2010, and validation

methods applied in this research regarding fire occurring in two provinces of Indonesia, are presented.

Chapter 4. The Conclusion presents an overview of the research results and introduces some points for possible on going research for remote sensing fire detection and burned area estimation. A summary of the research and results is a closing description of this chapter.

Appendices containing supporting data are also included.

CHAPTER 2

REVIEW OF LITERATURE

This chapter discusses some of the principles of remote sensing for fire detection and monitoring using electromagnetic energy. Section 2.1 introduces the general principles of satellite remote sensing, in particular the satellites typically employed in environmental remote sensing, including sensing of fires. This first section gives a basic explanation of remote sensing and the physical principles of electromagnetic energy radiation in the context of earth observing by satellite-borne sensors. Section 2.2 discusses thermal radiance as an essential domain of electromagnetic radiation from fire and basic principles related to detecting fire occurrence using the remotely sensed thermal radiation. Section 2.3 explains the methods of detecting fire using remote sensing satellite data, particularly MODIS data. This section also describes two algorithms (MOD14 and IndoFire) and how fire detection works. Some of the environmental parameters which affect the operation of the fire algorithm are discussed in Section 2.4. Such parameters are cloud cover, vegetation cover types, day and night time, and seasonal parameters (SOI and precipitation). The sensitivity of fire detection and relationships to the wet and dry seasons is described in Section 2.5. The issue of validation methods to assess the results of detecting fire is reviewed in Section 2.6.

2.1 Remote Sensing Principles

Remote sensing is defined as the "investigation of the characteristics of physical objects and environmental properties by the methods of recording, measuring and interpreting imagery and digital representations of energy patterns derived from non-contact sensor systems" (Lillesand and Keifer, 2004). Besides the science and technology point of view, remote sensing also encompasses the art of processing and interpreting data (Lillesand and Kiefer, 2000). Environmental remote sensing instruments are typically mounted on satellites or aircraft. The

remote sensing principle is similar to the way our body's three's senses: vision, smelling, and hearing work. That is, they do not need physical contact with objects to detect their properties. In remote sensing for fire monitoring, thermal properties of fire are sensed remotely from the sensors mounted on board the remote sensing satellites.

Remote sensing, in the context of environmental monitoring typically relies on the detection and measurement of the energy of electromagnetic waves e.g. the light intensity, the heat emitted by objects, and sometimes radio waves (Sabins, 1987). In remote sensing, energy reflected or emitted from the earth's surface is measured using sensors that are mounted on aircraft or satellite platforms. Satellite-borne remote sensing instruments detect electromagnetic energy that is a combination of radiation reflected and emitted by the earth's surface (Tso and Mather, 2009). The information collected by remote sensing methods is often formed into imagery data representing spatial features within the environment (Richards and Jia, 2006).

Objects at the earth's surface have different properties of absorption, reflection, and emission of the electromagnetic radiation. Water, soil, vegetation, buildings and roads exhibit different absorption and reflection characteristics at different wavelength regions of the electromagnetic spectrum (Chuvieco and Huete, 2010). Some materials at the earth' surface, such as fire, not only exhibit reflectance properties, but also exhibit thermal properties. Fire at the earth's surface (ground) will emit relatively high intensity thermal radiation that might be captured by remote sensing sensors (Chuvieco and Huete, 2010). The following sections describe the remote sensing principle of fire detection using satellite data. This discussion firstly introduces the general principles of electromagnetic radiation, including how electromagnetic energy interacts with the atmosphere and earth's surface, and leads to the thermal radiation in the range of electromagnetic energy in respect to fire radiation.

2.1.1 Electromagnetic Radiation

Electromagnetic radiation emitted from the sun is incident at the top of the earth's atmosphere (Figure 2.1), and can undergo scattering, absorption, reflection, and transmission, with some portion reaching the surface where it may be absorbed reflected, or transmitted (Campbell, 2002). Remote sensing data are collected by detecting and measuring the intensity of electromagnetic (EM) energy emitted or reflected by land surfaces such as soil, rock, vegetation and water (Chuvieco and Huete, 2010). A good understanding of the physical principles of EM energy and earth's surface interplay is important for the accurate use of remote sensing in many applications.

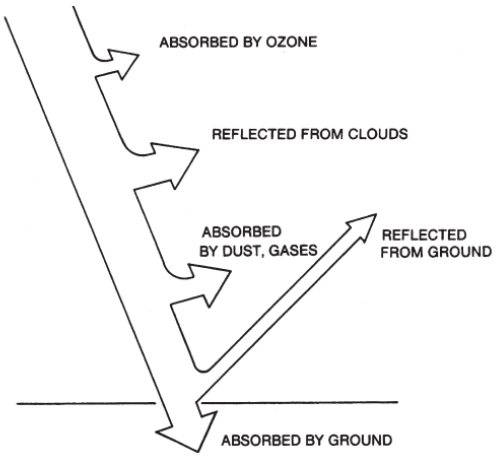

Figure 2.1. Electromagnetic energy from the sun transmitting through the earth's atmosphere to the surface (Campbell, 2002).

Every object has different responses to incident EM energy. The specific response characteristics may be used to identity an object by its spectral signature. The aim of remote sensing is to use the EM signals that are reflected or emitted to determine the object's physical properties. For example, fire mostly emits EM energy in the thermal infrared waveband, and it is the specific characteristic of fire as a hot object, the temperature, that allows remote sensing to determine the location and "intensity" of a fire. In certain stages of burning or condition, fire also emits EM radiation in the visible regions of the EM spectrum.

With respect to the satellite remote sensing for fire monitoring, a focus of this thesis research, this section discusses electromagnetic energy and its related characteristics that play a specific role in optical remote sensing. It will also

describe the physical point of view related to how electromagnetic radiation behaves when it interacts with a medium (atmosphere) and is incident on an object at the earth's surface.

2.1.2 Electromagnetic Radiation and the Atmosphere

The information acquired by a space-borne sensor from the observed surface is affected by surface properties, and varies with the wavelength of the electromagnetic radiation. However, spectral differences in the radiation are not only due to properties of the surface. While propagating through the atmosphere, the interactions between electromagnetic radiance energy and the atmosphere can arise in forms of scattering and absorption.

The upwelling electromagnetic energy from the earth's surface transmits partially through the atmosphere before being detected by the satellite sensors. Certain spectral bands of electromagnetic energy are transmitted more than others by the atmosphere. The atmospheric constituents that affect the spectral transmittance of the atmosphere include water vapour (H_2O), clouds, ozone (O_3), and other aerosols. The radiance energy which is not scattered or absorbed will pass through the atmosphere. Figure 2.2 shows the variability in spectral transmittance of the atmosphere. The figure shows a high value of transmittance in only certain bands of wavelength, termed "atmospheric windows". The radiation energy in the atmospheric window regions will be mostly transmitted through the atmosphere (Rees, 2001; Lillesand and Keifer, 2004). Remote sensing sensors mostly operate in atmospheric window regions to gain more information from radiation energy transmitted from the earth's surface.

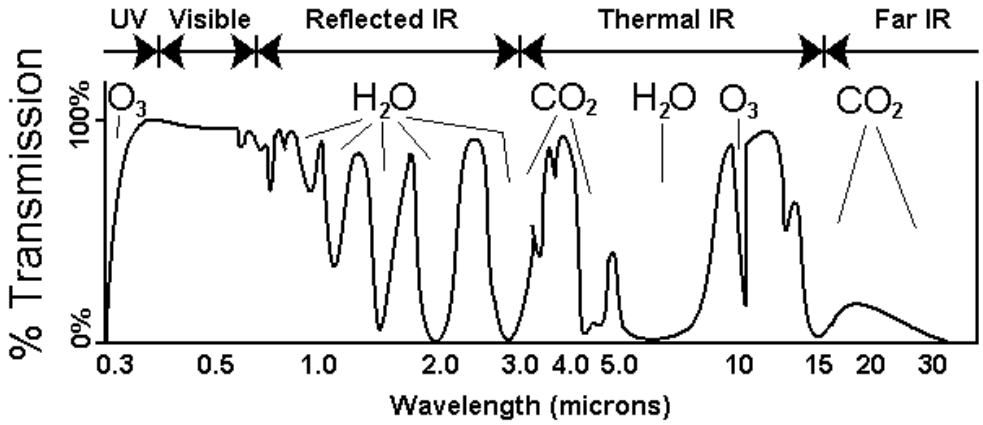

Figure 2.2. Plot of spectral transmittance of electromagnetic radiation through the atmosphere (Rice, 2012).

Figure 2.2 shows that CO_2 absorbs energy at wavelengths around 3.0 µm and 4.0 µm, H_2O absorbs at various bands from about 1.0 µm to 3.0 µm, and O_3 at 9.58µm (Philip, 2007). Therefore, the energy on those high absorption (low transmittance) wavelengths reaches the sensor with lower intensity. In addition, the atmospheric transmittance in the visible waveband from 0.3 microns to about 0.7 microns shows a line with high transmittance values. With respect to the atmospheric window, the band width of remote sensing instruments is designed to get the optimum information of object characteristics. The atmospheric windows commonly used in remote sensing are the windows from 0.3µm to 2.3µm for observations in the visible range and the near infrared (NIR), the window between 3µm and 5µm for observations in the mid infrared (MIR), and the window from 8µm and 14µm for observations in the thermal infrared (TIR) (Lillesand and Keifer, 2004).

With regards to the detection and monitoring of fire, which emits radiation in the thermal band, Figure 2.2 shows that the highest transmittance in the TIR band ranges between the wavelengths 3-5µm and 8-12µm. This is why the satellite sensors intended to measure the thermal radiation from hot objects in the earth's surface are designed with spectral bands at those wavelengths (Justice and Dowty, 1994; Flasse and Ceccato, 1996).

2.1.3 Electromagnetic Radiation's Interaction with the earth surface

When electromagnetic energy is incident on the earth's surface, particularly land areas, the energy might be reflected, absorbed (Lillesand and Keifer, 2004), or the absorbed energy re-emitted as thermal energy. The proportions of those three components differ depending on the incident electromagnetic wavelength and the surface properties. For different specific materials, the reflection and absorption vary for every wavelength. When different electromagnetic wavelengths interact with an object, different proportions of reflected or absorbed energy will result (Lillesand and Keifer, 2004). For example, trees reflect a different amount of energy from red and infrared radiation (Lillesand and Keifer, 2004; Chuvieco and Huete, 2010).

Reflection of electromagnetic waves by objects can be used to recognize the object's characteristics, but in some cases may be an unwanted effect. For example high intensity reflections from the earth's surface might affect the accurate detection of fire using remote sensing methods. The reflectance (ρ) of objects is defined as the value of reflected energy (E_R) from the objects to the incident energy (E_I) that strikes the object's surface. The reflectance, which is a function of wavelength (λ), is known as spectral reflectance and it is expressed as (Lillesand and Keifer, 2004):

$$\rho_\lambda = \frac{E_R(\lambda)}{E_I(\lambda)} \qquad (2.\ 1)$$

Where $E_R(\lambda)$ is the spectral upwelling (reflected) irradiance and $E_I(\lambda)$ is the spectral downwelling incident irradiance. The plot of the ratio of radiation reflected by different materials across the electromagnetic spectrum gives a unique signature or pattern, or a reflectance spectrum. The spectral reflectance of a surface is independent of the spectral nature of the incident radiation. A material can be recognized by its spectral reflectance signature if the detection system has enough spectral resolution to differentiate its spectrum from other materials. The earth's surface is made of soil, water, and vegetation; each surface type responds in different ways to the electromagnetic radiation spectrum. Figure 2.3 shows the typical spectral reflectance spectra of water, vegetation, sand, concrete, and snow.

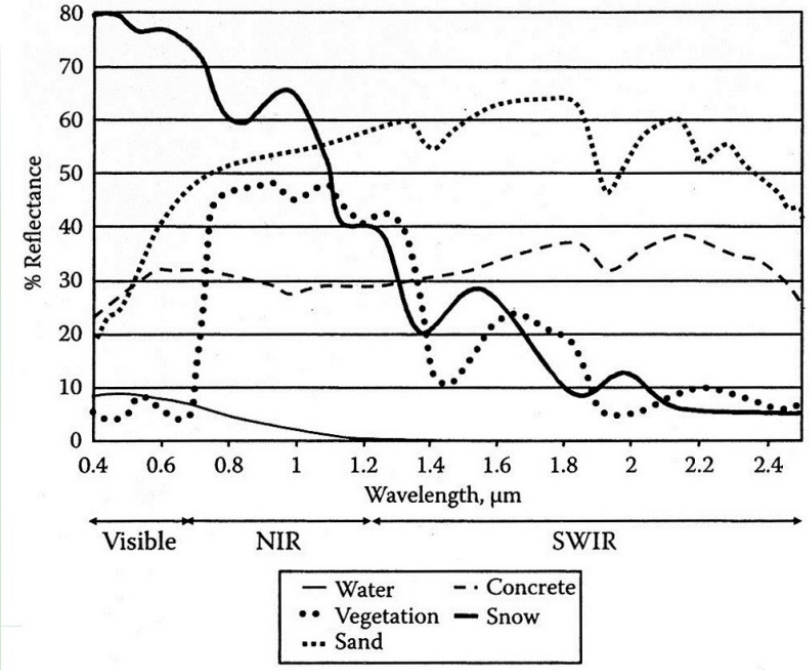

Figure 2.3. Spectral reflectance signatures for representative earth surface materials (Chuvieco and Huete, 2010).

Water shows the lowest reflectance values across the spectrum (less than 10%) with the highest value placed at the blue end of the electromagnetic spectrum. Water reflectance decreases with increasing wavelength of radiation. The reflectance of snow in the visible bands has the highest value of all materials in Figure 2.3 with a magnitude up to 80% at a wavelength of approximately 0.4μm. Therefore nearly all of the visible bands of radiation are reflected when they reach the snow surface and snow appears white. Their reflectance intensity decreases along with increasing wavelength until it has relatively constant values in the SWIR spectrum at wavelengths of more than 2.2μm. Concrete reflectance values increase by 10-24% in the visible range and are relatively constant in NIR bands. SWIR wavelength radiation is reflected by concrete with 30-40% reflectance. The sand reflectance pattern is similar to concrete but it has higher overall reflectance of between 20% and-70%.

In the remote sensing approach to fire detection, the materials described above can potentially interfere in fire detection and cause false detection. Giglio (2003) reported that fire has low reflectance in the near infrared band 0.86 μm. He

determined a pixel of remote sensing satellite data as potential fire if the pixel has reflectance value below 0.3 or 30%. Based on the reflectance values in the NIR band (0,86µm) in Figure 2.3, the material with reflectance values lower than 30% is water. So it might satisfy the requirement of fire pixel determination in terms of reflectance value. However the criteria to determine a fire pixel is not only by reflectance but also by brightness temperature which is sensed in the thermal infrared band. The brightness temperature of water is far below the fire brightness temperature. The brightness temperature of water is about 130 K (Johnson, 2002). Therefore water pixels will be rejected as fire pixels because pixels are categorized as fire if they have a brightness temperature of at least 310 K for day pixels and 305 K for night pixels (Kaufman, Justice, et. al., 1998; Giglio et al., 2003).

2.2 Thermal Radiance of Electromagnetic Radiation

Every object which has a temperature above absolute zero, that is 0 K or -273.15^{o} C, emits radiation in the thermal region (3µm to 14µm) of the electromagnetic spectrum (Levin, 1999; Rees, 2001). The emitted radiance is distributed over a range of wavelengths in a continuous spectrum and is known as spectral radiance. The spectral radiance of blackbody radiation in the absolute temperature, T, is expressed by Planck's function as (Rees, 2001):

$$L_\lambda = \frac{2hc^2}{\lambda^5 \left(e^{hc/\lambda kT} - 1\right)} \qquad (2.2)$$

where: L_λ = Spectral radiance (W m^{-2} sr $^{-1}$ µm^{-1})

h = Planck's constant = 6.625 x 10^{-34} W s^2

k = Boltzmann's constant = 1.38 x 10^{-23} W s^2 K^{-1}

c = Speed of light = 3 x 10^8 m s^{-1}

T = Object temperature (Kelvin)

With respect to Equation 2.2, we define $c_1 = 2hc^2$ and $c_2 = hc/k$, so that the equation can be rewritten as

$$L_\lambda = \frac{c_1}{\lambda^5 \left(e^{c_2/\lambda T} - 1\right)} \qquad (2.3)$$

where: c_1= 119106211.8 W m^{-2} sr^{-1} µm^{-4} and c_2 = 14387.86 K µm

By inputing a range of wavelength (λ) values at a certain temperature (T), a graphic of electromagnetic radiation energy over the given range of wavelength can be generated, as shown in Figure 2.4. The lowest graph represents the lowest radiance temperature and the radiance value increases when the temperature increases. It is obvious that the higher the temperature, the blackbody radiation peaks shift to smaller wavelengths. This phenomenon is commonly known as *Wien's Displacement Law*. In the mathematical formula, Wien's Displacement Law is expressed by (Chuvieco, 1999):

$$\lambda_{max} \, . \, T = b \qquad (2.4)$$

where λ_{max} = the peak wavelength in meters (m)

T = the temperature of the blackbody in Kelvin (K)

b = a constant of proportionality, called "Wien's displacement constant"
= 2.8977685×10^{-3} m K (Codata, 2010)

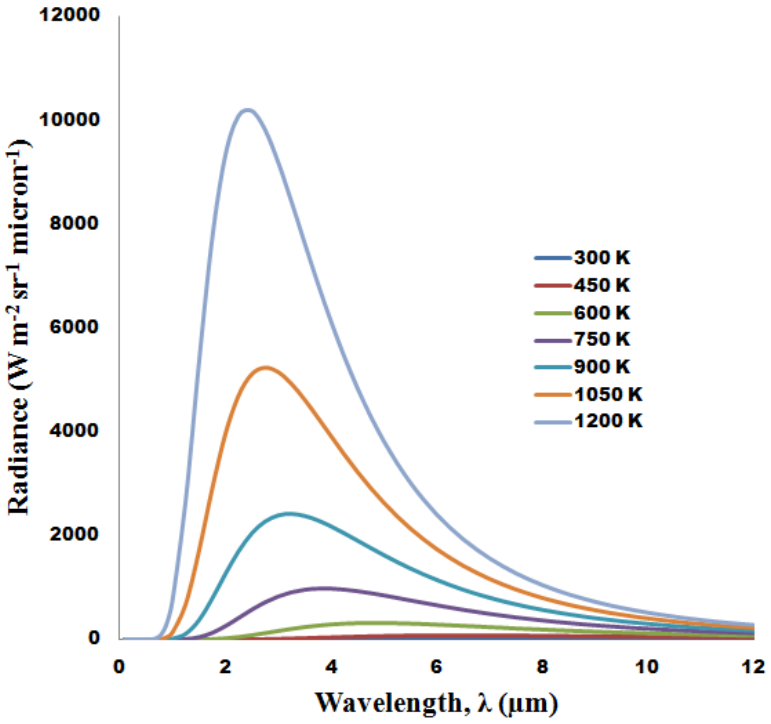

Figure 2.4. Plot of radiance curves calculated using Equation 2.3.

The formula of Wien's displacement law indicates that the higher the object temperature, the shorter the peak of wavelength of the emitted radiation spectrum. Based on Wien's formula, we can calculate the peak wavelength of electromagnetic

radiation from objects at specified temperatures; for example, a calculation of the sun's radiation peak wavelength. Suppose the surface temperature or effective temperature of the sun is 5778 K; the radiation spectrum peak wavelength will be 2.9×10^{-3} m.K / 5778 K = 5.0 x 10^{-7} m. This value sits in the green visible light spectrum range. Another example is a forest fire with a temperature of 360 K. The peak wavelength emitted from fire is 2.9 × 10^{-3} m K / 360 K = 8.0 x 10^{-6} m; therefore fire emits peak energy in the thermal infrared spectrum range. Most fires have a peak radiance in the range of 3-12μm, so the appropriate satellite sensor for fire detection purposes is designed to detect radiation in this spectral range.

2.3 Remote Sensing for Fire Detection

The possibility of identification of surface temperature in sub-pixel data of satellite remote sensing was introduced by Dozier (1981). In sub-pixel resolution, land area with varying temperature will be sensed in different wavelengths of thermal radiance by the satellite sensors (Dozier, 1981). Two main aspects of fire that contribute to its radiated energy are temperature and size. In remotely sensed data, a pixel temperature is an average temperature value of an area covered in one pixel. This value might be contributed to by different temperatures within different portions of sub-pixels (part of the pixels). A fire pixel may have some portion of un-burned area and burning area which may be flaming or smoldering. A hotter part will contribute more radiance proportionally for the pixel than the remaining part. By manipulating the integration of Planck's function (Equation 2.3) and based on the radiance values from channels at different wavelengths, it is possible to determine the radiant temperature of one sub-pixel area and the portion of the sub-pixels from the appropriate temperature. The portions of a pixel occupied by each temperature field are not necessarily contiguous. It is assumed that there are only two types of land class, the target and background (Dozier, 1981). Although Dozier has reported a method to determine the sub-pixel contribution due to burning, this has not been integrated into operational fire detection algorithms.

In remote sensing fire detection, a sub-pixel fire can be detected as fire if it has sufficient radiant flux as a contribution to the average temperature of the pixel so the pixel is possible to be flagged as fire (Robinson, 1991). The sensor used

should detect the radiated energy in the range of fire temperature wavelengths. For example, a forest fire has a temperature of 700 K. Based on the Wien's displacement (Equation 2.9), the peak emission wavelength from the fire is 2.9×10^{-3} m K / 700 K = $4.1\text{x}10^{-6}$ m. This wavelength of fire emission energy sits in the thermal infrared (TIR) spectrum range, so the appropriate detector for fire investigation is a thermal infrared sensor.

Sensors can be characterized by their spectral response function. Every sensor with a specific wavelength bandwidth has a specific response to various stages of fire occurrence in the landscape, such as flaming and smoldering. In the MODIS instrument, the thermal infrared sensors acting in the atmospheric window region are centred at 3.95 µm and 11 µm, that is, MODIS channels 21/22 and channel 31. The response of those 3.95 µm and 11 µm sensors, expressed by measured brightness temperature values, to the fraction of pixel occupied by fire is shown in Figure 2.5. With respect to the different responses of sensors 3.95 µm and 11 µm to the fraction of fire, Philip (2007) stated that the 11 µm sensor produced a pixel temperature 35 K lower than the 3.95 µm sensor when the pixel is occupied by 4% fire. The different responses to the temperature of these two sensors (3.95 µm and 11 µm) is then basically used in the fire detection algorithm.

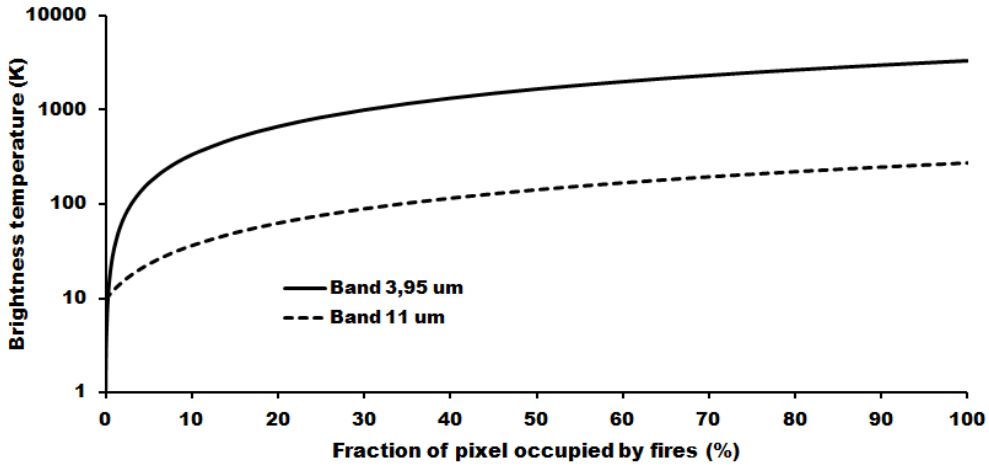

Figure 2.5. Response of the 3.95 µm and 11 µm MODIS bands to the fraction of pixel covered by fire (Philip, 2007).

In principle, fire detection algorithms exploit information from the detected objects in the thermal infrared bands. Every fire detection algorithm recognizes emitted fire energy in terms of pixel value. Although most fire detection algorithms utilize the same wavelength sensors, approximately 3.95 µm and 11 µm, they have slight differences in the fire detection methods such as: algorithm testing step orders, data pre-processing such as remapping or re-projecting, and the embedded algorithm threshold values.

The aim of a fire detection algorithm is to identify whether the image pixels of a surface area on a satellite overpass represent fire in an actively burning area. Satellite data which have been used to monitor fire on the earth's surface have been provided by the AVHRR (Advanced Very High Resolution Radiometer), VAS (Visible-Infrared Spin-Scan Radiometer Atmospheric Sounder), ATSR (Along Track Scanning Radiometer), and OLS (Operational Linescan System) instruments (Giglio et. al., 2000). NASA launched the MODIS instruments in 1999 and 2002, each equipped with more thermal infrared sensors than their predecessors, designed in particular for fire detection purposes (Kaufman et al., 1998; Giglio et al., 2003).

With respect to many existing models of fire detection using satellite remote sensing, the following section focuses only on the description of the MOD14 algorithm, arguably the current global "standard" fire detection algorithm applied to polar orbiting satellite remote sensing datasets. Also, the following section discusses the IndoFire algorithm which is used in Indonesia by the Ministry of Forestry, LAPAN, the Ministry of Environment and is based on the MOD14 algorithm.

Essentially, fire detection algorithm employs data which is captured by thermal infrared sensors (3.9 to 4 µm and 10.7 to 11.3 µm). MODIS is equipped with 5 thermal infrared sensors while NOAA-AVHRR has only 3 sensors in the same wavelength range. In addition, the MODIS instruments have better temporal resolution i.e. twice a day for each platform, the Terra and Aqua satellites.

2.3.1 MOD14 algorithm

The MOD14 algorithm, which was developed by the NASA Land Research Team, is based on the contextual algorithm applied to NOAA-AVHRR data. This

algorithm is designed to be applied to MODIS data (Giglio et al., 2003). The MOD14 algorithm produces a number of MODIS fire products, day/night fire occurrence, fire locations and other thermal anomalies (Justice et. al., 2002).

The MOD14 algorithm processes MODIS data at 1 km resolution and includes geolocation files as input. MODIS data can be accessed through many different sources depending on the application purposes. LAADs web[1] provides MODIS data and atmosphere products, Land Processes DAAC[2] (LPDAAC) at the U.S. Geological Survey EROS Data Center[3] (EDC) serves land products, snow and sea ice cover as Cryosphere data products can be accessed through the National Snow and Ice Data Center[4] (NSIDC) in Boulder, Colorado, and the intended Ocean color products and sea surface temperature products and other information related to these are available at the OCDPS at GSFC[5]. MODIS also provides direct access data from the spacecraft for the users who want to get x-band data using the MODIS Direct Broadcast signal. For fire observations, we used MODIS daily acquired datasets downloaded from LAADs web.

The processed result is a MOD14 file in HDF format which contains information about the number of fire pixels, latitude/longitude of the fire pixels, fire intensity, confidence level, and pixel classification. There are 9 classifications of pixels in the MOD14 file, provided as Scientific Data Sets (SDS) called “fire mask” as shown in Table 2.1. Detected fire pixels are classified into three categories based on their confidence level i.e. low-confidence-fire, nominal-confidence-fire, and high-confidence-fire which are noted as 7, 8, and 9 respectively.

[1] http://ladsweb.nascom.nasa.gov/data/search.html
[2] https://lpdaac.usgs.gov/
[3] http://eros.usgs.gov/find-data
[4] http://nsidc.org/data/
[5] http://oceancolor.gsfc.nasa.gov/

Table 2.1. MOD14 fire mask pixel classes (Giglio, 2005).

Class	Meaning
0	Not processed (missing input data)
2	Not processed (other reason)
3	Water
4	Cloud
5	Non-fire clear land
6	Unknown
7	Low-confidence-fire
8	Nominal-confidence-fire
9	High-confidence-fire

Note: A pixel class 1 is intentionally abandoned by Giglio (2005) with no stated reason since MODIS collection 3 active fire products.

The MOD14 algorithm has been reported to detect fire over several different areas such as the Canadian boreal forest (Li, Nadon, et. al., 2000), Southern Africa (Morisette, Giglio, Csiszar, and Justice, 2005), Brazil (Morisette, Giglio, Csiszar, Setzer, et. al., 2005), and showed satisfactory results. This broad global success makes the MOD14 algorithm arguably the global standard for fire detection.

However, the MODIS fire product or MOD14 algorithm was found to sometimes produce false detection for big fires (Nakayama et. al., 1999). Nakayama and Maki et al. (1999) made an improved method of the fire detection algorithm to be applied for detecting active fires in South Sumatra, Indonesia. Nakayama used a contextual algorithm, originally reported by Justice and Dowty (1994), to determine whether the pixel was a fire or not automatically by comparing the selected pixels with their neighbors. The algorithm can identify the occurrence of big fires better than the original MOD14 algorithm.

The probability of the occurrence of false detection by MOD14 is also decreased by adjusting some variables in the algorithm. The variables are the values of reflectance and temperature and also the accuracy of rejecting unwanted factors such as cloud, water, sunglint, and desert boundary (Giglio et al., 2003). Among those variables above, this research aims to investigate how significant the

changing of temperature values, particularly threshold values, are to the MOD14 algorithm results applied to MODIS data over Indonesia. The motivation for this work is previous research which reported that different temperature threshold values and research areas showed varying results in detecting fire (Prins and Menzel, 1992; Kaufman, Kleidman, et. al., 1998; Seielstad et al., 2002; Dayamba et al., 2010; Devineau et. al., 2010).

2.3.1.1 MODIS Instruments

The MODIS instruments are mounted aboard NASA's Terra and Aqua satellites. The MODIS instrument aboard the Terra satellite was launched on December 18, 1999, and that aboard the Aqua satellite launched on May 4, 2002. The orbit altitude of the two satellites is 705 km above the earth's surface. The MODIS Terra instruments acquired data for the first time on February 24, 2000. Aqua MODIS instruments started to take spatial data on June 24, 2002. The MODIS instrument channels have a spatial resolution of 250 m, 500 m, and 1 km at nadir, as shown in Appendix 1. The temporal resolution of MODIS satellites is 0.5 day. The Terra satellite crosses the Earth's equator at 10:30 and 22:30 local time and so it is known as Terra AM or Terra morning, while the Aqua satellite passes over the earth's equator at 13:30 and 01:30 and so it is known as Aqua PM (Chuvieco and Huete, 2010).

The MODIS data captured by the satellites are transmitted to ground station receivers. A ground station in White Sands, New Mexico, receives data transmitted by the MODIS instruments through the Tracking and Data Relay Satellite System (TDRSS). The data are then forwarded to the EOS Data and Operations System (EDOS) at the Goddard Space Flight Center. The raw data in level-0 from EDOS are processed by the MODIS Adaptive Processing System (MODAPS) into higher levels and products such as Level 1A, Level 1B, the geolocation file, the cloud mask product, the MODIS land product, and atmosphere products. All of these products are distributed into three Distributed Active Archive Centers (DAAC). MODAPS does not produce the ocean color product, but this duty is covered by the Ocean Color Data Processing System (OCDPS).

MODIS sensors were built to contribute to, amongst other needs, fire detection and fire monitoring purposes. For this reason the existing sensors were planned to have special and specific characteristics regarding fire monitoring activities. MODIS is also able to detect burn scars or burnt areas because of its unique spatial and radiometric capabilities. These capabilities improved the fire assessment, which were previously achieved by using the National Oceanic and Atmospheric Administration's - Advanced Very High Resolution Radiometer (NOAA-AVHRR) and the Geostationary Operational Environmental Satellite (GOES) systems (Li, Kaufman, et. al., 2000). From the first time of launching NOAA-AVHRR, the instrument performance characterization and the quality of the data produced in monitoring fires has been undergoing validation (Giglio et al., 2003). Furthermore, by taking advantage of the capability of the MODIS sensor, there is potentially a greater opportunity to develop automatic procedures to detect burn scars, and this issue challenges researchers to develop and implement algorithms to lead the MODIS production stream. The products are available at full resolution and as spatial summaries and temporal composites.

The MODIS instruments have 36 channels with spectral bands from 0.405 to 14.385µm, and they acquire data at three spatial resolutions: 250m (bands 1-2), 500m (bands 3-7), and 1,000m (bands 8-36). The multispectral sensors on the MODIS instruments span the visible, NIR, and TIR bandwidths.. Details of MODIS instrument specifications and characteristics are given in Appendix 1.

The MODIS sensor scans the earth with 10 simultaneous 1 km wide stripes (or 20 and 40 stripes at the 500m and 250m resolution respectively). MODIS sensors have triangular spatial response characteristics as shown in Figure 2.6. This response characteristic allows the possibility to detect fires in one or two adjacent pixels in the MODIS data depending on where the fires are located in the scene and how big the fires are (Kaufman et al., 1998).

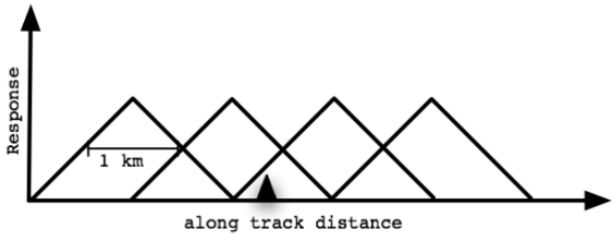

Figure 2.6. MODIS response across track (Kaufman et al., 1998)

2.3.1.2 MODIS Sensor Channel for Fire Detection

In terms of fire detection using satellite MODIS data, not all 36 channels of the MODIS instrument are employed. MODIS fire products are processed by utilising only seven bands of the MODIS instrument (Justice et al., 2002). The channels' specifications and purposes are given in Table 2.2.

Table 2.2. MODIS channels used for active-fire detection and characterization (Giglio et al., 2003)

Channel	Central λ (µm)	Purpose
1	0.65	Sunglint, coastal false alarm rejection, and cloud masking
2	0.86	Bright surface, sunglint, coastal false alarm rejection, and cloud masking
7	2.13	Sunglint and coastal false alarm rejection
21	3.95	Fire detection and characterization (high-range)
22	3.95	Fire detection and characterization (low-range)
31	11	Fire detection, cloud masking
32	12	Cloud masking

The main channels which are related to fire identification are channels 21, 22, and 31 with central wavelengths at 3.95 µm and 11 µm. The spectral response function (SRF) of MODIS channels 21, 22, and 31 are shown in Figure 2.7. Figure 2.7 (a) describes the spectral response of channel 21, ranging from 3.89 µm to 4.07 µm and centred at 3.98 µm. The spectral response of channel 22 shown in Figure 2.7 (b) ranges from 3.88 µm to 4.06 µm with centre at 3.97 µm. Channel 31 has a spectral response range from 10.5 µm to 11.6 µm. With respect to the wavelength

range of the spectral response curves, it is indicated that channel 21 and 22 responses are more sensitive to the wavelength changing of electromagnetic radiation compared to channel 31.

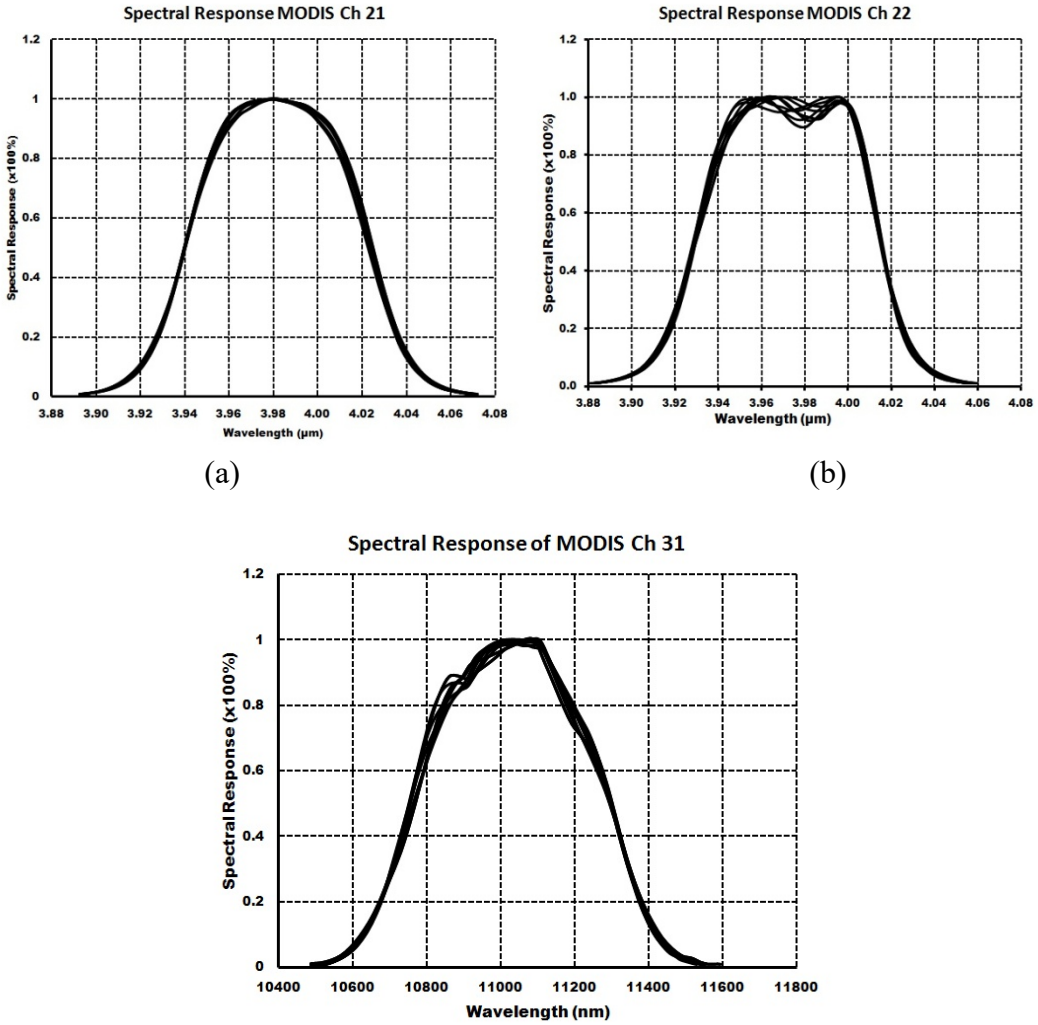

Figure 2.7. Spectral Response Function (SRF) of MODIS sensor channels (a) 21, (b) 22, and (c) 31 (Goessmann, 2007)

Moreover, the 3.95 μm and 11 μm sensor channels also respond differently to the pixel temperature, as shown in Figure 2.8. for a fire temperature at 1000 K (Christopher et. al., 2006), the 3.95 μm channel displays a more sensitive response compared to the 11 μm channel. It is indicated by a higher measured radiance value for the 3.95 μm channel compared to the 11 μm channel. Also, the non-fire temperature curve (450K) shows similar radiance values in the wavelength regions

of those two channels (3.95 μm and 11 μm). The different radiance values of fire and non-fire temperatures in the 3.95 μm channel is bigger than the difference of radiance values in the 11 μm channel. Thus, the remote sensing of fire detection by MODIS data uses the measured radiance of channel 31 as a background of the measured radiance in channel 21 or 22 (Goessmann, 2007). The brightness temperature's difference of channel 21 and 31, converted from measured radiance by using the Planck function, is an essential requirement in the fire detection algorithm step (Giglio et al., 2003).

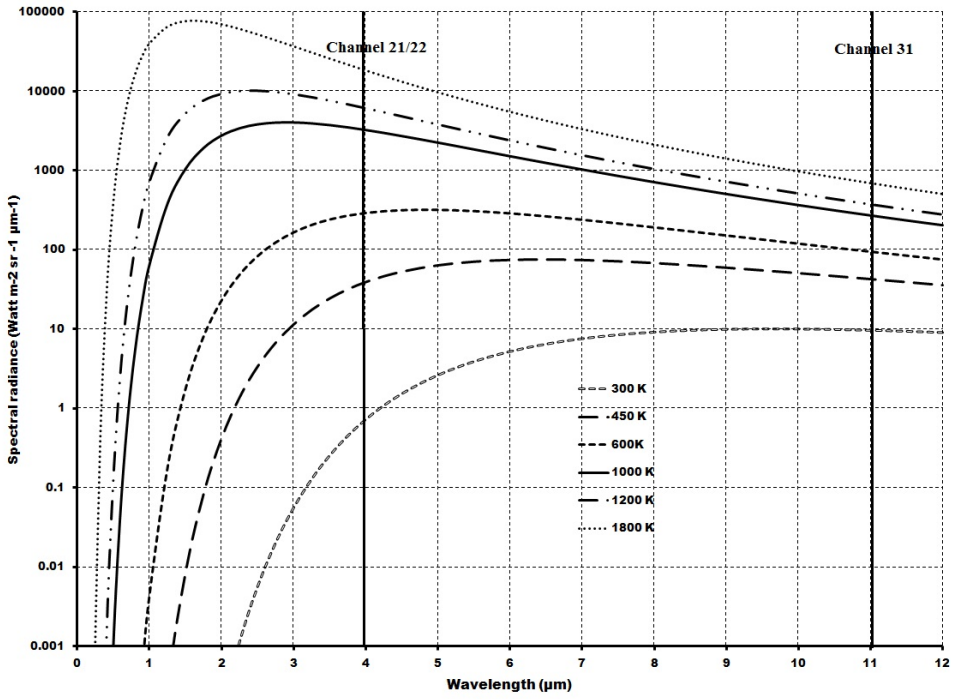

Figure 2.8. Planck function for blackbodies of different temperatures (Goessmann, 2007)

The sensitivity of the 3.95 μm and 11 μm channels are also different for the smoldering and flaming radiation (Christopher et al., 2006). Christopher et al. (2006) found that sensor sensitivity to the temperature is inversely proportional to the fire radiation wavelength, as summarized in Table 2.3. The temperatures 600 K and 1000 K indicate smoldering and flame temperatures respectively. The sensitivity ($\Delta T/\Delta f$) of the 3.95 μm channel is 800 when 5% of a MODIS pixel is covered by smoldering (at 600 K). Further, the sensitivity of this channel is 8300

when the pixel is only covered by 0.5% of active flame (1000 K). In contrast, the 11 μm channel shows less sensitivity for both smoldering and active burning.

Table 2.3. Information of the MODIS bands sensitivity used for fire detection (Christopher et al., 2006). f is the fraction of pixel burning.

Channel	Spatial Resolution	Saturation	Fraction of pixel that saturates the channel		Sensitivity (ΔT/Δf) at 600K	Sensitivity (ΔT/Δf) at 1000K
			1000K	600K		
3.95 μm	1000 m	500K	0.025	0.30	ΔT/Δf=800 at f=0.05	ΔT/Δf=8300 at f=0.005
11 μm	1000 m	400K	0.07	0.25	ΔT/Δf=485 at f=0.05	ΔT/Δf=1700 at f=0.005

Where: $\Delta\rho$ = change in the apparent surface reflectance

f = area covered by fire

Δf = change of area covered by fire

ΔT = temperature change in Kelvin

During the day, solar radiation interferes with the thermal radiation emitted from the earth's surface and it increases the spectral response of the 3.95 μm sensor. The interference of those two radiations are represented by the overlapping area under each curve shown in Figure 2.9. However, during the night the sensor receives only the Earth's radiant energy due to the lack of direct solar radiation. Therefore, the 3.95 μm band responds differently to day and night time hotspots. Figure 2.9 also shows that the solar radiance in the 11 μm region is close to zero. This means that solar radiation has negligible effect on the MODIS sensor in the 11 μm band and it responds only to earth's surface radiation at both day and night. These different responses play a significant role in the recognition of fire or other hotspots (Philip, 2007).

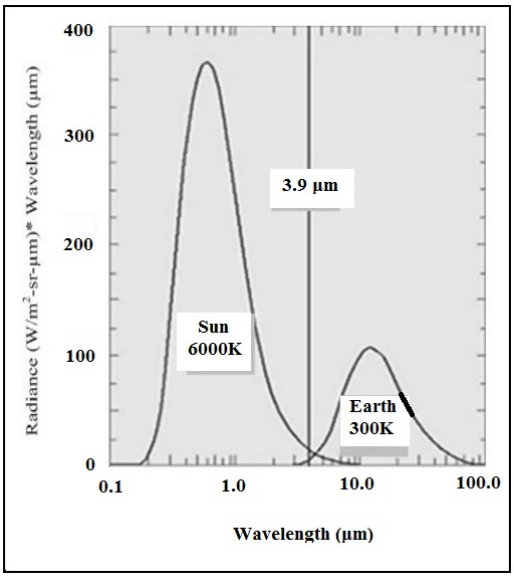

Figure 2.9. Effect of solar radiation on the 3.9 μm waveband (Philip, 2007).

The relationship between pixel temperature and radiance values at the 4 μm band (4 μm rounding up from 3.95μm) and the 11μm band can be calculated by Equation 2.3. The curves of radiance values of the 4 μm band and the 11 μm band for a range temperatures between 300 K and 700 K is shown in Figure 2.10. Increasing temperature causes an exponential increase of radiance in the 4 μm band, but increasing radiance values in the 11 μm band is almost linear. It shows that the higher the observed temperature, the bigger the difference in radiance (Δ_{rad}) values between the 4 μm band and the 11μm band (drawn in continuous black line curve).

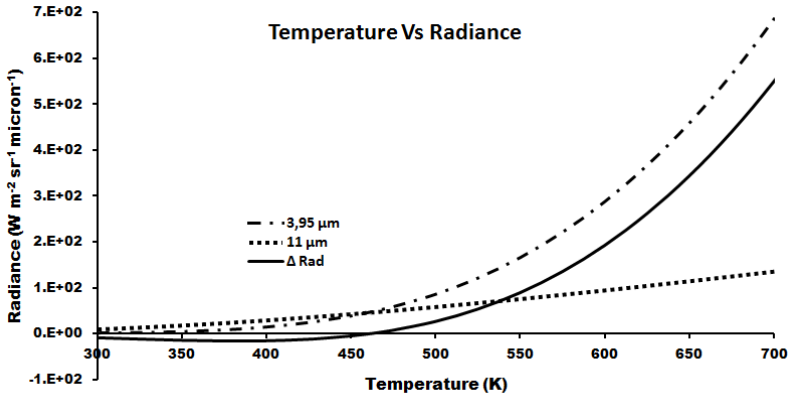

Figure 2.10. Plot of temperature and radiance for the 4μm and 11μm bands.

Data Conversion

The data captured by MODIS sensors are provided as raw data in 16-bit digital number (DN) format. These data are converted into appropriate physical values as required for fire detection such as reflectance and brightness temperature. Reflectance values in MODIS are obtained from channel 2 (0.86 µm). Converting the DN into a reflectance value is expressed by Equation 2.5.

$$\text{Reflectance} = \text{Reflectance scale} * (\text{DN} - \text{Reflectance Offset}) \quad (2.5)$$

Reflectance scale and reflectance offset values are specific for every MODIS dataset. For example in the MODIS dataset MOD021KM.A2009022.0340.hdf, the reflectance scale and reflectance offset are 0.00003 and 0 respectively. By using Equation 2.5, the reflectance value of the pixel with DN 6681 is $\rho_{0.86}$=0.00003 * (6681–0) = 0.2.

Another important value which is used in the fire detection algorithm is the brightness temperature. This is captured from channels 21 and 22 for T_4 (4 µm) and channel 31 for T_{11} (11µm). Unlike retrieving the reflectance value, generating the brightness temperature (T) refers to the Planck function (Equation 2.3). The brightness temperature value is obtained by inverting the Planck function to produce the inverse function expression.

$$T = \frac{c_2}{\lambda \, ln\left((c_1\lambda^{-5}/L)+1\right)} \quad (2.6)$$

where T = Brightness temperature of pixel (K)

c_1 = 2hc2 =119106211.8 W/(m2 sr µm4)

c_2 = hc/k = 14387.86 (K µm)

L = Spectral radiance (W m^{-2} sr^{-1} μm^{-1})

λ = wavelength (4µm for channel 21 and 22 and 11µm for channel 31).

As with the reflectance value, the spectral radiance value is retrieved from MODIS data in the digital number format, and the dataset also contains the radiance scale and offset. The radiance scale and radiance offset values are specific to every MODIS dataset. For the MODIS dataset in the previous example, the value of radiance scale is 0.00315 and radiance offset is 2730.583496. Thus the radiance value (L) of the example dataset with DN 3363 is L=0.00315*(3363-

2730.583496)=1.992. Then the brightness temperature is calculated by inputting the radiance value into Equation 2.6 and with 4 μm as the λ value for channel 21. The result (T_4 =327.745K) represents the brightness temperature value of the pixel of MODIS data with the DN 3363 stated above.

2.3.1.3 MOD14 Algorithm Assessment Steps in Fire Detection

The MOD14 algorithm consists of two main strategies, namely absolute fire detection and relative detection. Absolute detection is reserved for a strong fire, characterized by a large or high temperature fire. The absolute detection only considers the brightness temperature value which is measured from the 4 μm channels, that is channel 21 or channel 22. The next strategy is relative detection which is used to accommodate the detection of weaker fires that have elevated values from the surrounding pixels (background). This method considers the brightness temperature value from the 4 μm channel and also considers the difference of emitted thermal radiation recorded from the 4 μm and 11 μm channels. It has also been described that solar radiation in the day time affects the measured radiation value, particularly in the 4 μm channel. Thus, the impacts of solar radiation should be considered with respect to the threshold values of both the absolute and relative detection strategies particularly in day time fire detection algorithms (Giglio et al., 2003).

In order to reduce false fire detection, some additional pixel examinations are also included prior to the application of the fire detection algorithm. They are needed to exclude unwanted pixels such as missing data (null value), cloud pixels with a low temperature (cold) and high reflectance in visible wavelengths, water pixels with dark and cold characteristics, desert boundaries, and coastal edge pixels which look very bright but do not have a high temperature. Also, the strongly reflected solar radiation known as sunglint may cause false detection and the pixels affected must be removed from the assessment steps of the fire detection algorithm (Justice et al., 2002). Once the identification of pixels of cloud, water, sunglint, desert boundary, and coastal edge have been undertaken for the datasets, the fire pixels test algorithm is applied to the remaining pixels.

The MOD14 fire detection algorithm can be grouped into four tests—the preliminary test, absolute detection test, background pixels identification, and contextual test. The following sections describe each group of tests in determining the fire pixels.

Preliminary test

A preliminary test or prescreening stage is applied to obviously differentiate fire pixels or potential fire pixels from non-fire pixels. In this stage, imagery pixels are tested by the following algorithm (Giglio et al., 2003). Day time pixels are considered potential fire if $T_4 > 310$ K, $\Delta T = T_4 - T_{11} > 10$ K, $\rho_{0.86} < 0.3$ or the reflection angle is within 40^o, where sunglint may cause false detection (Justice et al., 2002), while night time pixels are tested using a reduced threshold, $T_4 > 305$ K, $\Delta T = T_4 - T_{11} > 10$ K. The reflectance value from the 0.86 μm channel is not taken into account as there is no reflectance at night. All satisfied pixels are considered potential fire pixels and progress to further tests; otherwise they are classified as non-fire pixels. Once all appropriate pixel values are examined then the MOD14 algorithm is applied to those values. Determining fire pixels from potential fire pixels that pass a preliminary test is performed in two categories, the absolute threshold test and the contextual test algorithm.

Absolute detection test

An absolute test is aimed to classify fire pixels with high brightness temperature. In the absolute fire algorithm, for day time imagery, pixels will be identified as fire pixels if the pixels fit the following conditions.

($T_4 > 360$ K) or

($T_4 > 330$ K and $T_4 - T_{11} > 25$ K)

For the night time the pixels will be classified as fire if:

(T4 > 330 K) or

($T_4 > 315$ K and $T_4 - T_{11} > 10$ K).

Note: *Nighttime pixels are defined as the pixels with solar zenith angle* $\geq 85^o$.

All pixels that pass the absolute detection requirements are marked as fire pixels and they do not need to proceed to the next assessments. However, the pixels that fail this test must be assessed by the next step, background characterization.

Background pixels identification

Background pixel identification is used to determine the relative threshold values in the contextual test. This assessment takes a window of increasing size until the condition is met. Assessing a valid background value commences with a 3x3 window centered on a potential fire pixel. The size of the square window is increased up to 21x21 pixels. When there are at least 25% of the pixels in the tested window and at least eight pixels satisfy the valid background criteria, then the window size increment is stopped and the appropriate pixels are marked as valid background pixels.

Pixels are considered a valid background if they meet four criteria: (1) made from usable observations, (2) must be land pixels, not water pixels, (3) are not identified as cloud, and (4) are not considered as fire pixels where $T_4 > 325$ K, $\Delta T > 20$ K for day time pixels and $T_4 > 310$ K, $\Delta T > 10$ K for night time pixels (Giglio et al., 2003). Once the number of valid background pixels in the tested window reaches the required criteria, then the "mean" and "standard deviation" is computed for the valid background pixels. After the background statistic values are computed, the contextual test is then applied to the window of pixels to define the fire pixels.

Pixels which do not meet the required criteria until the window size reaches 21x21 are flagged as unknown pixels. Because of the triangular MODIS sensor response along track (Kaufman et al., 1998), two adjacent along-track pixels identified as potential fire pixels (center of window) are not taken into account (Giglio et al., 2003).

Contextual test

It has been stated previously that statistical values of valid background pixels are needed in order to provide the required parameters in the contextual test. Detail of the required parameters are given in Table 2.4.

Table 2.4. Parameters and definitions in contextual test (temperature in Kelvin)

Parameters	Definitions
ΔT	Temperature difference of T_4 and T_{11} ($\Delta T = T_4 - T_{11}$)
$\overline{T_{4_b}}$	Mean of valid background pixel temperatures from 4 µm channel
δ_{4_b}	Standard deviation of valid background pixels from 4 µm channel
$\overline{T_{11_b}}$	Mean of valid background pixel temperatures from 11 µm channel
δ_{11_b}	Standard deviation of valid background pixels from 11 µm channel
$\overline{\Delta T}_b$	Mean of valid background pixel temperatures of $T_4 - T_{11}$
$\delta_{\Delta T_b}$	Standard deviation of valid background pixels of $T_4 - T_{11}$
$\overline{T_4{}'}_b$	Mean of background fire pixel temperatures from 4 µm channel
${\delta_4}'_b$	Standard deviation of background fire pixels from 4 µm channel

In the contextual test, the potential fire pixels will be characterized as fire pixels if they agree with several requirements as stated in the expressions below (Giglio et al., 2003).

a. The daytime pixels are considered as fire if the conditions below are met. Otherwise the pixels will be classified as non-fire.

$\left(\Delta T > \overline{\Delta T_b} + 3.5\, \delta_{\Delta T_b}\right)$ and

$\left(\Delta T > \overline{\Delta T_b} + 6\, K\right)$ and

$\left(T_4 > \overline{T_{4_b}} + 3\, \delta_{4_b}\right)$ and

$(T_{11} > \overline{T_{11_b}} + \delta_{11_b} - 4\, K$ or ${\delta_4}'_b > 5K)$

b. The nighttime pixels are classified as fire pixels if they satisfy the requirements:

$\left(\Delta T > \overline{\Delta T_b} + 3.5\, \delta_{\Delta T_b}\right)$ and

$\left(\Delta T > \overline{\Delta T_b} + 6\, K\right)$ and

$\left(T_4 > \overline{T_{4_b}} + 3\, \delta_{4_b}\right)$

2.3.2 IndoFire algorithm

Fire Watch Indonesia (FWI), otherwise known as the IndoFire system, was developed to fulfill the Indonesian government's need for a fire monitoring system as a base system for forest fire control and forest management. This fire

monitoring system is used by three authorized agencies for fire monitoring in Indonesia: the Forestry Ministry, the Ministry of Environment, and LAPAN (Lembaga Antariksa dan Penerbangan Nasional). The IndoFire system was built in 2007 as a collaborative project between the Indonesian government and the Australian Government, through AusAID and the Western Australian Government Department, Landgate (Indofire, 2007).

The IndoFire system processes MODIS data from L0 to L1B using SeaDAS (SeaWIFS Data Analysis System). SeaDAS is a comprehensive image analysis package for the processing, display, analysis, and quality control of ocean color data. Generated radiance data are then remapped from a swath-based HDF file to separate flat binary grid files in the chosen map projection (geodetic projection and datum WGS84) (Steber, 2013). This step is performed using the MODIS swath to grid toolbox (MS2GT) (NASA, 2013). Those processes run automatically through a program created by a Satellite Remote Sensing Services (SRSS) research group of Western Australia Land Information Authority (Landgate), customized for Indonesian environmental conditions.

Information is displayed as a constrained map for the area of Indonesia: latitude 6 N to 11 S and longitude 95 E to 141 E. Existing fire hotspots (FHS) and their images are also provided and can be downloaded freely from the IndoFire system website.[6]

The IndoFire system uses an algorithm based on a contextual MOD14 algorithm, with several modifications made at specific preprocessing steps and some threshold values. The preprocessing step changes include: remapping input data rather than satellite projected data; testing for saturation levels; testing for Not a Number (NaN) in bands 21 and 22; testing for false coastal FHS; marking cloud pixels; removing the classification scheme; and including the changeable parameters.

The IndoFire algorithm has been modified by enhancing the contextual fire detection algorithm for MODIS (Giglio et al., 2003). The algorithm has been divided into several classification steps: preliminary test to eliminate obvious non-

[6] http://IndoFire.landgate.wa.gov.au/IndoFire.asp

fire pixel; background pixels identification, to assess pixels surrounding the potential fire pixels that are not classified as fire; a relative test to determine fire pixels in the background pixels window; and some additional rejection tests. The additional rejection tests are used to eliminate false detections caused by cloud and water pixels, sunglint, desert boundaries, and coastal pixels.

A preliminary test of the MOD14 algorithm classifies pixels as either obvious non-fire pixels or those that may be fire pixels. The requirements applied in the IndoFire algorithm are similar to the MOD14 algorithm, but T_4 threshold values applied to channel 21 on the MODIS instrument are different. The IndoFire algorithm uses a T_4 threshold value of 316 K instead of 310 K. In other words, IndoFire considers pixels as potentially to be marked as fire if they have $T_4 > 316$ K, $\Delta T > 20$ K, and $\rho_{0.86} < 0.3$.

The next pixel examination steps include the classification of pixel imagery as fire or non-fire, as well as steps to reject false alarms (error). The pixel rejection steps in the IndoFire algorithm are the same as used in the MOD14 algorithm, in both method and required values. However, the IndoFire algorithm was not designed to identify a confidence level of detected fire as is included in the MOD14 algorithm.

The detection results of the IndoFire algorithm have been cross-checked using NOAA-AVHRR datasets over Indonesia from 2006 to 2008. The datasets were acquired from the Darwin Station in Australia, and were processed using the NOAA fire detection algorithm. Even though the NOAA algorithm was only run on the nighttime data, it still gave a general indication as to where the fires were located; the algorithm could also confirm whether a fire picked up by the MODIS algorithm during the day was really a fire if a fire was picked up in exactly the same location by the nighttime algorithm. Some fire hot spots detected from a small number of scenes by the IndoFire system were checked on the ground to validate the results (Steber, 2013).

2.4 Affected Parameters in Fire Detections

The acquisition of remote sensing data for fire detection is affected by many parameters. Four of these parameters will be discussed here: cloud coverage, solar

zenith angle (which represents day and night time), vegetation cover, and seasons. The effect of cloud coverage on the number of detected FHS is described in Section 2.4.1. Day and nighttime are explored in Section 2.4.2, and vegetation cover related to fire activity is explained in Section 2.4.3. The final parameter, seasonality, will be introduced in Section 2.4.4.

2.4.1 Cloud Coverage

One of the factors affecting detection of fires using a remote sensing system is cloud cover. Seielstad (2002) stated that on average, 53% of fires in Alaska were not detected remotely by fire detection algorithms due to interference by clouds. Flannigan and Haar (1986) found similar results, reporting that 59% of fires in central Alberta were undetected by fire detection algorithms due to cloud cover.

In addition, a high rate of false alarms in fire detection by remote sensing also occurs along cloud edges, especially in the application of contextual algorithms (Giglio et al., 1999). In the daytime clouds reflect the most solar radiation in the visible bands, which can elevate the measured T_4 value. The low temperature value of clouds will reduce the radiance value captured by channel 31 (T_{11}). This interference may lead to erroneous fire detection due to an increase of ΔT, the difference between T_4 and T_{11}. Giglio et al. (1999) suggest a method for cloud pixel detection, which produces only a small omission error for fire detection.

Hawbaker et al. (2008) have examined how cloud cover affects fire detection rate. They used the MODIS active fire product (MOD14 product) applied to the MODIS data over the United States. FHS detected by MOD14 were compared to the fires observed with an area ≥18 ha from pre-fire and post-fire Landsat images. Fires observed by Landsat were used as reference in this assessment. From 361 reference fires, Hawbaker et al. (2008) found that the MOD14 algorithm detected 82% of all fire observations. This means that 296 of the 361 reference fires were detected by the MOD14 algorithm, derived from both Terra and Aqua MODIS. Omission error was due to cloud cover.

2.4.2 Diurnal Influence

The solar zenith angle, which is defined as the angle between the sun and the vertical, has an important effect on thermal anomalies detected by a sensor. At a small solar zenith angle, the influence of solar radiation is very high in thermal band sensors. The thermal 4 μm band is sensitive to radiation from fire as well as solar radiation; the measured brightness and temperature on the 4μm band will increase as the solar zenith angle decreases. Increasing the solar zenith angle will increase a pixel's solar-radiated area, thus the apparent brightness and temperature of pixels decreases. In the case of the changes in solar zenith angle, a fire would be more prominent than its background at a large solar zenith angle compared to a smaller solar zenith angle.

Comparing the solar zenith angle effect to the two thermal bands (4 μm and 11 μm) shows that the temperature of measured pixels decreases more in the 4 μm thermal band than in the 11 μm (Kaufman et al., 1998). The decrease is noticed mainly for small fires (<100 ha); in the case of large fires (>100 ha), the temperature of the 4 μm band remains constant and that of the 11 μm band decreases. An illustration of solar zenith angle which can determine the day and night time data is given in Figure 2.11.

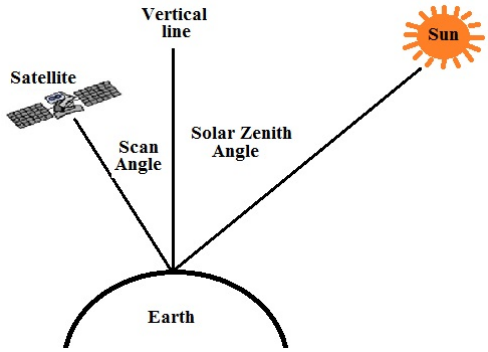

Figure 2.11. An illustration of solar zenith which can determine the day and night time data in remote sensing.

The investigation of diurnal fire patterns in this research is related to the solar zenith angle. The range of solar zenith angle values is used to classify the MODIS data as either day time or night time. Each pixel has a specific solar zenith angle value. Pixels with a solar zenith angle ≥85^{o} are classified as night time; otherwise

pixels are grouped as day time pixels (Giglio et al., 2003). Classification of day and night time pixel has been embedded in the MOD14 algorithm.

Observed fire activity during the day and at night shows different patterns (Cahoon et. al., 1992; Langaas, 1992) and the cycle tends to occur regularly on a daily basis (Prins and Menzel, 1992, 1994; Giglio, 2007; Roberts et. al., 2009). Many different sensors for fire detection give various results of diurnal fire cycles (Giglio, 2007). It is important for regional authorities and local governments to understand regional diurnal fire characteristics when monitoring and aiming to control fires. Some research related to diurnal fire characteristics contributes considerable knowledge to various methods for controlling fire (Prins and Menzel, 1994; Prins et. al., 1998; Giglio, 2007; Roberts et al., 2009).

Prins and Menzel (1992) have monitored day and night time patterns of fire activity using the Geostationary Operational Environmental Satellite (GOES) Visible Infrared Spin Scan Radiometer Atmospheric Sounder (VAS). The monitoring was performed in South America during August 1983 in areas of deforestation and grasslands. Observation was conducted using day and night time satellite datasets from two important channels for fire detection: 3.9 μm with a spatial resolution 13.8 km x 13.8 km; and the 11.2 μm channel with a resolution of 6.9 km x 6.9 km. Prins and Menzel (1992) found that the maximum number of fires detected occurred at 12:21 local time and the minimum number was detected at 18:31 local time (note that local time is UTC -3 hours).

Furthermore, Cahoon et al.(1992) published different findings, showing that many fires occurred at night time. They worked using Defense Meteorological Satellite Program (DSMP) data over Africa spanning 1986-1987. They concluded that a strong diurnal fire cycle occurred at night time.

The day and night time fire pattern has also been studied in 1988 by Langaas (1992). Langaas observed the daily fire activity in Gambia over two weeks, finding that the peak number of fires occurred at 14:30 local time and the minimum number was found at 02:30 local time. In the following year, Langaas continued the same research for Senegal using NOAA-10 and NOAA-11 AVHRR data, as he used for Gambia. Observations for the Senegal region were shorter (8 days long). Langaas reported that more fires occurred in the evening.

Another investigation of diurnal fire cycles was performed by Prins and Menzel (1994) by adding average fire temperatures of instantaneous sub-pixel areas within fire pixels, using Matson and Dozier's (1981) technique. The observation data were taken from GOES-7 VAS between 31 August and 7 September 1993. They found the peak number of total fire areas were observed at 12:30 local time (15:30 UTC). They had slightly different results when they obtained observation data from an instrument with a higher resolution (0.9 km) – the GOES-8 VAS – during the week of 5-11 September 1994. The peak of fire numbers was detected in the late afternoon at 15:00 local time (18:00 UTC) (Menzel and Prins., 1996).

Moreover, Giglio (2007) monitored the diurnal fire cycle in 15 tropical regions around the world using VIRS and MODIS datasets. His method counted fire hotspots in VIRS images within a prescribed area and matched them to the local hour observations. The prescribed areas included Brazil, Southeast U.S.A., Sahel, Central Africa, South Africa, Southeast Asia, Borneo, Australia, and India. He observed that the distinct patterns of diurnal fire cycles occurred maximally between the early afternoon and late afternoon for all investigated areas. In general, fire activity has only one peak value during the day, except in Northern Australia and Eastern Sahel where there are two peak fire times, one in mid- morning (about 9.00-10.00 local time) and one in the afternoon (15.00-18.00 local time). Giglio (2007) has also reported that the burning time period was observed to occur between 13:00 and 18:30 local time, but in the heavily forested regions the peak time of active fires occurred earlier.

2.4.3 Vegetation Cover Types

The relationship between fire occurrence and vegetation cover types has been studied by many researchers. The research areas of interest vary in vegetation cover types, and global location, such as Central Africa (Bucini and Lambin, 2002), Indonesia (Miettinen and Liew, 2005), and Central U.S.A. (Tulbure et al., 2011). Indonesia is a tropical area with diverse vegetation cover types, which often encounter fires. In some tropical habitats, a small fraction of vegetation is tree cover, while the greater proportion is comprised of herbaceous growth (Giglio,

2007). The low vegetation (herbaceous growth) dries faster and provides finer, lighter fuel for biomass burning. In the dry season, which is generally associated with higher temperatures, their availability is more abundant and lasts longer. Fire ignition in these conditions will increase very easily throughout the day. On the other hand, another extreme condition occurs when the land is covered mostly by trees, such as the tropical rainforest. Weather conditions in the tropics are primarily humid, which prevents the occurrence of fire ignition. If fires occur in the tropical rainforest, the fire is usually short lived (Kauffman and Uhl, 1990).

Miettinen and Liew (2005) have investigated the relationship between vegetation cover change and fire activity in the Riau province of Indonesia in 1986, 1998, 2000, and 2002. Research shows that change in primary vegetation in Riau province is strongly affected by fire, while change in secondary vegetation was less affected by fire. In some areas, fire is used to maintain vegetation cover types intentionally; for example, fire is used to change rubber-harvesting forest into palm oil plantations. The names and definitions of land classifications including vegetation cover types in Indonesia refer to the vegetation naming rules as given in Table 2.5.

Table 2.5. Names and definitions of land classifications (Anonymous, 2010a). Classification is divided into categories of vegetated (includes low vegetation and high vegetation categories) and non-vegetated areas.

No	Land classifications	Definitions
Low vegetation cover category		
1	Swamp bush	Shrubs and former forest in inundated areas
2	Shrubland	Former Dry Forest, now dominated by Shrubs, dominated by low vegetation and no longer showing the former water flow/scar's logging
3	Dry land farming with mixed shrubland	Agricultural land with fallow soils interspersed with shrubs and logged forest.
4	Dry land farming	Agricultural land in dry environments (formerly several vegetation types).
5	Rice field	Wetland agriculture characterized by patterns of embankments

No	Land classifications	Definitions
6	Transmigration	Cultivated land including agriculture and settlements
7	Savanna / Grassland	Few scattered trees over tussock grass
High vegetation cover category		
8	Plantation	The entire plantation area, planted or not
9	Secondary swamp forest	The whole appearance of forest in swampy areas that show previous logging
10	Secondary dry land forest	The whole appearance of forest that shows previous logging
11	Secondary mangrove forest	Mangrove forests and palm that has been cut and has groove patterns in it
12	Harvesting forest	The entire industrial forests area, either planted or not
13	Primary dry land forest	Forests that have not been logged, including vegetation naturally low-growing in the massive rock
14	Primary swamp forest	The whole appearance of forest in swampy areas, including peat swamp which do not exhibit logging signs
15	Primary mangrove forest	Mangrove forests and palm located around the coast that have not been cut
Non-vegetated category		
16	Clear land	The whole appearance of open land without vegetation
17	Water body	All the appearance of water, including the ocean, rivers, lakes, reservoirs, coral reefs and mud beach
18	Fish pond	The place for fishing activities or salting that appears with the pattern bund around the coast
19	Swamp	Swamp appearance that has not been forested
20	Settlement area	Urban settlement areas either in cities, rural areas, ports, airports, industrial areas, and so forth, which shows a dense pattern of grooves
21	Mining	Open land used for mining activities (coal, tin, copper, etc.)

No	Land classifications	Definitions
22	Airport/Harbour	The berthing place for aircraft or ships with passenger facilities and loading or unloading of goods

2.4.4 Seasonal Parameters (Precipitation and SOI)

Indonesia is a tropical area, located at the Equator. There are two seasons in Indonesia: the rainy (wet) season, and the dry season. The wet season generally has a high level of precipitation that can reduce the frequency of fire occurrence. Each of the two seasons lasts for approximately 6 months. Usually the dry season ranges from June to November and the wet season occurs from December to May (Yasunari, 1981; Kishore et. al., 2000; Langner et. al., 2007). The length of the two seasons may vary, and may be affected by climate parameters such as the El-Nino and La-Nina phenomenon.

El-Nino and La-Nina might change the seasonal time period. A strong El-Nino causes the occurrence of an early dry season or a delayed wet season (Irianto, 2003). In contrast, the La-Nina effect induces a longer wet season, which leads to increased precipitation.

The El-Nino and La-Nina can be indicated by the Southern Oscillation Index (SOI). The SOI is defined as the difference in sea level pressure at Tahiti and Darwin or $SOI = P_{Tahiti} - P_{Darwin}$. The SOI values can be a negative or positive number. The positive SOI values are usually associated with El-Nino phenomena and the negative SOI values are related to La-Nina phenomena (As-syakur, 2008). The relationship between fire, drought, and El-Nino in Borneo has been studied by Wooster, Perry, and Zoumas (2012) for two decades. They used detected FHS from 1980 to 2000 by using NOAA AVHRR data, which passed over Borneo. They found that the rising magnitude of active fires occurred during an investigation period was caused by decreasing precipitation, a short term climatic factor, due to the impact of the El-Nino phenomenon.

2.5 Sensitivity of Fire Detection Algorithm

MOD14, a fire detection algorithm, was created to use MODIS data instead of AVHRR data. The MODIS channels wavelength bands are relatively close to the AVHRR channels; therefore the design of the two algorithms is similar. Both AVHRR and MODIS use two infrared channels – 3.73 μm and 11 μm channels for AVHRR, and 4 μm and 11 μm channels for MODIS – that are notated by T_4 and T_{11}. MODIS sensors are sensitive to temperatures up to 450 K and 400 K for channels 4 and 11 μm respectively; this temperature is higher than the AVHRR saturation temperature (Kaufman et al., 1998).

Indonesia has a large forest area, including rainforest and plantation forest. Plants absorb a high amount of incident solar energy to drive their photosynthesis process and the solar energy is re-emitted at night in the thermal wavelength range. During the day, plants tend to be cooler than their surroundings because extra energy is needed when plants transpire in releasing water vapor (Chuvieco and Huete, 2010). To obtain accurate fire detection data during daylight, lower threshold values should be used in these forest areas, compared to the threshold values of other regions. This indicates also that the threshold value for night fire detection in dense forests could be higher than other regions.

A sensitivity assessment of a fire detection algorithm called "MODIS-like daytime active fire detection model" has been done using NOAA-AVHRR data over Alaska (Seielstad et al., 2002). In this assessment, Seielstad et al. (2002) related the false detection with the threshold value applied in the algorithm. They found that reducing the threshold value used in the assessed algorithm increases the false detection rate. Their results suggested that the threshold value utilized in the algorithm should be higher for Alaska compared to the MODIS fire algorithm threshold, which is 310K. Seielstad et al. (2002) proposed that the optimal threshold value is between 314K and 315K.

Further research in assessing the MOD14 algorithm was conducted by Wang et al. (2007). They reported that the MOD14 algorithm was not sensitive to fires in the South-Eastern United States, as the fires were generally small and cool. Pixel brightness temperature in the investigated area is mostly less than 310K; as a result the MOD14 algorithm showed a lot of false detection. Wang suggested decreasing

the threshold value (293K) to elevate the sensitivity of the fire detection algorithm applied in the area of the South-Eastern United States.

Based on both sensitivity assessments described above, the applied threshold value could be different for every different area. For example, the threshold value of 310K is too low to be applied in Alaska (Seielstad et al., 2002) but that value was too high for the South-Eastern United States region (Wang et al., 2007). The sensitivity assessment for the fire detection algorithm applied to MODIS data over Indonesia, particularly in Riau and Central Kalimantan provinces, is conducted in this research.

2.6 Validation Activities

The measurement of every physical object's properties needs a validation process to ensure the given information is accurate. A validation process includes accuracy and sensitivity assessments of uncertainty calculations. Section 2.6.1 describes the research conducted regarding the validation assessment of the fire detection algorithm; validation employed SPOT high resolution images. Further, Section 2.6.2 discusses the validation assessment by using collected ground data.

2.6.1 Validation Using SPOT High Resolution Imageries

The SPOT satellite does not have thermal infrared channels, which are considered essential in fire detection. The only SPOT band that could potentially detect a hot object is the Short Wave Infrared (SWIR) band, at 1.6 μm wavelength, onboard the SPOT 4 satellite. Unfortunately this band is dominated by solar radiation that cannot be involved in fire detection applications. However, the high-resolution imagery products represent a benefit of the SPOT satellite; this high resolution imagery allows the visual detection of fires.

CRISP (Center of Remote Imaging, Sensing, and Processing) has a receiver for SPOT satellite data; CRISP has used SPOT imagery for forest fire monitoring since 1997. The CRISP's researchers use the high-resolution SPOT images to detect fires and measure the length of existing smoke plumes; the images also can be applied for recognizing location and vegetation cover types of the area where fires occur (CRISP, 2001). The high-resolution SPOT imagery covers a smaller

area compared to the moderate resolution MODIS data. However, the high-resolution imagery can provide more accurate fire detection results, particularly for smaller fires.

Liew et al. (2003) conducted active fire detection research using SPOT data. They used 17 SPOT images that were acquired over 10 days in August-September 2002 and May-July 2003 to validate the MODIS fire product. The applied strategy was based on the visibility of smoke plumes produced by fire. However, not all fire ignitions produce smoke that can be detected by this method. If a fire is entirely a chemical reaction, smoke plumes will not rise as a combustion product, particularly in intense fires. However this condition is not common for tropical areas with high humidity; therefore the smoke plumes method is appropriate for a humid environment such as Indonesia's (Liew et al., 2003).

Liew et al. (2003) classified the detected fire from SPOT images into four classes based on smoke plume observations: fires with faint and mostly unseen smoke are classified as Class 1; Class 2 accommodates fire with smoke plumes less than 1 km long; Class 3 contains fires with 1 to 10 km smoke plumes; and finally Class 4 contains fires with more than 10 km smoke plumes long (Liew et al., 2003). From the 17 SPOT images acquired over 10 days, Liew et al. counted 275 existing fires, with 62 fires in Class 1, 78 fires in Class 2, 77 fires in Class 3, and 58 fires in Class 4.

An error assessment was carried out using the proximity method by creating 1 km radius circled areas around MODIS fire spots. Valid MODIS fires are marked if there are one or more fires identified in the SPOT image within 1 km radius from its point (Liew et al., 2003); otherwise the MODIS fire spot is considered a commission error. The opposite condition, omission error, is justified where there is no MODIS fire spot within a 1-km radius of an identified SPOT fire. As a research conclusion, the commission error rate was 26.8% while the omission error rate was 34.2%. The omission and commission error described was analysed over Sumatra and Borneo.

In addition, the commission error of 26.8% is potentially related to new burn scars with high temperatures that have not produced smoke yet. In contrast, the 34.2% pixels not detected by the MOD14 algorithm but considered as fire in SPOT

images, are caused by the high reflectance value of MODIS channel 2 (0.86 µm). The high reflectance value (more than 0.3) is a result of smoke plume reflection, so they are rejected by the MOD14 algorithm in the preliminary test.

2.6.2 Validation Using Ground Data

Fire information from ground-based data is generally provided only in limited regions and time periods (Cardoso et. al., 2005). Remote sensing methods for fire detection can cover extended areas and time periods, but the accuracy of the detection results must be assessed. Comparing fire observed on foot and fire detected from MODIS data is used as a validation method (known as the data validation method) by Cardoso et al. (2005), Tanpipat et al. (2009), and Vetrita et al. (2012). To enhance the interpretation of satellite fire data for the Amazonia region, Cardoso collected ground-based data on fires in 2001 and 2002 using a simple and passive method to compare with estimates from MODIS fire products using error matrices. The matrix data of Cardoso et. al (2005) showed that the number of fires observed on foot (ground data) was 138, while the number of hotspots detected by MODIS was 3, and only 1 fire matched the ground data. The data show that much of the fire observed on the ground cannot be detected by the MODIS fire product. It was suggested that the discrepancy was caused by time differences between ground observations and satellite overpasses.

In addition, Tanpipat et al. (2009) validated FHS detected by the MODIS fire algorithm applied to MODIS datasets over Thailand. Ground observation data was utilized in the validation to assess detection accuracy of the fire algorithm. The observation was conducted based on MODIS hotspot locations, which consider area accessibility as an important site selection criteria. Tanpipat found one false alarm in the burned and ash-covered area; this was due to the latent heat of the burned area, which gives the area a high temperature although the fire has died. Overall, the research resulted in high detection accuracy (97.67%) of MODIS fire detection over Thailand.

Similarly, Vetrita et al. (2012) have used ground data to validate the detected FHS occurrence at Riau province in 2011 based on the IndoFire algorithm. They collected ground data based on the FHS location detected by IndoFire. They

considered the IndoFire detected FHS as valid if ground data indicated fires occurring within 2 or 3 days around the date of the detected FHS. The other valid fire pixel consideration is the distance of the in-situ fire observed, and the location of the detected FHS data points; if the distance is within 2 km radius, then the detected FHS from IndoFire is considered as a valid detection. Vetrita also found some small burned areas in the field but none of these areas were detected as fire by the IndoFire algorithm. Based on Vetrita's validation, the detection's accuracy of the Indofire algorithm over Riau was 43%. This is possibly caused by small burned area size; the minimum burned area size to possibly be determined as fire by the MODIS fire detection algorithm is suggested by Giglio et al. (2009) to be 120 ha, (MOD14).

2.7 Summary

In summary, in Section 2.1 we discussed the principles of remote sensing as the observation of the Earth's surface from space. Explanation of remote sensing terms were focused on satellite remote sensing, as this research conducts analysis using satellite remote sensing data. Also described was the interaction of electromagnetic radiation with observed objects, and how the satellite sensors capture object properties from the Earth's surface as a fundamental theory which is used in fire detections. In addition, Section 2.2 highlighted the physical principle of thermal electromagnetic radiation and its relationship to the surface temperature and brightness temperature. Formulas to covert the captured electromagnetic radiation energy into physical properties of objects are also given in this. The fire detection algorithm principle is described in Section 2.3; the emitted radiance of fire in thermal wavebands determines the band of the sensor to be used to detect fire. The different stages of fire with their specific temperature characteristic has also been introduced in this section. The MOD14 algorithm, as the most commonly applied fire algorithm and also as a basis of the IndoFire algorithm in Indonesia is further explained, including the pixel classification results, sensors sensitivity, solar radiation effects which have an impact on the strategy of day and night time fire detection. Section 2.4 described the parameters that impact the fire detection methods. The parameters introduced are cloud coverage, the time of observing data

(day and night time), vegetation cover types, and seasonal parameters such as precipitation and SOI. The cloud coverage impacts on the detected FHS number, day and night time relates to the applied threshold values, while vegetation cover types and seasonal parameters affect the fire occurrence patterns. The sensitivity of the fire detection algorithm applied to different regions has been described in Section 2.5. The reported research regarding the assessment of fire algorithm sensitivity suggested it was appropriate to apply different threshold values in the fire detection algorithm applied in different regions. Finally this chapter concluded with discussion on the validation processes, outlined in Section 2.6. Validation using SPOT data is applicable for fire detection results due to their high spatial resolution although they do not have a thermal band sensor. The applied technique is using visual analysis based on the smoke produced from fire. The other research approaches to validation of fire detection results is through the use of ground check data. Ground data validations have been reported for different areas such as the Amazonia region, Thailand, and Indonesia. Based on the ground data validation methods, the same fire detection algorithm, MOD14, showed different accuracies when it was applied in those different regions.

CHAPTER 3

RESULTS AND ANALYSIS

Chapter two has introduced the review of literature regarding fire detection using satellite remote sensing data starting with the principles of remote sensing of electromagnetic radiation with a focus on the thermal infrared region. Two fire algorithms (MOD14 and IndoFire) were also described in the previous chapter with a focus on their use in Indonesia and investigation into the key parameters which influence the accuracy of fire detection using remotely sensed data. This chapter presents a study of the trends of Fire Hotspot (FHS) activity during the decade 2001-2010 and analyses the operation of the MOD14 algorithm when applied to MODIS datasets over Indonesia, with a focus on the provinces of Riau and Central Kalimantan (Kalteng). The term FHS refers to the number of fire affected pixels detected using remote sensing data. The decadal study is based largely on fire activity data generated by the IndoFire system (Landgate, 2007). The sensitivity of the fire data to perturbation of parameters in the MOD14 algorithm is investigated and the results are presented in the context of the decadal study. Factors affecting the operation of the algorithm include cloud cover, vegetation cover type, and seasons.

This chapter is divided into six sections. Section 3.1, 'Fire detection and cloud coverage', describes the remote sensing-derived fire activity trends for a decade in Indonesia based on IndoFire data. The impact of cloud coverage is analysed, and there is a discussion regarding approaches to estimating the true number of fires based on extrapolation from the partial views of selected geographical regions most often available from satellite imagery. Section 3.2 covers diurnal figures of fire activity in the chosen province area in respect to the Section 3.1 description. Section 3.3, 'Fire activity and vegetation cover type relationships', investigates the relationship between numbers of FHS and the different vegetation cover types over Riau and Kalteng province during 2009.

Section 3.4, 'Precipitation, Southern Oscillation Index (SOI), and fire activity', discusses the relationship between season's parameters (precipitation and SOI) and the number of occurring FHS. Section 3.5, 'Sensitivity analysis of the MOD14 algorithm', presents an analysis of the sensitivity of the MOD14 fire detection algorithm to the changes of the temperature threshold values, with reference to the changes in the operation of the algorithm in the wet and dry seasons. Finally, Section 3.6, 'Validation of MOD14 algorithm results', discusses how the detected FHS using the MOD14 algorithm may be validated using high resolution SPOT imagery and ground data, with Riau and Kalteng provinces as focus regions.

3.1 Fire Detection and Cloud Coverage

Indonesia is characterized as a country that deals with a lot of fire (Hoffmann et al., 1999; Page et al., 2002; Tacconi, 2003). Trends of fire occurrence based on IndoFire data are given in a time series for the decade 2001-2010 as shown in Figure 3.1. IndoFire-derived total FHS data for Indonesia were acquired within latitude 6°N to -11°S and longitude 95°E to 141°E. Figure 3.1 indicates that the highest number of FHS occurred in 2006 with approximately 120,000 FHS.

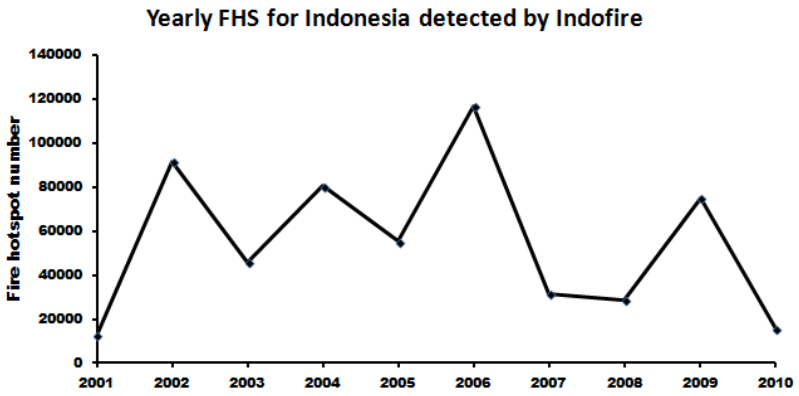

Figure 3.1. FHS trend in Indonesia for a decade. Yearly data is the sum of detected FHS by IndoFire for the whole Indonesian area.

Indonesia has 33 provinces, as shown in Figure 3.2, which contain different geographic characteristics. The number of FHS data in every Indonesian province for the decade 2001-2010 detected by the IndoFire system is given in Appendix 3.

The order of data in Appendix 3 is sorted according to the total number of detected FHS for the decade per area (sq.km) in every province. The table indicates that detected FHS in Indonesia are not distributed evenly for every province; fire may occur more densely in some provinces than in others. The Riau province is the most prone to fire, followed by Kalteng province. The location of both provinces in the Indonesian map is displayed in the marked areas of Figure 3.2.

Figure 3.2. The location of Riau and Kalteng provinces within Indonesia. Coordinate positions of Riau province is in between latitude -1.3 S to 2.5 N and longitude 100.0 E to 104.0 E while Kalteng province is located in between latitudes 1.0 N and -3.5 S and longitudes 110.5 E and 116.0 E. These coordinates are used to border the data searching related to those two province areas (Riau and Kalteng).

In addition, an investigation of fire activity trends was conducted based on province area. Trends of fire activity in Indonesia for 10 years in every province are shown in Appendix 4. Most provinces show the peak of the fire season occurs between June and November every year, which is generally recognized as the dry season. Conversely, between December and May, which is recognized as the wet season, the number of fires tends to be relatively lower. However, there are some provinces where the peak fire season occurs in arbitrary months throughout the 10 year time series. For example, signal peaks in the fire season in Riau occur in both dry and wet seasons over the ten year time series, while peaks in the fire season in Kalteng occur in the dry season only.

Furthermore, the accuracy of detecting fire occurrence using satellite remote sensing data has been reported to be affected by cloud coverage, as described in

Section 2.4.1. The cloud cover potentially obscures the remote sensing observations of fire occurring on the Earth's surface. This section presents a study of the relationship between patterns of fire activity and cloud coverage over the area of investigation in Indonesia. Cloud coverage data were obtained from NASA - GES DISC (Goddard Earth Science Data and Information Services Center) through the Giovanni GES DISC website[7]. The patterns of Monthly time series FHS numbers derived from IndoFire versus fraction of cloud cover derived from Giovanni- GES DISC for Indonesia over the decade 2001-2010 are displayed in Figure 3.3.

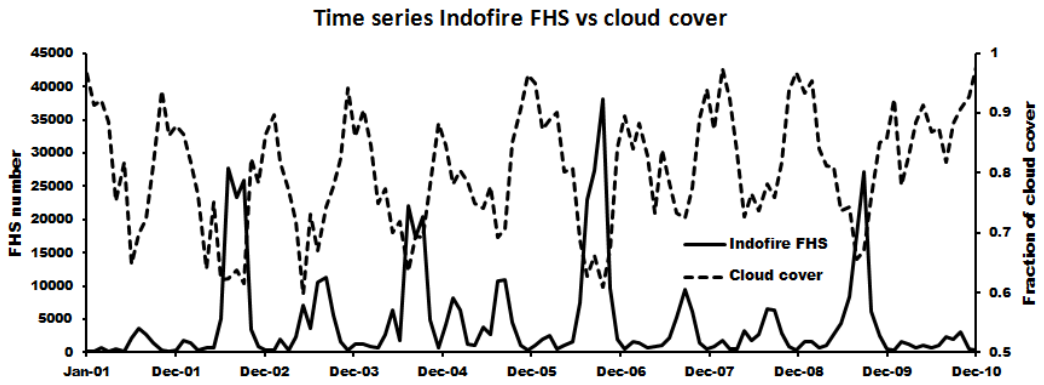

Figure 3.3. Monthly time series of number of FHS derived from IndoFire and fraction of cloud cover derived from Giovanni- GES DISC for Indonesia over the decade 2001-2010.

The scatter plot of detected FHS and the fraction of cloud coverage for Indonesia over the decade 2001-2010 is shown in Figure 3.4. From the figure we can observe that the increasing fraction of cloud coverage tends to decrease the number of detected FHS.

[7] http://gdata1.sci.gsfc.nasa.gov/daac-bin/G3/gui.cgi?instance_id=MODIS_MONTHLY_L3

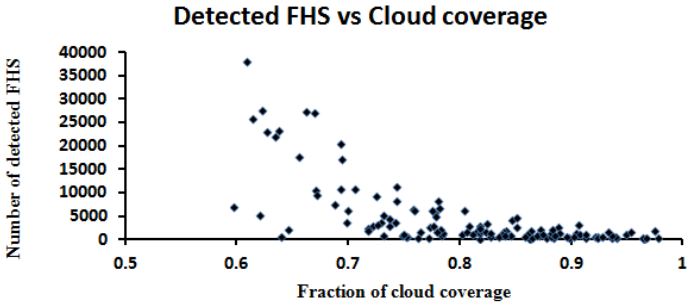

Figure 3.4. Scatter plot of the number of detected FHS and the fraction of cloud cover for Indonesia over the decade 2001-2010.

In a 2-tailed test of correlation at 0.01 significance level the correlation coefficient for the data is -0.665. This suggests that there is strong negative correlation between the fraction of cloud coverage and the number of detected FHS. The high fraction of cloud coverage relates to the smaller number of detected FHS and vice versa. This phenomenon is also observed in Figure 3.3.

Based on the monthly cloud cover data for Indonesia over a decade as displayed in Figure 3.3, the highest values of cloud cover are shown to occur around December to February every year, a period which is usually categorized as wet season months (Yasunari, 1981). Conversely, the cloud cover is commonly low in the months of July to September, and these months are classified as the dry season (Yasunari, 1981). The minimum monthly cloud cover value of 59.8% occurred during June 2003 and the maximum cloud cover value of 97.8% occurred during December 2010.

An associated FHS pattern for the decade 2001-2010 over Indonesia can show a better description of the relationship between detected FHS and cloud cover seasonally. The monthly number of FHS detected using IndoFire, as shown in Figure 3.3, indicates that the highest number of FHS occurred around July to October (within the dry season) and the lowest number of FHS was detected around December to March, which are normally wet season months. These patterns give a reasonable relationship between cloud cover and the occurrence of fire. Increasing cloud cover, mostly occurring during the wet season, corresponds to a low frequency of fires and so the number of FHS is low. In contrast, the low

fraction of cloud cover mostly occurs within the dry season, which is associated with high numbers of detected FHS.

Since cloud coverage obstructs the detection of FHS by satellite, the true number of fires within the area is potentially greater than the number of FHS detected by satellite alone. The true number of fires can be approximated by using an extrapolation technique. The approach adopted here is to estimate the number of FHS for the whole Indonesian area based on observations that are free from cloud. The extrapolation's approach used in this research is described by Equation 3.1.

$$FHS_{Extrapolation} = \frac{\text{Number of detected FHS}}{1 - \text{Fraction of Cloud Coverage}} \quad (3.1)$$

The actual number of fires (referred to here as extrapolated FHS data) potentially provides a more realistic overview of the year-to-year variability in fire occurrence; however, it is important to note that there is the potential for obtaining different results of occurring fire activity due to differences in the cyclic nature of variability in cloud cover. The extrapolated FHS numbers based on monthly cloud coverage data is shown in Figure 3.5.

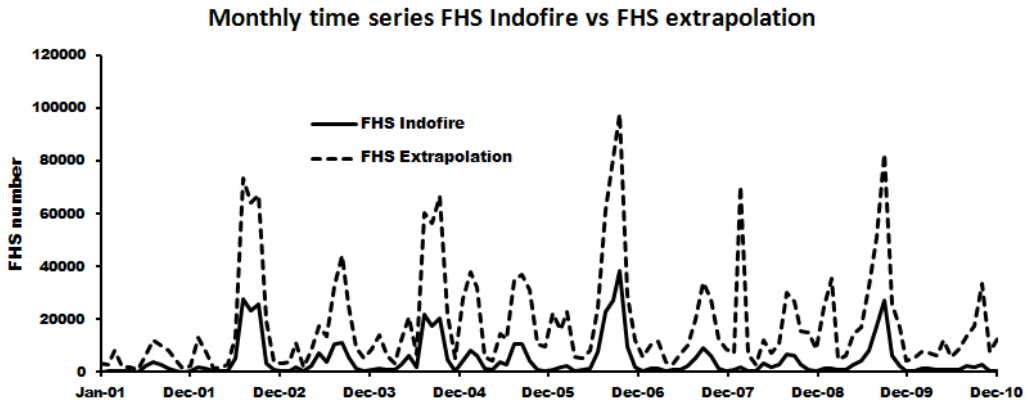

Figure 3.5. Monthly time series of FHS detected by IndoFire and the extrapolated number of fires based on monthly cloud cover data, acquired from Giovanni-GES DISC (Goddard Earth Science Data and Information Services Center), over Indonesia for the decade 2001-2010.

The cloud cover over Indonesia may also be considered in terms of annual averages, shown in Figure 3.6. The annual cloud fraction is derived from the

average of monthly cloud fraction data for every year. The figure shows a relatively high fraction of cloud coverage over Indonesia, between 70% and 90%.

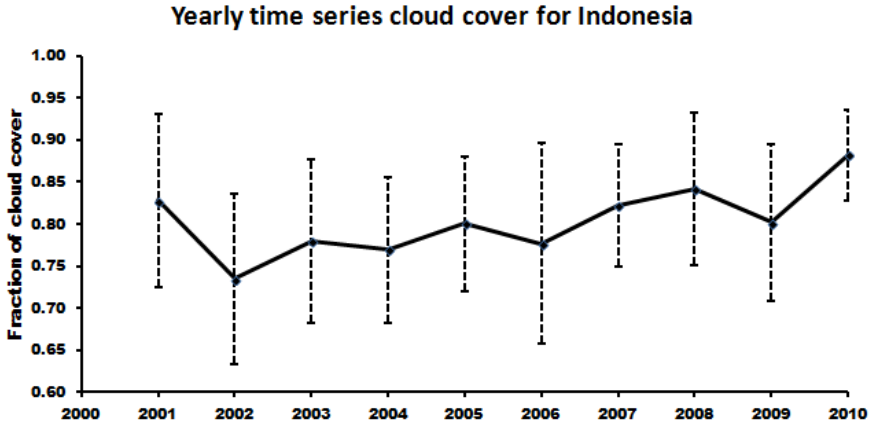

Figure 3.6. Yearly time series cloud cover for Indonesia (Latitude 6N to 11S and Longitude 95E to 141E) for the decade 2001-2010. Data are derived from the average monthly cloud cover data every year from Giovanni GES DISC (Goddard Earth Science Data and Information Services Center). Error bars represent the standard deviations of cloud cover for the region selected.

The extrapolated number of FHS based on the annual average data is shown in Figure 3.7. The yearly extrapolation data based on annual fraction of cloud coverage tends to be higher compared to the sum of monthly extrapolation data in a year. The difference between yearly and monthly FHS extrapolation was found to be 10.91%. Extrapolating the number of observed FHS based on cloud cover for a lower range of time will better describe actual fire activity, because an estimation of the number of FHS is made in almost real conditions of cloud coverage. For example, extrapolating the number of FHS based on yearly cloud coverage patterns will implicitly estimate the fire activity in the dry season (which normally has low cloud coverage) based on an average of dry and wet season cloud coverage. The yearly cloud coverage data is an average of cloud cover in a year, and the greatest contribution of cloud cover comes from the wet season. In contrast the average number of FHS in a year is mostly derived from fire in the dry season. It is possible to generate a false estimation of the number of FHS; however, predicting the number of FHS based on monthly cloud patterns will minimize the false estimation of fire activity in the dry season using cloud coverage of the wet season. Therefore,

monthly data of cloud coverage more accurately describes the pattern of cloud cover related to the seasons in Indonesia (dry and wet seasons).

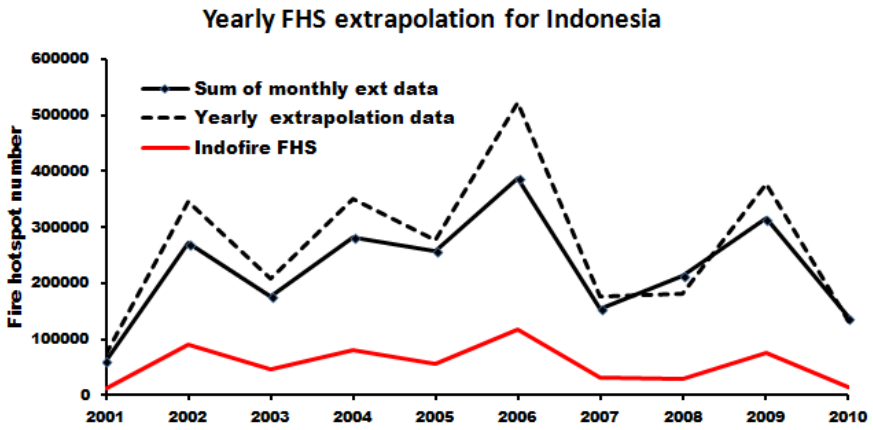

Figure 3.7. Yearly patterns of IndoFire FHS and extrapolated FHS data of Indonesia for a decade (2001-2010). Yearly extrapolation data are derived in two ways: first, by extrapolating yearly FHS data referring to yearly cloud cover (dashed line); and second, by summing monthly extrapolation data in a year (black solid line).

With respect to the previous discussion, the extrapolated number of FHS on a monthly basis gives a better description of fire activity and it gives a more accurate description of conditions of cloud cover to be used in the extrapolation of FHS. Hence, the extrapolation method based on monthly cloud coverage data is considered better than annual averages for extrapolating the yearly FHS number.

3.2 Monthly Patterns in Fire Activity

Section 3.1 discussed the importance of cloud coverage in estimating the actual number of FHS that occur, based on the number of FHS observed. In this section, firstly we discuss the temporal patterns of the number of FHS detected and the temporal patterns of cloud coverage over the areas investigated i.e. Kalteng and Riau Provinces. In 2009 there was a long drought as a result of the strongest El-Nino in the decade 2001-2010 (Wang et. al., 2012); Riau and Kalteng shared a peak fire season during that year (see Figure 3.1). Monthly FHS patterns overlaid by cloud coverage (CC) patterns for the two provinces for the whole year of 2009 are displayed in Figure 3.8.

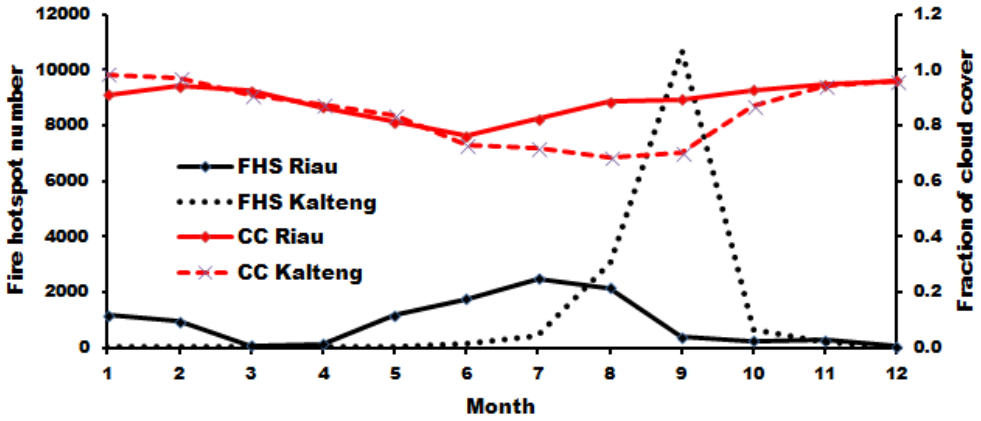

Figure 3.8. Plot of monthly FHS distribution overlaid by cloud coverage (CC) for Riau and Kalteng provinces during 2009

Figure 3.8 shows different monthly patterns of FHS distribution in Riau and Kalteng provinces. A unimodal curve of peak fire season occurring once in the year is shown in Kalteng, while Riau has a bimodal curve pattern indicating that it has two peak fire seasons, i.e. in January and July, as displayed by the black solid line of Figure 3.8. Based on this figure, the peaks of fire frequency occurred in July 2009 for Riau province and September 2009 for Kalteng province. Therefore, the months of July 2009 and September 2009 are the focus of analsyis for diurnal fire activity in Riau and Kalteng respectively.

Patterns of cloud cover over Riau and Kalteng are also displayed in Figure 3.8. By comparing the patterns of the number of fires and existing cloud cover shown in Figure 3.8, it can be seen that the decreasing fire numbers in Riau province during March and April are not solely impacted by cloud cover; the low or high number of FHS observed is not only due to cloud coverage but possibly describe the real pattern of fire activity. Fire activity in Riau province mainly affects human activities such as developing palm oil, timber, and conflict of logging companies (Sizer et. al., 2014).

However, in terms of the number of FHS detected, cloud cover still affects the probability of the number of real fires on the ground. Estimation of the actual number of FHS in the whole province is approached by the extrapolation technique described in the previous section. The curves of both detected FHS and

extrapolated FHS in Riau and Kalteng during 2009 is shown in Figure 3.9 and Figure 3.10.

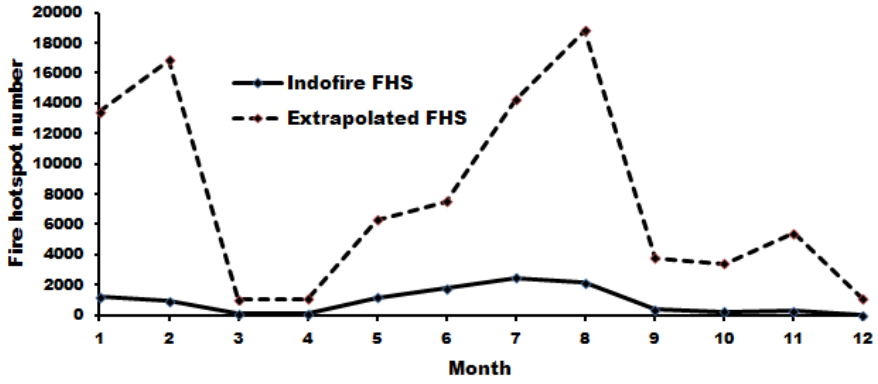

Figure 3.9. Detected number of FHS from IndoFire and the extrapolated estimate for Riau provinces during 2009

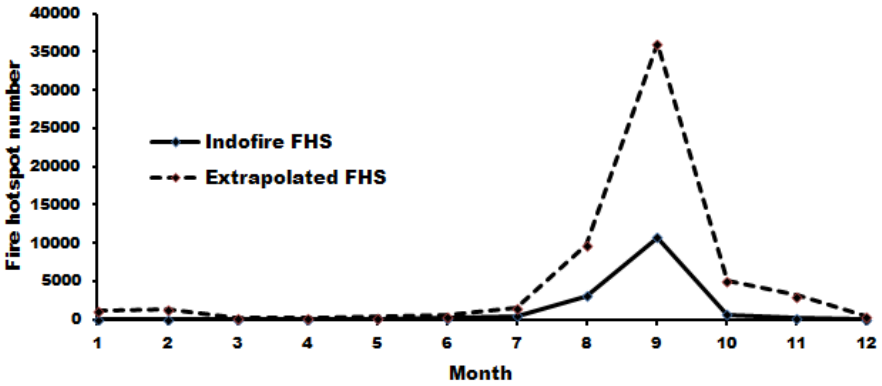

Figure 3.10. Detected number of FHS from IndoFire and the extrapolated estimate for Kalteng province during 2009.

The detailed data of Figure 3.9 and Figure 3.10 are given in Table 3.3. The calculation data suggests that the number of detected FHS from IndoFire is on average only 11% of the estimated actual number of fires in Riau province, as displayed in column D of Table 3.3. For the Kalteng province, the IndoFire system on average only detects 15% FHS based on the extrapolated FHS values, as displayed in column H of Table 3.1.

Table 3.1. Data of detected FHS numbers from IndoFire (column A and E) and the extrapolated estimate during 2009 over Riau and Kalteng provinces. The extrapolation FHS numbers (column C and G) are calculated based on monthly cloud coverage (column B and F) retrieved from Giovanni GES DISC website data. The ratio between the number of FHS detected by IndoFire and the extrapolated estimate is given in column D and H).

Month	Riau Province				Kalteng Province			
	A (FHS_{Ind})	**B** (cloud)	**C** (FHS_{Ext})	**D (A/C)**	**E** (FHS_{Ind})	**F** (cloud)	**G** (FHS_{Ext})	**H (E/G)**
January	1186	0.91	13477	0.09	17	0.99	1133	0.02
February	961	0.94	16860	0.06	41	0.97	1323	0.03
March	75	0.93	1027	0.07	19	0.91	213	0.09
April	142	0.87	1068	0.13	37	0.88	301	0.12
May	1177	0.81	6294	0.19	60	0.84	364	0.17
June	1766	0.77	7515	0.24	138	0.73	507	0.27
July	2482	0.83	14264	0.17	450	0.72	1590	0.28
August	2164	0.89	18817	0.12	3073	0.68	9725	0.32
September	396	0.90	3771	0.11	10715	0.70	36077	0.30
October	241	0.93	3394	0.07	677	0.87	5129	0.13
November	275	0.95	5392	0.05	184	0.94	3119	0.06
December	41	0.96	1079	0.04	15	0.96	385	0.04
Average	**908.8**	**0.9**	**7746.6**	**0.11**	**1285.5**	**0.8**	**4988.8**	**0.15**

With respect to the Figure 3.9 and Figure 3.10, the trends of number of detected FHS and its extrapolated values are different for Riau and Kalteng provinces. In the month of February in Riau province, the number of FHS detected is lass than January but for the extrapolated value the FHS increases relative to January. A similar condition is also occurs in the month of August. This issue leads us to carry out further investigation into the extrapolation method based on the fraction of cloud coverage.

3.2.1 Cloud cover and Land fraction

Cloud cover possibly obscures the satellite's sensor view of the Earth's surface in both land and water areas. The presence of cloud cover in a satellite scene impacts on the appearance of the fraction of land and water. To describe that

matter, Figure 3.11 shows an example of a scene containing water, land, cloud, and fire pixels. This figure clearly shows that cloud not only obscures the view of the land but also obscures the water.

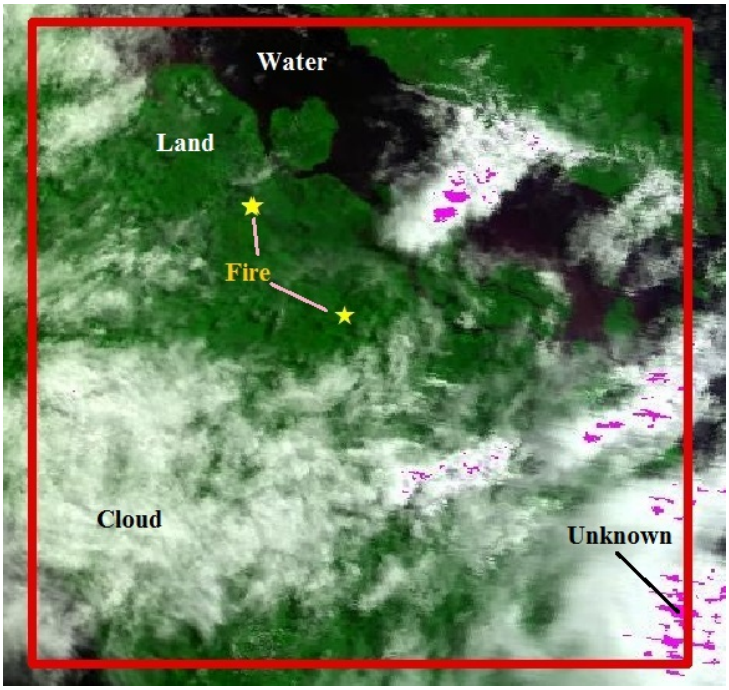

Figure 3.11. MODIS scene showing different fractions of land, water, cloud, fires, and unknown within a bordered area.

However, fire only occurs on the land, therefore the land fraction issue is more important than just the cloud fraction itself. There is a relationship between cloud cover and the fraction of land which is viewed from satellites. The presence of cloud cover in a satellite scene impacts on the appearance of the earth's surface, specifically the fraction of visible land. An increasing percentage of cloud cover will decrease the fraction of visible land and therefore decrease the chance of accurately detecting the number of FHS, as fires can only occur on land.

The cloud fraction and land fraction appearance on MODIS data can be extracted from the fire mask of the MOD14 product. It has been stated that the fire mask has 9 pixel classifications. Water, Cloud, and Land pixels are noted by numbers 3, 4 and 5 respectively (see Table 2.1). In this discussion, the total number of a scene's pixels within a rectangular border, which represent a province area, is termed the maximum pixels of the image. In the case where the whole province

area is covered in a scene, the maximum pixels of the scene are equal to the maximum number of pixels for the whole province.

As noted above, percentage of cloud cover, fraction of appearance of land and water, and the number of FHS detected can be counted from the MOD14 fire mask data. This research determined the number of pixels in each class automatically using the MATLAB script as given in Appendix 5. The input data, which is processed by the MATLAB program, is the gridded fire mask obtained from the MOD14 products. The fraction of cloud cover is defined as the number of cloud pixels divided by the maximum number of the scene's pixels. A similar calculation is applied to get the fraction of water pixels: the number of water pixels is divided by the maximum number of scene pixels.

In addition, the missing data, which are flagged as "0" in the fire mask files, represent the area within a border not covered by the scene. This issue occurs when the scene only covers part of the province area. This is illustrated in Figure 3.12, which shows the missing data in the black area on the top-right corner of the image. The missing data describes the fraction of reduction of each scene's coverage to the whole province area.

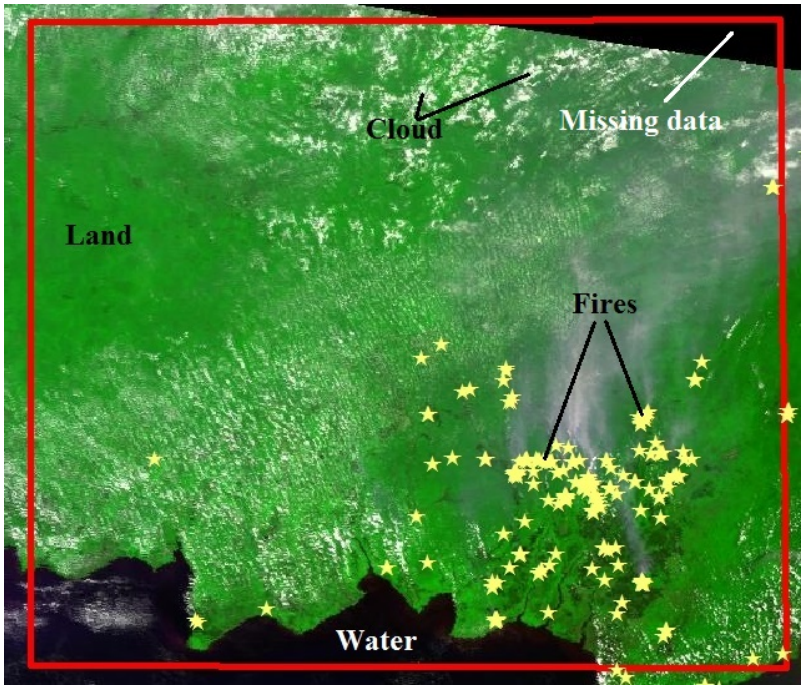

Figure 3.12. Image of MODIS scene for 20 September 2009 : 02.45 UTC. The scene does not cover all of the Kalteng province area. The figure shows the portions of land, water, cloud, and detected FHS.

If there are no images free from cloud cover, the assumption is made that the cloud has the same probability in covering land or water area. The proposed mathematical expression to calculate the number of cloud pixels over land is:

$$\text{Cloud}_{\text{over land}} = \frac{\textbf{(land+fire) pixels}}{\textbf{(land+fire) pixels+water pixels}} \text{ x cloud pixels} \quad (3.2)$$

Hence the maximum number of land pixels in a province is the sum of land pixels, fire pixels and cloud pixels over the land area. The number of land pixels for the whole province in the image area is calculated by:

$$\text{Land}_{\text{whole province}} = \text{land} + \text{fire} + \text{Cloud}_{\text{over land}} \quad (3.3)$$

The number of land pixels for the whole province is used as a basis for calculating the land fraction.

However, the number of pixels in the scene is affected by the position of the bordered area, whether the pixels are located in the middle of scene or in the edge of scene. Thus, the fractional calculation of each classification of pixels in the fire mask is performed in the gridded MOD14 file product to ensure consistency of the number of pixels within the border area investigated. This consistency cannot be achieved when we use the un-gridded MOD14 files because of the warping of the view effect.

3.2.2 Diurnal analysis of Cloud fraction

Diurnal fire activity will be described in this section; the data used are daily MODIS datasets over two Indonesian provinces, Kalteng and Riau, covering the months of September 2009 for Kalteng and July 2009 for Riau.

The Giovanni system does not provide daily cloud coverage, it only provides data on a monthly basis. Therefore, the diurnal analysis of the daily FHS uses the fire mask data from the MOD14 products flagged as cloud pixels. The MOD14 product was processed by the MOD14 algorithm with a modified threshold value (refer to IndoFire threshold, i.e. 316 K). The algorithm also produces a file product called “fire mask” which consists of 9 classes of pixels, as displayed in Table 2.1.

The data for this diurnal analysis are retrieved from the months of July 2009 for Riau province and September 2009 for Kalteng province. The reason is that these two months have the biggest peak fire seasons in the associated provinces, as

shown in Figure 3.9 and Figure 3.10. The diurnal analysis is performed in the UTC time point of view for the whole period. The number of pixels for each class in the fire mask file's product is counted within the given bordered area shown in Figure 3.11 for Riau province and Figure 3.12 for Kalteng province.

It has been discussed previously that the percentage of cloud cover affects the appearance of land and water in the Earth's surface imagery. The relationship between the relative proportions of cloud, land, and water diurnally is shown in Figure 3.13 for Riau province and Figure 3.14 for Kalteng province. In Riau province, the average fraction of visible land, water, and cloud is 41.63%, 26.73%, and 31.64% respectively during July 2009. Kalteng data for September 2009 shows the average of land, water, and cloud is 65.53%, 8.22%, and 26.25% respectively. These data describe a higher average of cloud cover over Riau compared to Kalteng. Furthermore, the area of visible water in Riau is larger than Kalteng and consequently the land area shows an inverse trend.

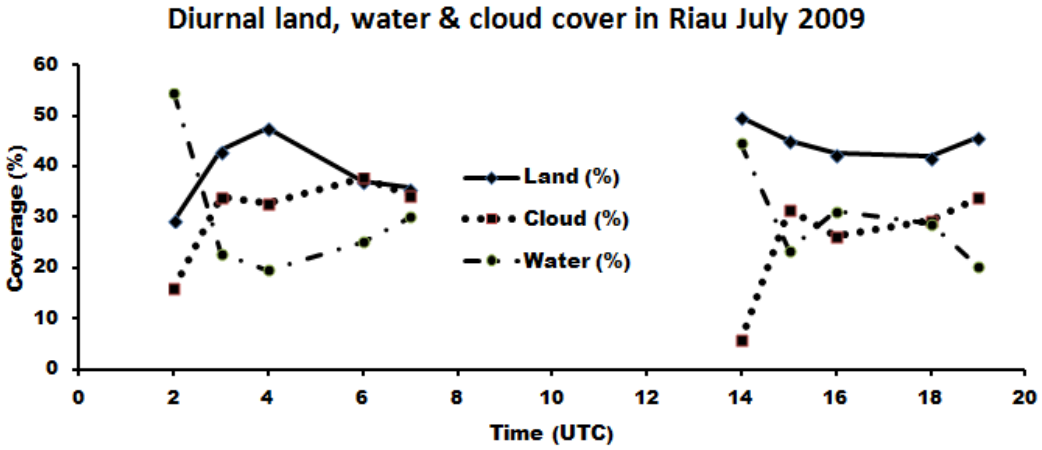

Figure 3.13. Diurnal pattern of percentage of visible land, water and cloud coverage over Riau province for July 2009

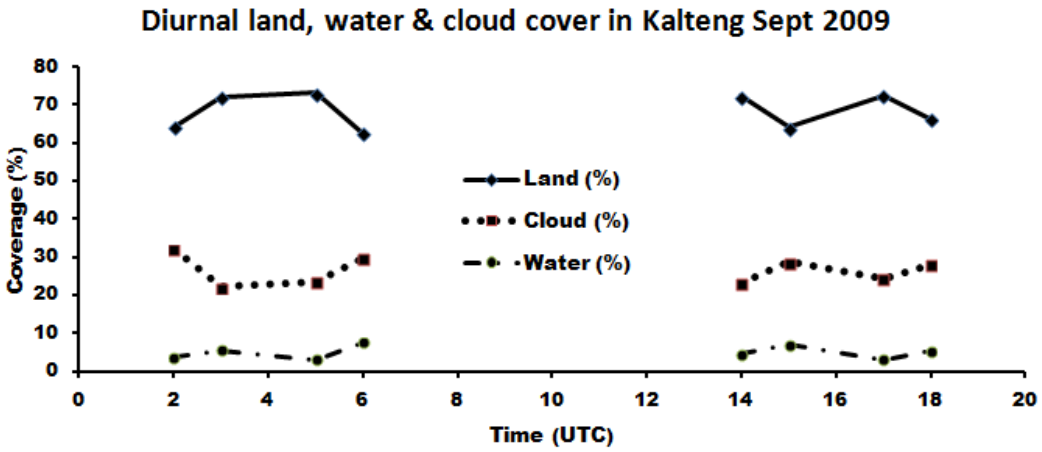

Figure 3.14. Diurnal pattern of percentage of visible land, water and cloud coverage over Kalteng province for September 2009

Based on the data described above, we conclude that Riau province has a larger portion of water area than Kalteng province. Riau's water area is almost a quarter, or 41840/185565 = 22.5%, of the province area. In comparison, the water area in Kalteng province is smaller: only 14809/306000 = 5% of the whole province area. The percentage of visible land area values in Riau vary around an average value of 41.8%, while in Kalteng the percentage land area is higher with an average visible land area of 68.5 %. Cloud cover in Kalteng affects the land area visibility more than the water area; therefore, the cloud cover is closely related to the number of FHS detected in Kalteng. In contrast, the cloud cover in Riau does not affect the land area visibility significantly; the fire activity pattern in Riau is less affected by the cloud cover pattern.

3.2.3 Daily analysis of FHS and Land fraction

Essentially the earth's surface consists of land and water, so the high fraction of water appearance in the scene will reduce the fraction of land. The total land area in the scene, in terms of a cloudy image, can be calculated by an extrapolation method similar to that used to estimate the number of FHS.

Since fire is only possible on land, the next extrapolation method for fires will consider the fraction of land observed in the scene. A fraction-based extrapolation calculation is considered a better way to describe the estimated number of FHS on

land. Let us say there are 10 FHS detected in the scene with 60% cloud cover. 80% of cloud cover is over the water area. This means the FHS extrapolation should be based on (20% x 60%) = 12% of cloud cover over land. Hence, an improved extrapolated number of FHS is 10/(100-12)% = 11.4 FHS. For the above illustration, extrapolating the number of FHS by considering only total cloud cover gives a result of 10/(100-60) = 25 FHS; there is an over extrapolated number by 15 FHS.

The land fraction calculation is performed by a different method to the calculations of cloud coverage and water fraction; the calculations only divide the pixel number of cloud or water by the maximum number of scene pixels. Land fraction is defined as the ratio of the number of land plus fire pixels to the maximum number of land pixels in the whole province area. The maximum number of land pixels in the whole province area is the number of land pixels, including fire pixels, observed when the cloud-free scene covers the whole province area.

Based on the resulting land fraction value, the extrapolated number of FHS in the province area is obtained by the formula:

$$\text{FHS}_{\text{extrapolation}} = \text{FHS} \times \frac{\mathbf{100}}{\mathbf{Land\ fraction}} \tag{3.4}$$

Where

$$\text{Land fraction} = \frac{\mathbf{(Land+Fire)\ pixels}}{\mathbf{Whole\ land\ pixels\ in\ a\ province}} \tag{3.5}$$

For example, we take one scene for each of Riau and Kalteng provinces to get the number of land pixels as a reference for further calculations of the extrapolated number of FHS. A scene of MODIS data passing over Riau province on 30 July 2009 at 18.30 UTC has 143,659 land pixels, 56 fire pixels, 41,837 water pixels, and 13 cloud pixels. Based on equation 3.3, we assume that the number of cloud pixels over land is:

$$\text{Cloud}_{\text{over land}} = \frac{\mathbf{(land+fire)\ pixels}}{\mathbf{(land+fire)\ pixels+water\ pixels}} \times \text{cloud pixels}$$

$$= \frac{\mathbf{(143659+56)}}{\mathbf{(143659+56)+41837}} \times 13 = 10 \text{ pixels} \tag{3.6}$$

So the number of land pixels for the whole Riau province in the image area is:

$$\text{Land}_{\text{whole province}} = \text{land} + \text{fire} + \text{Cloud}_{\text{over land}}$$
$$= 142659 + 56 + 10 = \mathbf{143{,}725} \text{ pixels} \quad (3.7)$$

The second example of calculating land pixels takes a scene over Kalteng province on September 27th, 2009 at 18.10 UTC with 287,893 land pixels, 419 fire pixels, 14,663 water pixels, and 3,025 cloud pixels. Using the approach described by Equation 3.7, the resulting number of cloud pixels over land in Kalteng is 2,879 pixels; the number of land pixels for the whole Kalteng province area in the image is therefore **291,191** pixels. The number of land pixels, which are 143,725 for Riau and 291,191 for Kalteng, are then used as reference numbers to calculate the fraction of the land in every scene using the expression given in Equation 3.6.

It has been mentioned that land fraction in every MODIS scene varies due to the 16 day cycle of MODIS. Therefore, the fire characteristics between scenes cannot be properly compared; instead we use the extrapolation method described. If there is 100% land fraction, meaning that the scene covers the whole province area and is free from cloud, then the extrapolated number of FHS is equal to the number of FHS detected. However, if the land fraction is less than 100%, the extrapolated number of FHS is calculated by the mathematical expression given in Equation 3.5.

For example, the captured scene over Riau province on 1 July 2009 at 06.40 UTC has 87,349 land pixels and 54 fire pixels. Based on Equation 3.6, and using the total number of land pixels as 143,725, the land fraction of the scene is:

$$\text{Land fraction} = \frac{(87349+54)}{143725} = 60.8\% \quad (3.8)$$

and so the extrapolation of FHS number is:

$$\text{FHS}_{\text{extrapolation}} = 54 \times \frac{100}{60.8} = 89 \text{ pixels} \quad (3.9)$$

This calculation of extrapolation of FHS number is applied to the whole available scene for both Riau province during July 2009 and Kalteng province during September 2009.

Those results affect the patterns of extrapolated estimates of FHS based on cloud coverage and land fraction in each province, as shown in Figure 3.15 and Figure 3.16. The Figures show that patterns of extrapolated numbers of FHS based on cloud coverage and land fraction are similar in Kalteng province but not in Riau

province. This result is used as a reference in the next discussion of the extrapolation method for detected number of FHS; performing extrapolation calculations is based on land fraction.

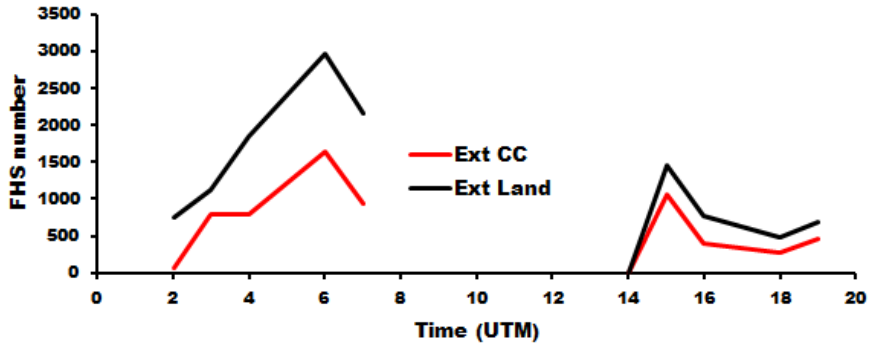

Figure 3.15. Diurnal pattern of Extrapolated estimate of FHS number based on cloud coverage and land fraction calculation over Riau province for July 2009

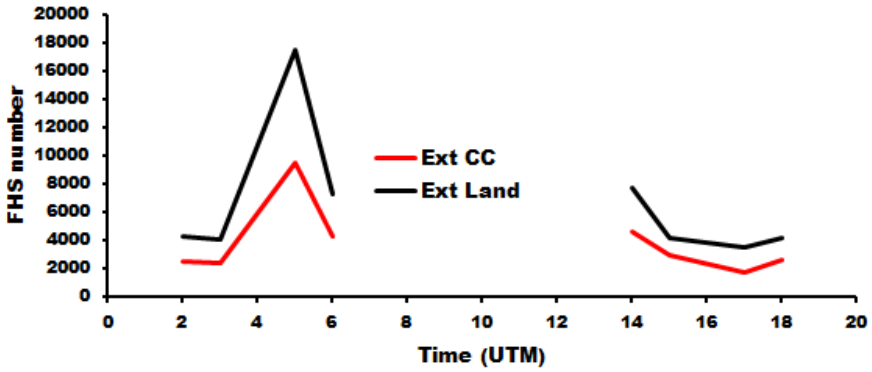

Figure 3.16. Diurnal pattern of Extrapolated estimate of FHS number based on cloud coverage and land fraction calculation over Kalteng province for September 2009

The diurnal characteristics of active fire have been reported by Giglio (2007) which showed that the peak fire time in Southeast Asia mostly occurred in the afternoon between 14.00 and 17.00 local time. In this research investigation, we apply MODIS data from the narrower area of Southeast Asia with a focus on Indonesia, specifically Riau province during July 2009 and Kalteng province during September 2009, to analyse the diurnal fire characteristics. Datasets have been obtained from LAADS web of NASA Goddard Space Flight Center for the months considered and have been processed using the MOD14 algorithm to produce a fire

mask showing FHS occurrence. Using the fire mask data, we can count the number of pixels classified as land, water, and cloud.

As described earlier, the number of fires occurring in a province cannot be determined solely by detected fire from every scene of remote sensing imagery because the scenes cover a different fraction of area within the province; hence the given value is a partial estimation number. When the scene covers the complete province area, the number of detected FHS is a good approximation of the number of FHS over the whole province.

The pattern of FHS numbers for Riau and Kalteng provinces are shown in Figure 3.17 and Figure 3.18. Uncertainty in estimation values for the number of actual FHS is represented by the error bars for each data point. Figure 3.17 shows the diurnal extrapolation of FHS pattern for Riau province with peak fire time occurring at 6:00 UTC (13:00 local time). The data points in Riau associated with 14:00 UTC consisted of 2 scenes which were devoid of fires. Because in these cases no fires were detected at 14:00 UTC, no standard deviation value can be calculated. Thus, the error bars for this data point are not drawn. In general the average number of FHS detected is 842 pixels, which sits within uncertainty ranges calculated for every data point. The peak number of FHS occurring at 6:00 UTC is 2,237 pixels or about 2.6 times bigger than the average number of FHS.

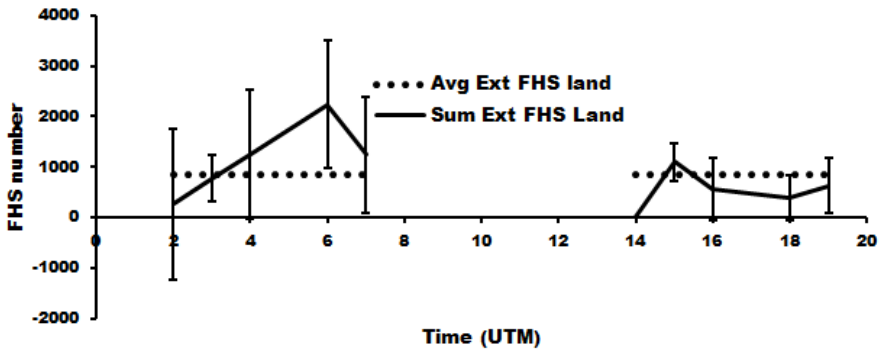

Figure 3.17. The pattern of diurnal extrapolation FHS for Riau province during July 2009 corrected by land fraction.

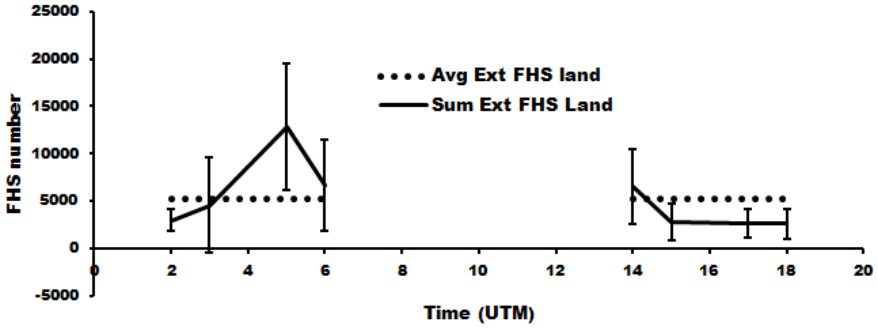

Figure 3.18. The pattern of diurnal extrapolation FHS for Kalteng province during September 2009 corrected by land fraction.

Further, the diurnal extrapolation of FHS pattern in Figure 3.17 for the Kalteng province shows that the peak fire time occurs at 5:00 UTC (13:00 local time). This time is similar to the peak fire local time in Riau province that is 14:00. The average number of FHS detected during September 2009 is 5,156 pixels and the detected number of FHS at 6:00 UTC is 12,822 pixels, or about 2.5 times bigger than the average number of FHS.

This finding refers to the effect of thermal radiation from the sun, which is related to solar zenith angle. The smallest solar zenith angle occurred at midday, about 12:00 local time. There is a lag of time for the thermal radiation from the sun to increase the surface temperature, which is known as the thermal response (NOAA, 2014). This could be a reason the fire peak occurs at 13:00, or 1 PM local time. This peak time of thermal solar radiation at the Earth's surface is in agreement with Lindsey's (2013) statement. The hottest time of day occurs at 13:00 local time, thus the fire susceptibility is also in the highest level at this time. These results are slightly different to the Giglio (2007) studies which reported that the peak fire time in Southeast Asia was at 14:00 local time.

Table 3.2. FHS number detected by the MOD14 algorithm and its extrapolation number with regard to the land fraction at Riau and Kalteng provinces

Riau July 2009	**Time (UTC)**											
Time (UTC)	**2**	**3**	**4**	**6**	**7**		**14**	**15**	**16**	**18**	**19**	**Avg**
Sum of FHS number	52	512	584	1044	614		0	722	289	193	316	
Sum of extrapolated FHS	260	769	1250	2237	1237		0	1100	553	387	622	
Land fraction (%)	6.9	45.2	31.6	35.1	28.4		7.2	49.9	37.6	40.4	45.9	32.8
FHS number/Extrapolated FHS (%)	20.0	66.5	46.7	46.7	49.6		0.0	65.6	52.2	49.9	50.8	44.8

Kalteng Sept 2009	**Time (UTC)**									
Time (UTC)	**2**	**3**	**5**	**6**		**14**	**15**	**17**	**18**	**Avg**
Sum of FHS number	1737	1798	7124	3056		3493	2013	1320	1828	
Sum of extrapolated FHS	2937	4521	12822	6619		6505	2723	2568	2550	
Land fraction (%)	41.1	44.4	40.6	42.0		45.6	48.3	37.9	44.2	43.0
FHS number/Extrapolated FHS (%)	59.1	39.8	55.6	46.2		53.7	73.9	51.4	71.7	56.4

Details of the statistical data for diurnal FHS number in both Kalteng and Riau provinces is displayed in Table 3.2. Comparison of the diurnal pattern of the number of FHS detected by the MOD14 algorithm, and the extrapolated FHS numbers, are shown in Figure 3.19 for Riau province and Figure 3.20 for Kalteng province. Those figures show that the pattern of both observed FHS numbers and their extrapolated numbers are similar. The curve's representing the extrapolated number of FHS follow the pattern of the observed FHS.

On average the original number of FHS detected by the MOD14 algorithm in Riau province is 44.8% of the extrapolated number of FHS, while in Kalteng province the original number of FHS from MOD14 is 56.4% of the extrapolated number of FHS. This difference is caused by the lower land fraction in Riau province (32.8%) compared to Kalteng province (43%).

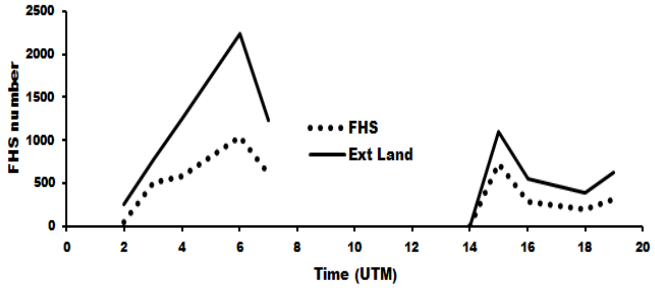

Figure 3.19. Diurnal patterns of FHS number detected by MOD14 compared to the extrapolated number of FHS based on the land fraction over Riau province for July 2009

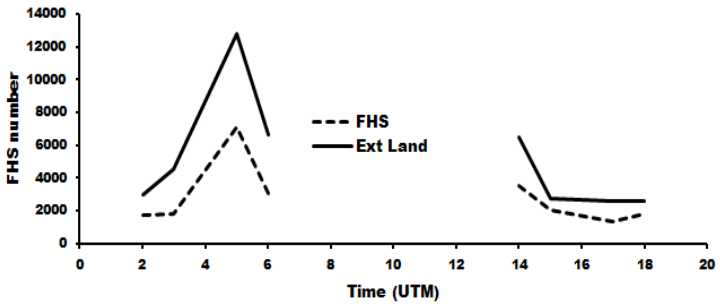

Figure 3.20. Diurnal patterns of FHS number detected by MOD14 compared to the extrapolated number of FHS based on the land fraction over Kalteng province for September 2009

3.2.4 Summary

In conclusion, the diurnal FHS pattern analysis was conducted by considering land fractions. With regard to the daily MODIS data in July and September 2009, the land fraction in Riau is 32.8%. This number is lower compared to the land fraction of 43% in Kalteng province. Consequently, the extrapolated FHS number based on land fraction in Riau is also lower (44.8%) compared to extrapolated FHS numbers in Kalteng (56.4%). Diurnal FHS patterns in both Riau and Kalteng province show the same time of occurring peak fire time, which is 13:00 local time. This peak fire time is related to the peak time of solar thermal radiation.. This result is slightly different than that of Giglio's (2007) research, which found the diurnal peak fire time for Southeast Asia to be between 14:00 and 16:00 local time.

3.3 Fire Activity and Vegetation Cover Types

Vegetation cover type is another parameter affecting fire characteristics detected from satellite remote sensing. This work links to the research previously introduced in Section 2.4.3 about vegetation cover affecting fire activity. It has been described that land surfaces covered by different vegetation have different characteristics; low vegetation dries faster and is longer lasting in the dry season (Giglio, 2007), while high vegetation may reduce fire risk due to its cooling and humid influence on the environment as a result of the leaf evapotranspiration (Kaufman et. al., 1990). The differences in vegetation cover characteristics have been investigated in respect to their relationship to fire activity patterns.

In this research we want to determine the percentage of low and high vegetation cover in Kalteng and Riau provinces. It has been indicated in Section 2.4.3 that low vegetation cover has a greater potential as a fuel for biomass burning. In theory, a greater percentage of low vegetation cover leads to increased risk of fire occurring. The relationship between fire density and the percentage area of low and high vegetation will be investigated and discussed in this section. The investigation was conducted in various vegetation cover classifications, which were created by the officer of the Forestry Ministry of Indonesia for Kalteng and Riau provinces. There are 22 classes of land classifications that include 7 classes of non-

vegetated areas and 15 classes of vegetated areas. The details of the land classification data and their areas are given in Table 3.3.

Table 3.3. Land classifications and their proportions for Kalteng and Riau on 2009

No	Land Classifications	Kalteng Area		Riau Area	
		Ha	Fraction (%)	Ha	Fraction (%)
Low vegetation categories		**5460011**	**24.61**	**3153877**	**31.98**
1	Swamp bush	2395639	10.80	847532	8.59
2	Shrublands	1700622	7.67	783877	7.95
3	Dry land farming with mixed shrublands	816934	3.68	875260	8.87
4	Dry land farming	153538	0.69	398548	4.04
5	Rice field	347944	1.57	239541	2.43
6	Transmigration	45332	0.20	8544	0.09
7	Savanna / Grassland	2	0.00	574	0.01
High vegetation categories		**15774765**	**71.13**	**5954437**	**60.36**
8	Plantation	1097986	4.95	2655763	26.92
9	Secondary swamp forest	3476642	15.68	1222005	12.39
10	Secondary dry land forest	5116494	23.07	914573	9.27
11	Secondary mangrove forest	21846	0.10	167108	1.69
12	Harvesting forest	118773	0.54	414442	4.20
13	Primary dry land forest	5902416	26.61	230414	2.34
14	Primary swamp forest	37623	0.17	344619	3.49
15	Primary mangrove forest	2984	0.01	5514	0.06
Non-vegetated areas		**944507**	**4.26**	**756519**	**7.68**
16	Clear land	253127	1.14	456360	4.63
17	Water body	144302	0.65	123077	1.25
18	Fishpond	3436	0.02	3639	0.04
19	Swamp	418451	1.89	27510	0.28
20	Settlement	69408	0.31	111199	1.13
21	Mining	55681	0.25	33869	0.34
22	Airport/Harbour	103	0.00	865	0.01
Total		**22179283**	**100.00**	**9864832**	**100.00**

This research is focused on biomass burning activities, so the non-vegetated areas with almost no potential to be burned will not be taken into account in further discussions. We are only concerned with the 15 classes of vegetated areas. Referring to the vegetated land cover definitions given in the previous chapter (Table 2.5), the 15 classes of vegetated areas are then divided into low vegetation and high vegetation (trees) categories. The first category, low vegetation cover, includes the classes of swamp bush, shrublands, dry land farming with mixed shrublands, dry land farming, rice field, transmigration, and savanna/grasslands. The vegetation cover types classified as high vegetation include plantations, secondary swamp forest, secondary dry land forest, secondary mangrove forest, harvesting forests, primary dry land forests, primary swamp forests, and primary mangrove forests. Three vegetation types in the high vegetation categories are considered as primary forests namely primary dry land forest, primary swamp forest, and primary mangrove forest. Primary forests have not experienced logging activity and are in their naturally grown condition.

Data in Table 3.3 show that both Kalteng and Riau province areas were mostly (more than 90%) covered by vegetation in both low and high vegetation categories. The proportion of low vegetation in Kalteng was only about 1/4 of the land area, while vegetation cover classified as high vegetation occupied the majority of the land area (71%). Additionally in Riau province, the low vegetation portion was higher, almost 32%, and the percentage of high vegetation area was about 60%. This finding indicated that the fraction of low vegetation categories in Riau was larger than in Kalteng province. Among all low vegetation categories, swamp bush represented the biggest percentage (10.80%) of low vegetation in Kalteng province. However, the data for Riau province showed that swamp bush represents 8.59% (ranked second after dry land farming and shrublands area with 8.87%) of low vegetation category areas.

Furthermore, in the high vegetation cover category, the fraction of primary dry land forest was the largest area (26.62%) in Kalteng province; in Riau province the area of primary dry land forest was only 2.34% (the 7th rank). The largest area in Riau province in the high vegetation category was classified as plantation (which is defined as being unchanged plantation for at least 2 years). Plantation covered

more than a quarter (26.92%) of the total Riau province area. In contrast, plantations in Kalteng covered less than 5% of the province area.

The other vegetation classes covering areas of more than 10% in Kalteng were secondary dry land forest, secondary swamp forest, and swamp bush, and the remaining 10 vegetated land classes occupy less than 10% area for each class within the Kalteng province area. Similarly, Riau province also showed an un-balanced proportion of vegetation cover type areas, with only 5 of 15 vegetated land classes covering more than 5% fractional area for each class including plantations, which had the biggest portion.

The fire activity in specific vegetation classes is analysed further in the following discussion. The analysis will be focused only on 2009 data because the available vegetation cover data is only for 2009. The occurring fires were counted in every vegetation cover type of 15 classes of vegetated area. To describe the ratio of occurring FHS and the vegetation cover area, we have calculated the FHS density as a representation of area per FHS. With respect to the data of Table 3.5, the data of occurring fire as well as the density of fire for every vegetation cover type are presented in Table 3.4. From those two tables (Table 3.3 and Table 3.4) we conclude that Kalteng province has an area of about a quarter (24.61%) under low vegetation cover with an average fire density of 588 ha per FHS. In this low vegetation cover area, swamp areas in Kalteng on average show 1 fire in every 343 hectares and it is considered as the area most impacted by fire during 2009. The remaining 71.13% of the area in Kalteng has high vegetation cover with lower average fire density (4,162 ha for every fire). The plantation cover type areas are considered to be the most fire prone areas in the high vegetation category, with 938 ha per FHS.

Fire activity in Riau province showed similar patterns, but it had different proportions of high and low vegetation. The area under low vegetation cover was larger (31.98%) than the same low vegetation category in Kalteng. The bigger portion of low vegetation cover area in Riau leads to the greater fire density as shown in Table 3.4. Fire density under low vegetation area in Riau was 529 ha per FHS.

Looking at a specific area of low vegetation cover, fire density in swamp bush areas of Riau showed the highest rate of fire occurrence, with 1 fire in every 262 hectares on average. The data in Table 3.4 also shows that swamp bush areas in Kalteng have the highest density of occurring fire. This data indicates that swamp bush was the area that suffered the most fires in both Kalteng and Riau province. Swamp bush areas in Riau had a risk of fire 1.3 times higher compared to the same types of areas in Kalteng. In summary, Riau province was much more fire prone than Kalteng. This result confirms the Giglio (2007) report because Riau has a greater area of low vegetation cover types which dry easily and increases fire susceptibility.

Table 3.4. Land classifications and the related number of FHS for Kalteng and Riau for 2009. Density numbers represent the area (in hectares) per detected fire.

No	Land Classifications	Kalteng Area		Riau Area	
		FHS	Density	FHS	Density
Low vegetation categories		**9285**	**588**	**5958**	**529**
1	Swamp bush	7020	341	3233	262
2	Shrublands	1001	1699	1513	518
3	Dry land farming with mixed shrublands	666	522	39	6142
4	Dry land farming	477	1713	1061	825
5	Rice field	81	1896	107	3725
6	Transmigration	40	1133	4	2136
7	Savanna / Grassland	0	-	1	574
High vegetation categories		**3790**	**4162**	**2552**	**2333**
8	Plantation	2095	1659	850	1438
9	Secondary swamp forest	1170	938	959	2769
10	Secondary dry land forest	482	10615	318	2876
11	Secondary mangrove forest	32	3712	384	1079
12	Harvesting forest	4	5462	3	55703
13	Primary dry land forest	6	6271	23	14983
14	Primary swamp forest	1	5902416	14	16458
15	Primary mangrove forest	0	-	1	5514
Total		**13075**	**1624**	**8510**	**1070**

Tansey et. al., 2008 state that fire must cover at least 15 hectares (ha) of a MODIS pixel to be detected. In contrast, rescribed burning areas (based on the information of local forestry officer) are typically less than 15 ha. We therefore conclude that the detected FHS likely represent the larger wild fires.

3.3.1 Wet and Dry season's fires over vegetation cover classification

The analysis of fire activity in different vegetation cover types has also been carried out for dry and wet season data. The dry season FHS data were taken from the months of June to November 2009, while wet season FHS data were chosen from the months of December to May 2009. Detected fire data for both dry and wet seasons over different vegetation classes are presented in Table 3.5 for Kalteng province and Table 3.6 for Riau province.

Data of fire activity in Kalteng province show that 12947/13075 or 99% of fires occurred in the dry season during 2009 and only 1% of fires occured in the wet season. Meanwhile, 5873/8510 or about 69% of fires in Riau occurred in the dry season of 2009 and there was a relatively high number of fires (2637 or 31%) in the wet season. The higher number of fires occurring in the wet season in Riau province is possibly due to a lower fraction of high vegetation type compared to Kalteng province. Kaufman, Tucker, and Fung (1990) reported that high vegetation has a significant cooling and humidifying impact on the atmosphere. This cool and humid effect will decrease fire susceptibility. This finding confirms the Giglio (2007) statement that low vegetation cover dries fast and Riau province tends to be burned in both dry and wet seasons.

A different type of fire pattern is shown in the Kalteng data. The data show that the dry season is the time of most dangerous fire hazard and the wet season is relatively safe from burning. The recorded number of FHS indicates that almost all fires in 2009 arise in the dry season, while fire in the wet season only represents 1% of all fires during the year of 2009.

Table 3.5. Density analysis of wet and dry season FHS numbers for different land classes in **Kalteng** province of Indonesia for 2009. Density = area (ha) per FHS.

No	Land Classifications	Dry season		Wet season	
		FHS	Density	FHS	Density
Low vegetation categories		**9216**	**592**	**69**	**79131**
1	Swamp bush	6983	343	37	64747
2	Shrublands	990	1718	11	154602
3	Dry land farming with mixed shrublands	660	527	6	57991
4	Dry land farming	466	1753	11	74267
5	Rice field	78	1968	3	51179
6	Transmigration	39	1162	1	45332
7	Savanna / Grassland	0	-	0	-
High vegetation categories		**3731**	**4228**	**59**	**267369**
8	Plantation	2082	1670	13	267434
9	Secondary swamp forest	1129	973	41	26780
10	Secondary dry land forest	479	10682	3	1705498
11	Secondary mangrove forest	30	3959	2	59386
12	Harvesting forest	4	5462	0	-
13	Primary dry land forest	6	6271	0	-
14	Primary swamp forest	1	5902416	0	-
15	Primary mangrove forest	0	-	0	-
Total		**12947**	**4820**	**128**	**165897**

Table 3.6. Density analysis of wet and dry season FHS numbers for different land classes in **Riau** province of Indonesia for 2009. Density = area (ha) per FHS.

No	Land Classifications	Dry season		Wet season	
		FHS	Density	FHS	Density
Low vegetation categories		**4021**	**784**	**1937**	**1628**
1	Swamp bush	2309	367	924	917
2	Shrublands	893	878	620	1264
3	Dry land farming with mixed shrublands	12	19962	27	8872
4	Dry land farming	722	1212	339	2582
5	Rice field	80	4982	27	14761
6	Transmigration	4	2136	0	-
7	Savanna / Grassland	1	574	0	-

No	Land Classifications	Dry season		Wet season	
		FHS	Density	FHS	Density
High vegetation categories		**1852**	**3215**	**700**	**8506**
8	Plantation	617	1981	233	5245
9	Secondary swamp forest	686	3871	273	9728
10	Secondary dry land forest	224	4083	94	9730
11	Secondary mangrove forest	307	1350	77	5382
12	Harvesting forest	2	83554	1	167108
13	Primary dry land forest	9	38291	14	24616
14	Primary swamp forest	7	32916	7	32916
15	Primary mangrove forest	0	-	1	5514
Total		**5873**	**3999**	**2637**	**3454**

3.3.2 Vegetation cover related to the diurnal fire patterns

There is a relationship between diurnal fire characteristics and vegetation cover, as it has been reported by Giglio (2007). He wrote that fires in the tropical region mostly occurred during the day in the herbaceous (low vegetation cover) regions. The peak number of fires in the low vegetation cover increased in early to late afternoon. Meanwhile, the high vegetation cover tended to restrict fire ignition and therefore the occurring fires were mostly surface fires and short-lived.

In this research, the investigation of diurnal fire activity related to the existing vegetation cover has been performed during 2009. The data are taken from the months of peak fires in 2009; July in Riau and September in Kalteng province. The fire data are associated with the vegetation cover types of occurring fires. The diurnal fire distribution associated with vegetation cover types in July 2009 is shown in Figure 3.21 and Figure 3.22 for Riau province; diurnal fire distributions for Kalteng province in September 2009 are shown in Figure 3.23 and Figure 3.. Graphs are grouped into low vegetation cover and high vegetation types as described earlier with regard to the works by Giglio (2007).

Low vegetation cover category in Riau

i

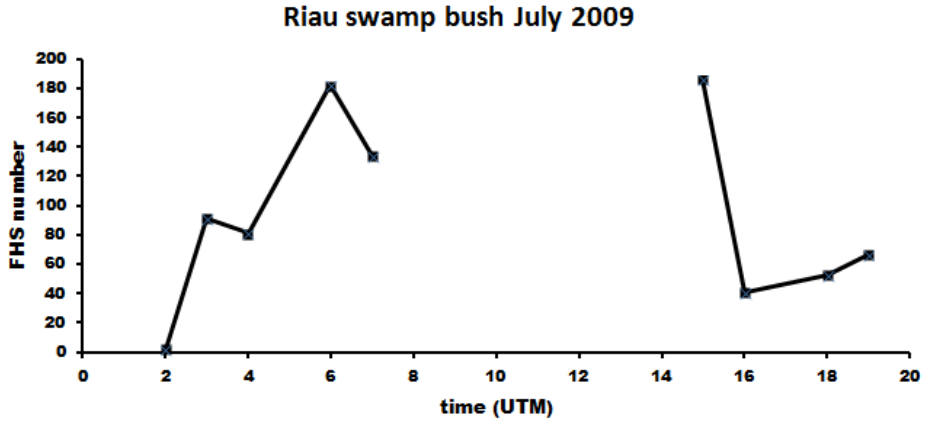

ii

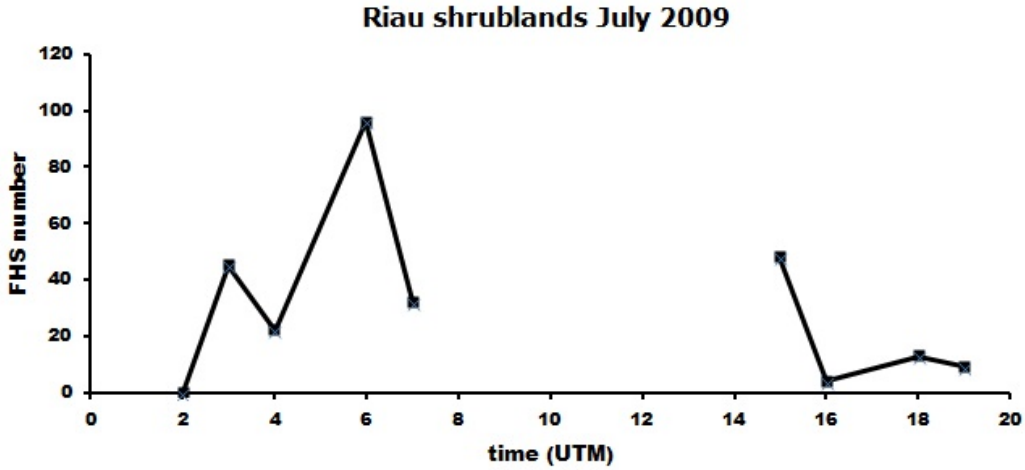

iii

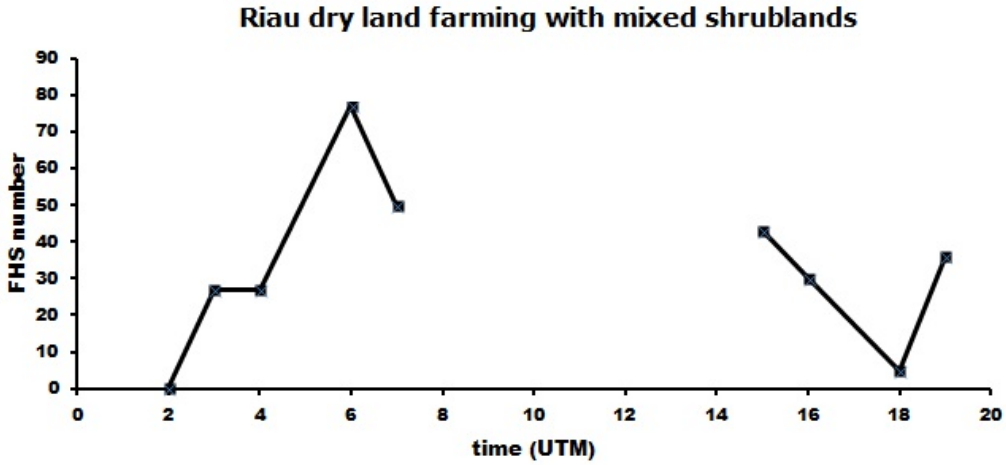

Figure 3.21. Diurnal fire occurrence over various vegetation cover types for the low vegetation category for Riau province for July 2009; the local time equals UTC+7

iv

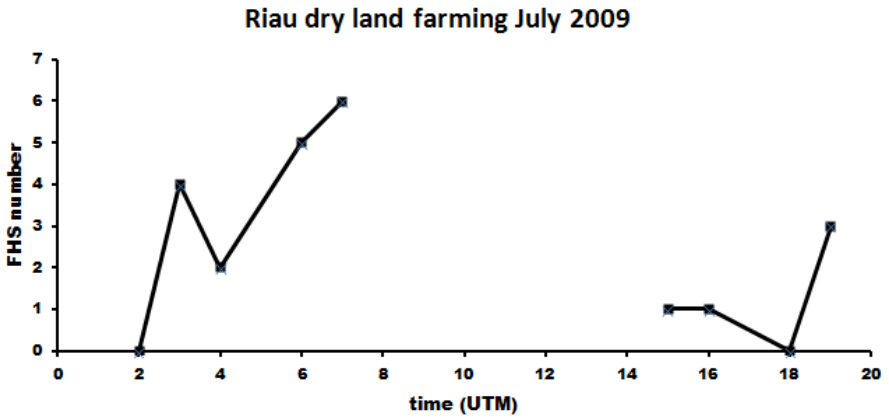

v

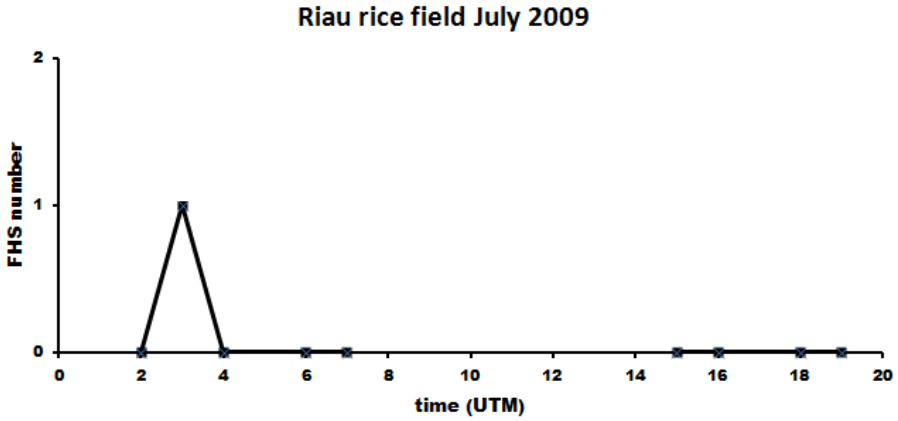

vi

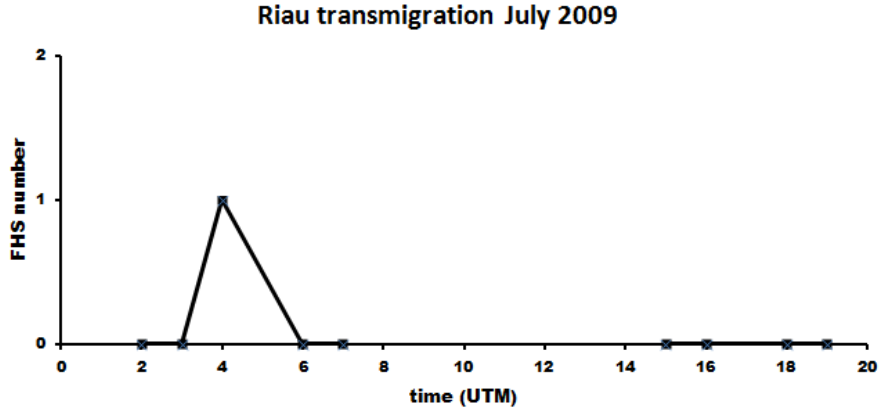

Figure 3.21. Diurnal fire occurrence over various vegetation cover types for low vegetation category for Riau province for July 2009; the local time equals UTC+7

High vegetation (trees) cover category in Riau

vii

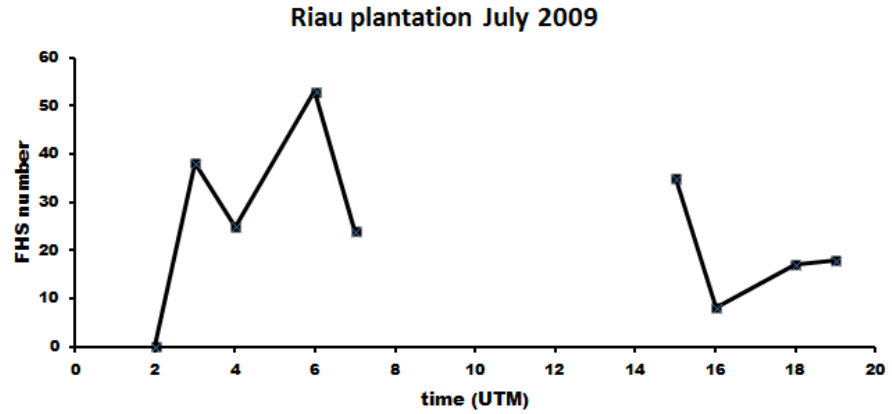

viii

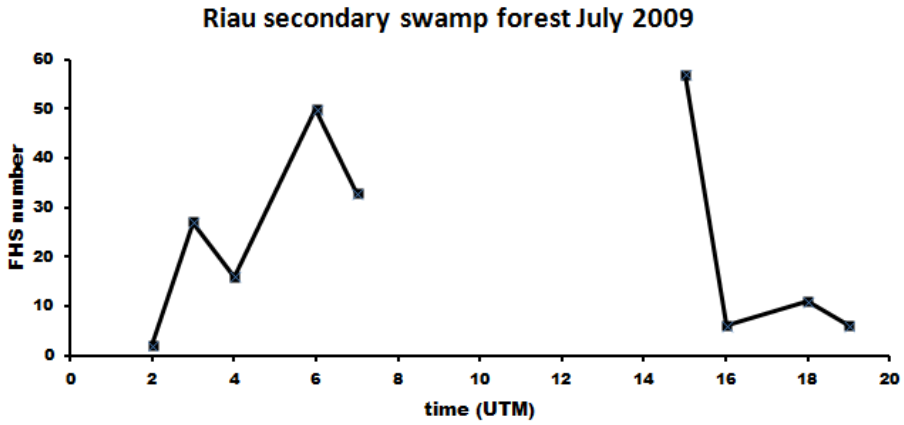

ix

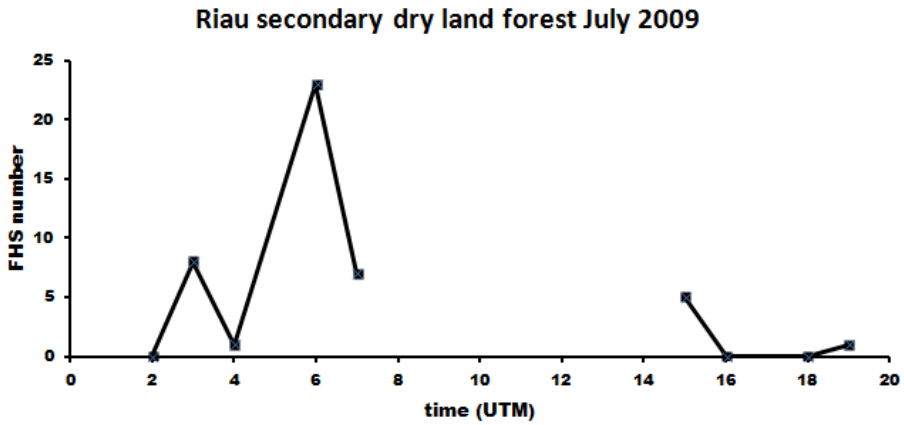

Figure 3.22. Diurnal fire occurrence over various vegetation cover types for high vegetation (trees) category for Riau province for July 2009; the local time equals UTC+7

x

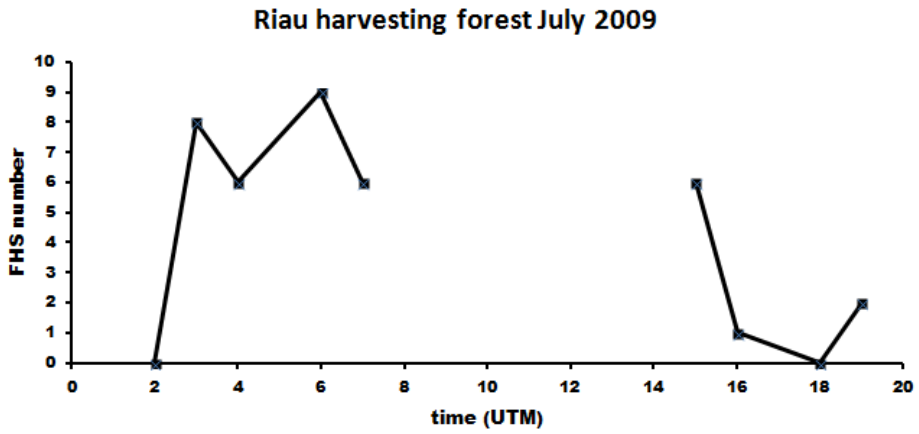

xi

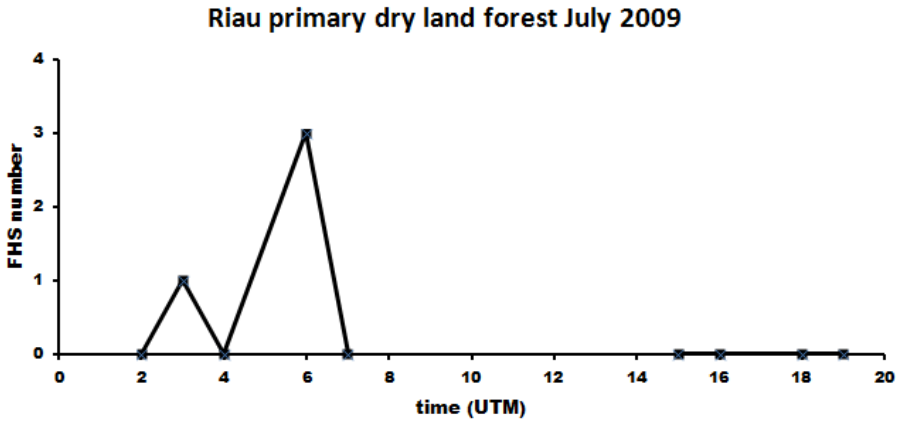

xii

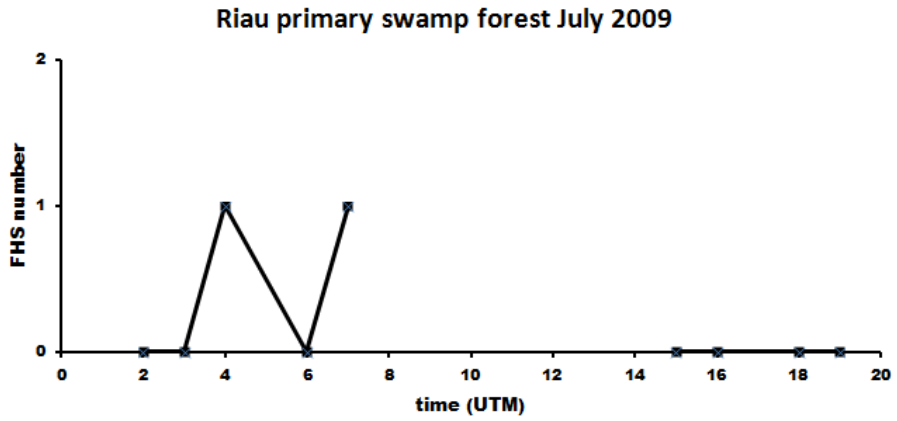

Figure 3.22. Diurnal fire occurrence over various vegetation cover types for high vegetation (trees) category for Riau province for July 2009; the local time equals UTC+7

Low vegetation cover category in Kalteng

i

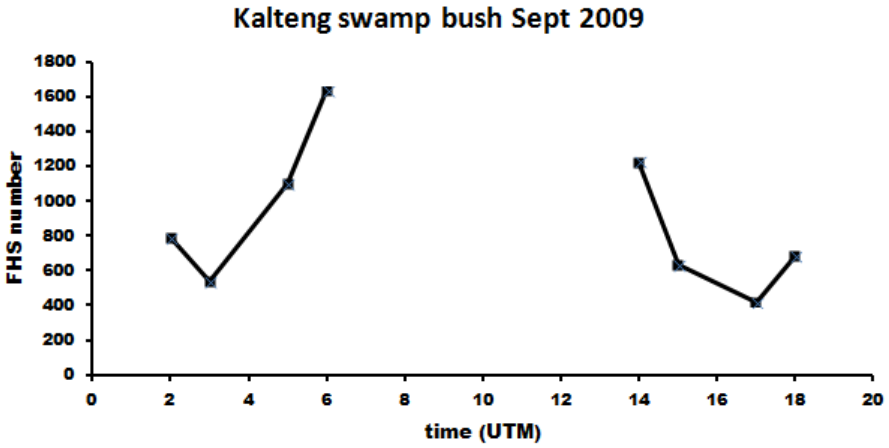

ii

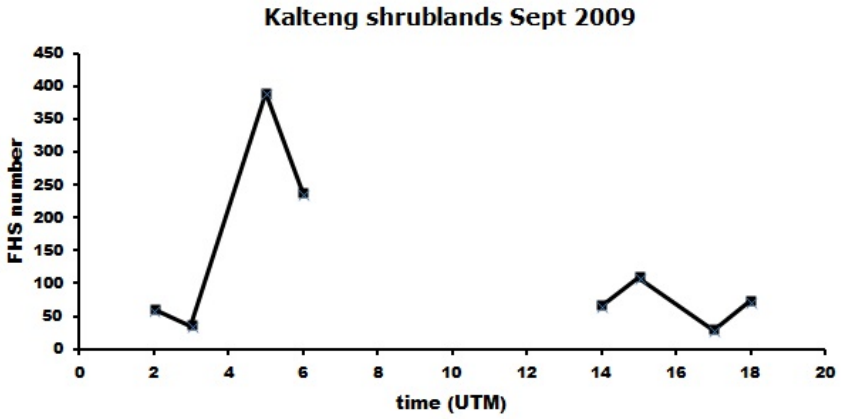

iii

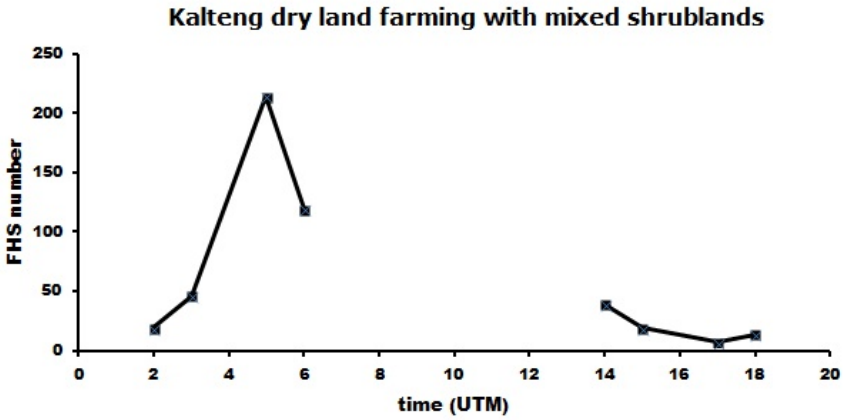

Figure 3.23. Diurnal fire occurrence over various vegetation cover types for the low vegetation category for Kalteng province for September 2009; the local time equals UTC+8

iv

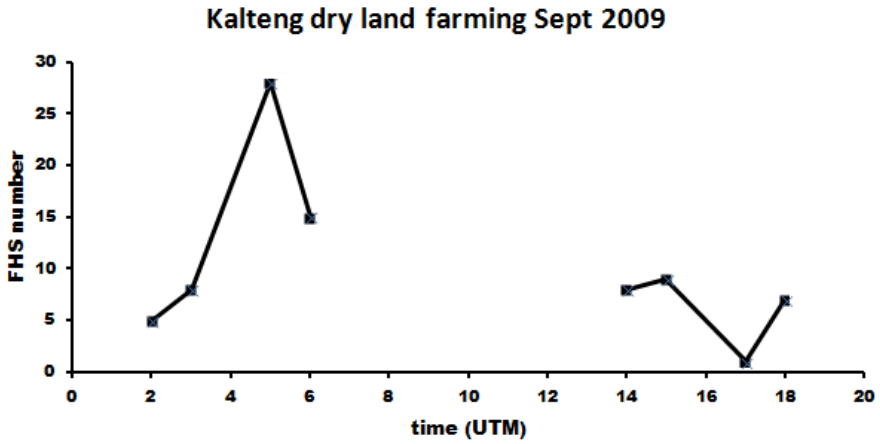

v

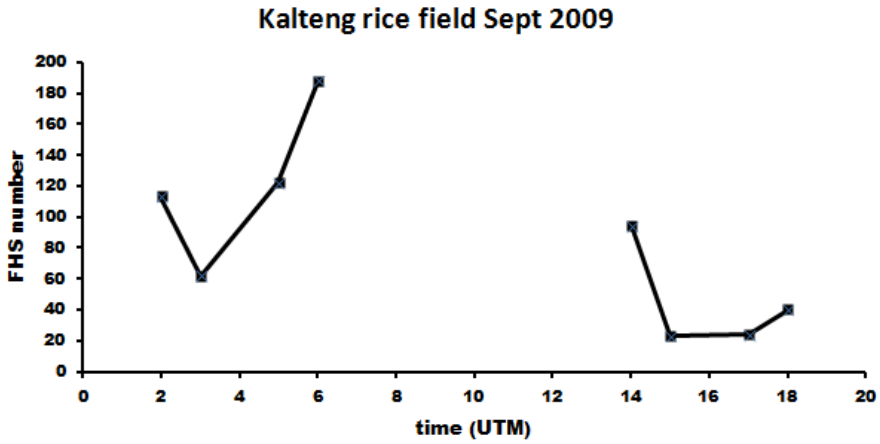

vi

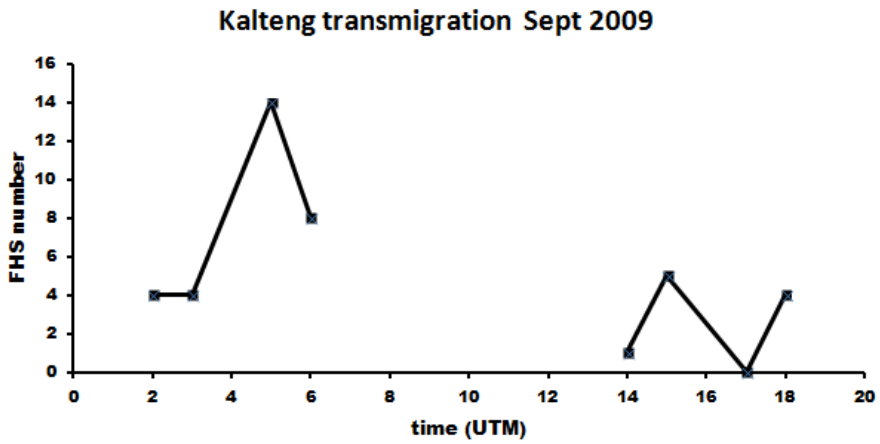

Figure 3.23. Diurnal fire occurrence over various vegetation cover types for the low vegetation category for Kalteng province for September 2009; the local time equals UTC+8

High vegetation (trees) cover category in Kalteng

vii

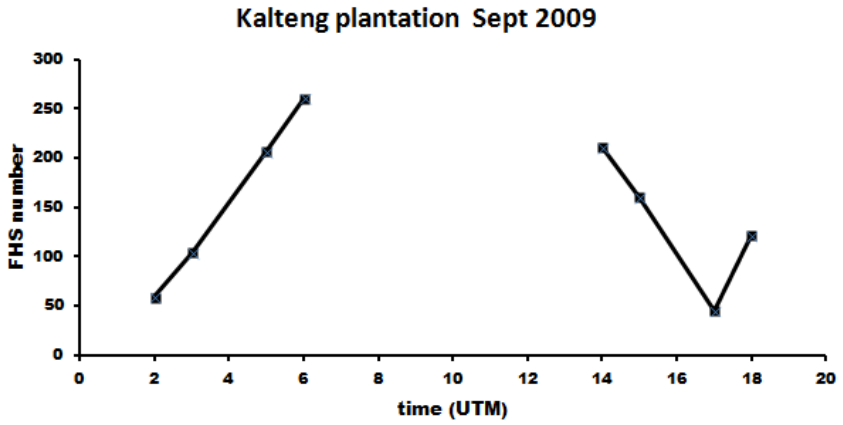

viii

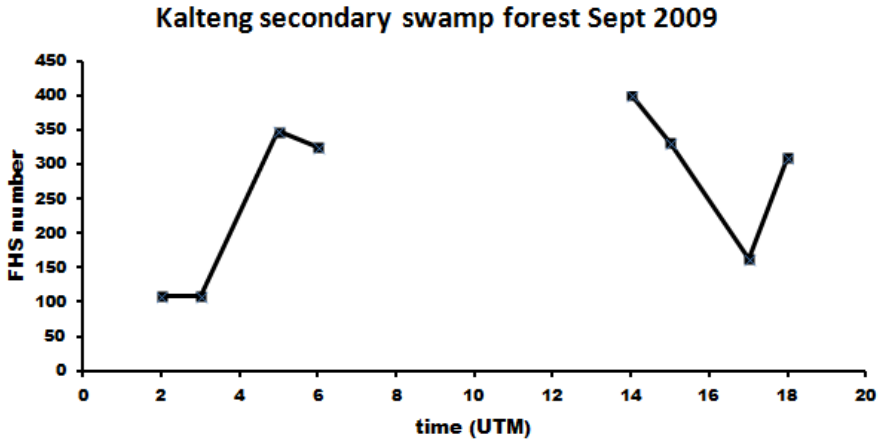

ix

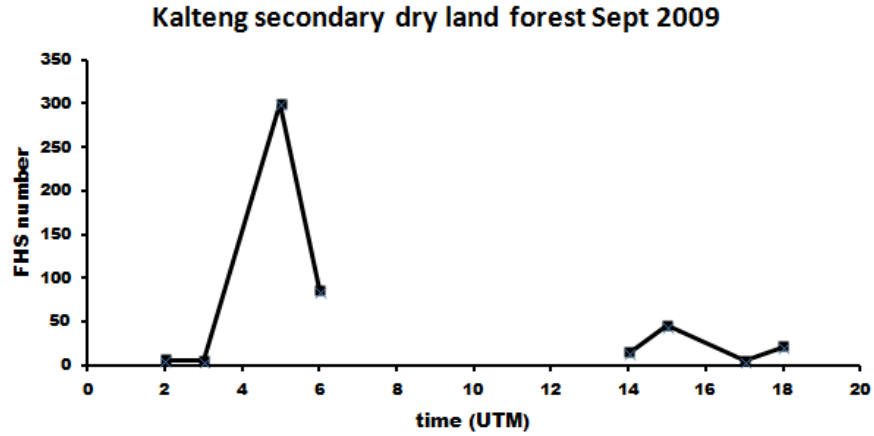

Figure 3. 24. Diurnal fire occurrence over various vegetation cover types for the high vegetation (trees) category for Kalteng province for September 2009; the local time equals UTC+8

x

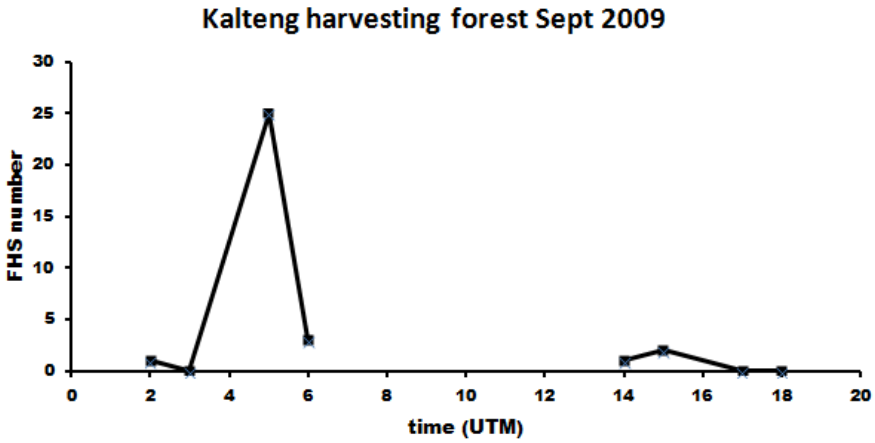

xi

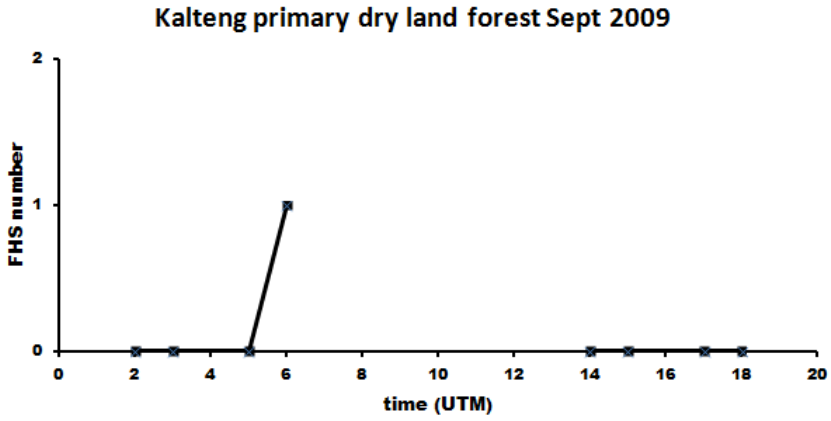

xii

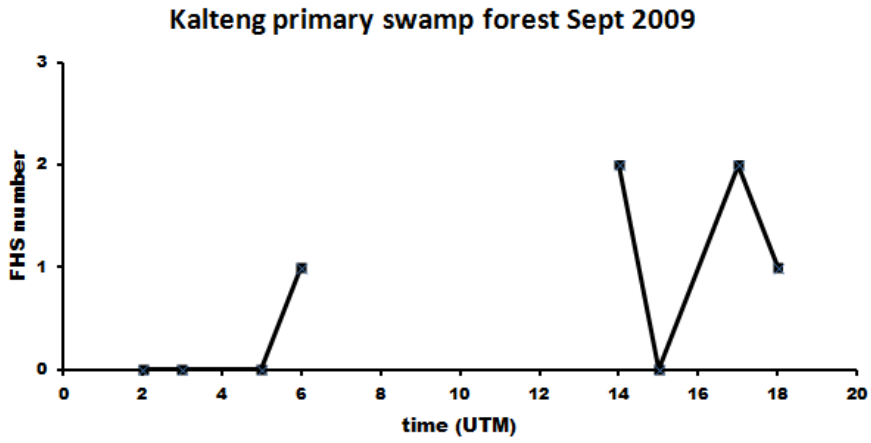

Figure 3.24. Diurnal fire occurrence over various vegetation cover types for the high vegetation (trees) category for Kalteng province for September 2009; the local time equals UTC+8

The available MODIS data are morning and afternoon. The morning data for Riau are between 3 and 7 UTC and the afternoon data are between 15 and 19 UTC. Morning data for Kalteng are between 2 and 6 UTC and the afternoon data are

between 14 and 18 UTC. All of these times are associated with the local time of 10 AM to 2 PM for the morning and 10 PM to 2 AM for the afternoon. There are no MODIS data between 2 PM and 10 PM local time because the satellites do not overpass the area.

Based on the fire data in Riau province as shown in Figure 3.21 for the low vegetation category and Figure 3.22 for the high vegetation category, the maximum number of fires in all types of vegetation cover occurred at about 06:00 UTC(13:00 local time). The greatest number of fires occurred in low vegetation cover, particularly in the shrublands classification. The exceptions occurred with a small number of fires such as in rice fields and transmigration areas. This single fire may have been a controlled fire because it was only a single fire (Crutzen and Andreae, (1990),.

Similar fire patterns over various vegetation types in Kalteng are shown in Figure 3.23 for the low vegetation category and Figure 3. for the high vegetation category. Most fires occurred at 13:00 local time (5 AM UTC). In some vegetation areas such as swamp bush, rice field, and plantation, fires persisted until 14:00 local time. These results confirm that in the day time (early and late afternoon) low vegetation cover is dry and easy to burn (Giglio, 2007).

3.4 Precipitation, SOI, and Fire Activity

In this section we discuss seasonal meteorological effects with respect to FHS occurrence in Riau and Kalteng provinces. Parameters which have an effect on the temporal distribution of FHS include climate variables such as precipitation and SOI (Giglio et. al., 2006; Dayamba et al., 2010; Savadogo, 2012). Dayamba et al. (2010) reported a strong correlation between the fire season, defined as high numbers of fire occurrences, and the dry season. Dayamba et al. (2010) researched the relationship between fire occurrence characteristics and the seasonal parameter's patterns. They reported that the trends of occurring fires have a parallel relationship to the dry season periods. The dry season was divided into three ranges of time i.e. early, mid, and late dry season. The fire patterns followed the dry season division. The early fire season occurs in the early dry season, mid fire season was associated with the mid dry season, and the late fire season was also

related to the late dry season. This section discusses the impacts of wet and dry seasons on the number of FHS detected, focusing on the Riau and Kalteng provinces of Indonesia; these are the two biggest provinces in Indonesia prone to being burned.

The focus of this work is assessing the time lag and correlation between time of rainfall and fire occurrence. Data for the decade 2001-2010 (time series datasets of FHS, SOI, and precipitation) have been obtained to analyse the relationships between FHS and climate variability. FHS data have been acquired from the IndoFire system, SOI data have been sourced from the Australian Government's Bureau of Meteorology website[8], and monthly precipitation data have been accessed from the TOVAS (TRMM Online Visualization and Analysis System) website[9]. The spatial extent for the study encompasses the focused provinces, which are the most prone to fires, based on the numbers of FHS detected as given in Appendix 3 (see the province's location at Figure 3.2).

Time series data analysis aims to recognise patterns in sequential data over time. Examining the relationships between multiple related parameters is another application of time series data analysis. In this manner, we want to examine the relationship of three parameters of the monthly time series research data (the number of FHS, SOI, and precipitation level) for the decade 2001-2010. Pallant (2011) reported that time-series data analyses are best extracted from datasets with 50 or more data points; this time-series data analysis is considered fit to analyse the relationship of FHS, SOI, and precipitation level parameters because this research has 120 time-series data points for each stated parameter. The relationships in the data are determined using a cross correlation analysis method. The assessment is performed on the monthly time-series data with no time lag, lag+1 month, lag+2 months, lag+3 months, and lag+4 months. This assessment aims to find the correlation of FHS and SOI and the correlation of FHS and precipitation level. The assessment results are presented in Table 3.7 and Table 3.8, which represent the assessment results for Riau and Kalteng respectively.

[8] http://www.bom.gov.au/climate/current/soihtm1.shtml#top
[9] http://gdata1.sci.gsfc.nasa.gov/daac-bin/G3/gui.cgi?instance_id=TRMM_Monthly

The results of the assessment given in Table 3.7 show that correlation coefficients of FHS with both precipitation level and SOI in Riau province have peak values in the lag+2 month. The peak value of -0.34 is associated with fire and precipitation correlation, and the peak value of -0.28 is associated with fire and SOI correlation. This indicates that the precipitation and SOI level corresponds to the next two months of fire activity. For example, SOI and precipitation during January 2009 will have the highest correlation with the fire activity during March 2009.

Table 3.7. Correlation coefficient between fire activity (FHS) and climate parameters (precipitation and SOI) in Riau province

No	Parameters	Correlation coefficient
1	FHS	1
2	SOI lag 0	-0.24
3	SOI lag +1	-0.22
4	SOI lag +2	**-0.28**
5	SOI lag +3	-0.19
6	SOI lag +4	-0.14
7	Rain lag 0	-0.17
8	Rain lag +1	-0.26
9	Rain lag +2	**-0.34**
10	Rain lag +3	-0.28
11	Rain lag +4	-0.20

The above evaluation results of parameters' correlation for a decade of data (2001-2010) shows that precipitation and SOI are most related to the following two months of fire occurrence in Riau province (Cahyono et. al., 2013). A negative sign in the coefficient values indicates that increasing SOI and precipitation causes a reduction in the fire occurrence in the Riau province.

The same investigation of FHS and climate parameter correlation was also performed on the Kalteng data to determine whether the occurrence of fires are directly impacted by rainfall or whether the impacts are delayed. The results of the coefficient relationship assessment for Kalteng data are displayed in Table 3.8. It shows that the peak value of correlation coefficient for FHS and SOI value occurs in lag +2 month with -0.28; meanwhile the peak of coefficient relationship for FHS

and rainfall occurs in lag 0 with a value of -0.34. These results indicate that Kalteng province has slightly different characteristics compared to the Riau province. Rainfall in Kalteng province affects the fire occurrence in the same month of rain. These things implicitly suggest that the seasons, indicated by the rainfall rate, have the same pattern as fire activity. Decreasing rainfall rate in the beginning, middle, or end of a season directly affects the fire activity in that season.

Table 3.8. Correlation coefficient between fire activity (FHS) and climate parameters (precipitation and SOI) in Kalteng province

No	Parameters	Correlation coefficient
1	FHS	1
2	SOI lag 0	-0.22
3	SOI lag +1	-0.25
4	SOI lag +2	**-0.28**
5	SOI lag +3	-0.25
6	SOI lag +4	-0.22
7	Rain lag 0	**-0.34**
8	Rain lag +1	-0.33
9	Rain lag +2	-0.28
10	Rain lag +3	-0.12
11	Rain lag +4	0.07

Finally, we conclude this section with the relationship between fire activity and rainfall. In Riau province, the occurrence of rainfall is correlated to the next two months of fire activity. A different trend is shown in the correlation of rainfall and fire activity for Kalteng province; this province is characterized by a direct impact of rainfall on fire activity. Comparing these results to the Dayamba et al. (2010) work, the Riau fire pattern does not show that early, mid, and late fire seasons are associated with early, mid, and late dry seasons respectively, because the occurrence of rainfall has a closer correlation with the next two months of fire activity. However, Kalteng province seems to agree with Dayamba's (2010) work because the rainfall impacts the fire activity in the same month, which means that early, mid, and late fire seasons are associated with early, mid, and late dry seasons respectively.

3.5 Sensitivity of the MOD14 Algorithm in Wet and Dry Seasons

It was introduced in Section 2.5 that the sensitivity of the MOD14 algorithm varies when applied to different regions. To enhance the understanding of how the MOD14 algorithm responds to the MODIS datasets over Indonesia, this section will discuss the analysis of sensitivity of the MOD14 algorithm applied to MODIS datasets over Riau and Kalteng provinces of Indonesia, the two regions of interest. The fire detection sensitivity in this section is defined as the change in number of detected FHS as the threshold value is changed, when the algorithm is applied to the MODIS data. Therefore, the sensitivity assessment in this section is based on threshold values changes. If the algorithm is sensitive to changes , this suggests it might be appropriate to vary the threshold values for different conditions.

The sensitivity analysis is applied to the MODIS datasets over Indonesia for the two seasons, dry and wet, as described by Yasunari (1981). The dry season usually occurs between June to November, while the wet season usually occurs in the period of December to May (Yasunari, 1981; Kishore et al., 2000). The sensitivity analysis aims to describe and compare FHS detection sensitivity characteristics in the two seasons. Two months of MODIS data were examined in this research. Data acquired in August 2009 represent the dry season and data for February 2010 represent the wet season. For these two months there is a total of 93 data points: that is, 50 data points for the dry season and 43 data points for the wet season.

The analysis was performed on the seasonal MODIS data by modifying the threshold (T_4). Essentially, this preliminary test filters or detects all pixels that may be considered fire pixels. When the pixels' temperatures fall below the threshold value, these pixels are not classified as fire pixels. Consequently, decreasing or increasing threshold values will impact by increasing or decreasing the number of detected FHS respectively.

The first experiment was performed to determine the lowest and highest temperatures of threshold values at which the maximum number of fires is detected and when no fires are detected. The lowest threshold value was considered to be the value which enabled the fire algorithm to detect the maximum FHS number. No additional numbers of FHS were detected when the threshold value was reduced

below this limit. Conversely, the highest threshold value is determined when the fire algorithm cannot detect any pixels as a fire or simply when no fire pixels are detected. Note, the threshold value used in the MOD14 algorithm is 310K .

The assessment results showed that 300 K was the lowest threshold because reducing threshold value from this point did not impact on the additional number of detected FHS. In contrast, the highest threshold value was determined to be 350 K because fire pixels were still detected in some datasets by applying the threshold value above 350 K, but on average only 2% of total detected fire is found. This means that 98% of fires have been either detected or not by changing the threshold value from 300 K to 350 K. Thus the sensitivity assessment is applied in the threshold values changing from 300 K up to 350 K in one degree steps. The number of detected FHS is recorded in every changing step of threshold values.

The plot of the distribution of detected FHS numbers for various threshold values applied to each MODIS dataset for both dry and wet seasons is shown in Figure 3.25 and Figure 3.26. Every curved line represents the FHS distribution pattern of each MODIS dataset. The dashed black lines in both figures represent the patterns of average value for all datasets in each season. The maximum number of FHS detected by the MOD14 algorithm varies for every assessed MODIS dataset; hence the shapes of the curves of response of the algorithm for each datasets, as well as the average value curves on these separate figures, cannot be compared directly. Merging the average curve patterns of the FHS distribution for each season in one chart will help the pattern analysis. However, displaying the real number of average detected FHS still does not give a clear picture of fire distribution characteristics in terms of response of the fire detection algorithm for MODIS datasets applied.

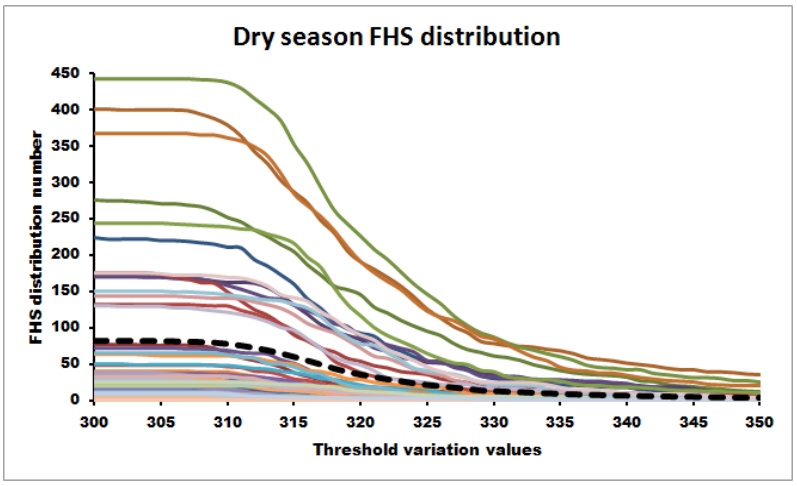

Figure 3.25. Detected FHS distribution in various threshold values for 50 datasets of dry season in August 2009. Each solid line represents the FHS distribution of each MODIS dataset. The average FHS distribution is drawn by the dashed line.

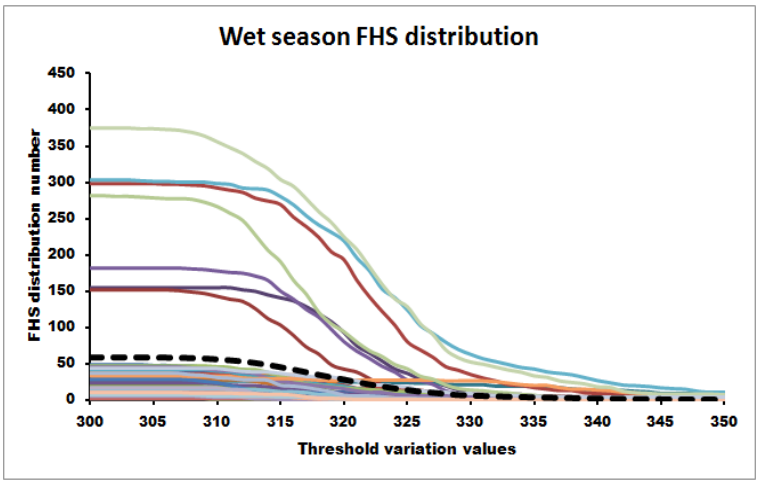

Figure 3.26. Detected FHS distribution in various threshold values for 43 datasets of wet season in February 2010. Each solid line represents the FHS distribution of each MODIS dataset. The average FHS distribution is drawn by the dashed line.

Similar curve patterns are shown in both Figure 3.25 and Figure 3.26. They indicate the relatively constant number of FHS from 300 K to 310 K, then the number of FHS decreased steeply from a threshold of about 310 K to about 325 K, and then the change in the number of FHS gradually decreased from 325 K to 350 K. This finding indicates that the sensitive threshold value in determining fire pixels ranges from 310 K to 325 K.

The pattern of the normalized number of detected FHS gives a better description of how the fire algorithm responds to the changing threshold values. By

normalizing all the curves, the maximum numbers of detected FHS are indicated at the same value: that is, 1 or 100% in the normalized scales and the minimum numbers of detected FHS are placed at the same value, 0. The graphs of normalized number of detected FHS for the dry and wet seasons of MODIS datasets over Indonesia are displayed in Figure 3.27 and Figure 3.28.

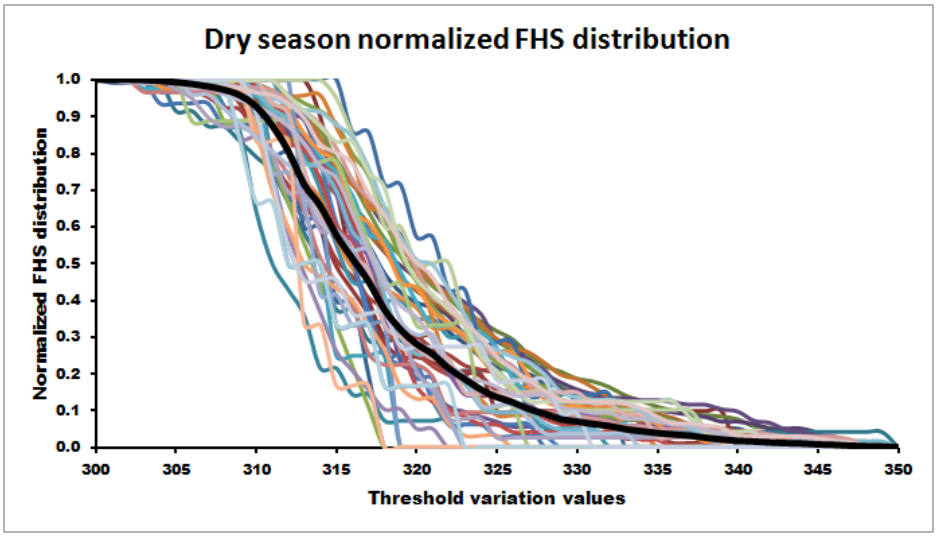

Figure 3.27. Normalized detected FHS distribution for various threshold values for the dry season

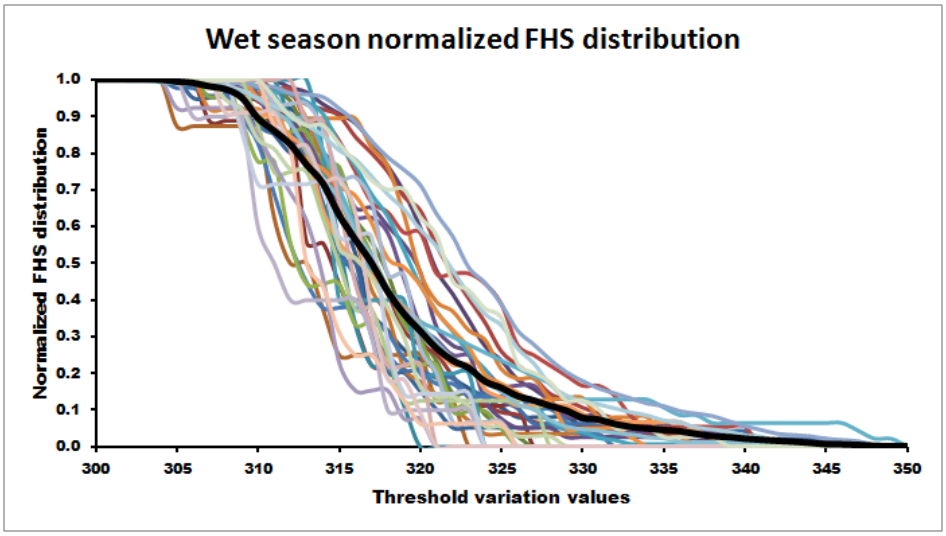

Figure 3.28. Normalized detected FHS distribution for various threshold values for the wet season

The trend of the normalised curves is analysed to compare the algorithm response and sensitivity between both dry and wet seasons. The normalized curves

of average fire distribution for the wet and dry seasons are shown in Figure 3.29. The wet season curve shows that the number of decreasing FHS is steeper compared to the number of decreasing FHS in the dry season, with the steepest curves in the threshold values ranging from 310 K to 325 K. This suggests that the MOD14 algorithm responses are more sensitive to the wet season data than those generated from the dry season in terms of variation of changing threshold value. Figure 3.29 also indicates that the application of the fire detection algorithm may need a lower threshold value for the wet season compared to the dry season.

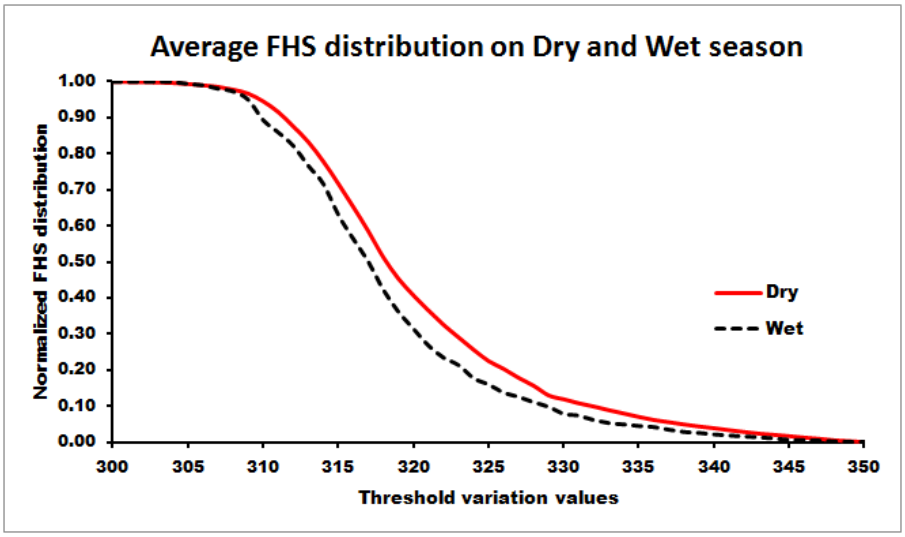

Figure 3.29. Average patterns of normalised algorithm response for detected FHS distribution for various threshold values for both dry and wet seasons

The "Mann-Whitney test" statistical analysis was used to show the characteristics of the reduction pattern of the assessed data (Pallant, 2011). Essentially, the Mann-Whitney test is used to compare median values of two independent groups, in this case normalised FHS distributions in both the dry and wet seasons. With respect to the fire algorithm response to the threshold values, the reduction number of FHS along with the increase of threshold value is related to the sensitivity response of the fire algorithm to the MODIS data. The results of the Mann-Whitney test applied to the dry and wet data suggest that the rate of reduction of FHS numbers in the wet season is larger than in the dry season, as displayed in Figure 3.30. It appears that wet season datasets have a more sensitive response to the threshold value compared to the dry season datasets. This result

supports the previous comment that the application of the fire detection algorithm may need a lower threshold value for the wet season compared to the dry season.

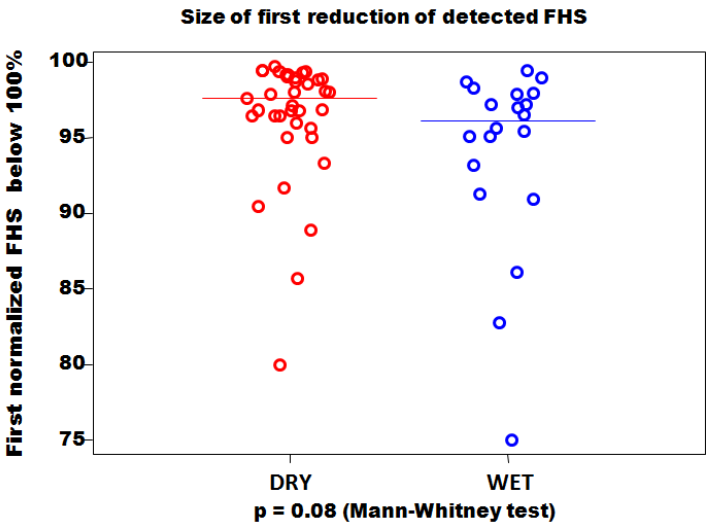

Figure 3.30. First reduction of normalised detected FHS distribution in both dry and wet season

The comparison of results between dry and wet seasons of fire distribution patterns, as shown in Figure 3.29 and the Mann-Whitney test, indicates that the MOD14 algorithm responds differently to dry and wet season MODIS datasets. The statistical analysis test is employed to examine the significant difference of responses of the algorithm in both dry and wet seasons.

Since the number of FHS detected in every season are not related to each other, the number of fires in the two seasons are regarded as independent variables, thus the t-student test is considered to be appropriate to examine the significance of the independent variables (Pallant, 2011). The t-student test is performed on the average of normalized data of the number of FHS detected in dry and wet seasons. There are 51 pairs of data, representing the data step of temperature changes from 300 K to 350 K. The data were tested using a t-student test implemented in SPSS. The t-student test results, with a significance (2-tailed) of < .001, are shown in Table 3.9. Pallant (2011) makes the point that the significance (2-tailed) values less than 0.05 indicate that there is a significant difference between the two variables tested. The significance (2-tailed) value of the t-student test reported by SPSS was

< .001 for the dry and wet season data. This means that both curves are significantly different.

Table 3.9. T-student test of detected FHS in dry and wet seasons

Season	Number of data	Mean	Std. Deviation	Std. Error Mean	Sig (2-tailed)
Dry	51	0.4055	0.39520	0.05534	0.000
Wet	51	0.3692	0.39506	0.05532	0.000

We have analysed the patterns of average detected FHS number distributions for the dry and wet season datasets, performed the Mann-Whitney test, and applied the t-student test, with the conclusion that the MOD14 algorithm responds differently in dry and wet season datasets over Indonesia. The results indicate that a lower threshold value may be more appropriate for the wet season MODIS datasets over Indonesia. This result leads to the importance of determining the best threshold value for fire algorithms that fit dry and wet season datasets.

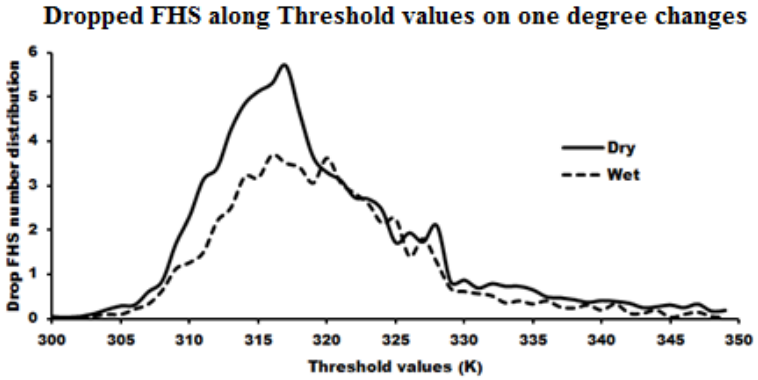

Figure 3.31. Decrease of FHS number detected in dry and wet seasons for various threshold values

However, the sensitivity of the fire detection algorithm has not been determined yet. Our approach of assessing algorithm sensitivity is analyzing the decreased number of FHS detected for every step of threshold value change. The pattern of the average decrease of the detected FHS number for dry and wet seasons in one-degree step threshold variation is shown in Figure 3.31. Based on the figure and the statistics data displayed in Table 3.10, the biggest decrease of detected FHS occurs in the most sensitive range of threshold values between 310 K

and 325 K. The biggest decrease value in the dry season occurs at 317 K, while in the wet season it occurs at 316 K. This indicates that the most sensitive MOD14 algorithm response occurs at the threshold 317 K for dry season datasets and at 316 K for wet season datasets.

Table 3.10. Statistics for the average number of FHS detected and the average decreased number of FHS for dry and wet season datasets at various threshold values in 1 degree steps.

Threshold values	Dry		Wet	
	Avg FHS	Avg Decrease	Avg FHS	Avg Decrease
310	77.96	2.32	55.95	1.28
311	75.64	3.14	54.67	1.51
312	72.50	3.40	53.16	2.21
313	69.10	4.26	50.95	2.51
314	64.84	4.84	48.44	3.21
315	60.00	5.12	45.23	3.19
316	54.88	5.30	42.05	3.70
317	49.58	5.70	38.35	3.51
318	43.88	4.64	34.84	3.42
319	39.24	3.64	31.42	3.07
320	35.60	3.30	28.35	3.63
321	32.30	3.12	24.72	3.07
322	29.18	2.74	21.65	2.84
323	26.44	2.70	18.81	2.60
324	23.74	2.46	16.21	2.16
325	21.28	1.72	14.05	2.26

The result of the MOD14 algorithm response in terms of the decreased number of detected FHS implies that the threshold value of 317 K is recommended for the dry season and the threshold value of 316 K is suggested for the wet season. To see the impact of the misuse (not recommended usage) of threshold values in dry and wet seasons to the number of detected FHS number, we calculated the

percentage of the number of detected FHS between 316 K and 317 K threshold values by dividing the number of detected FHS in the associated threshold values (as recommended) in each of the dry and wet seasons. Based on the data shown in Table 3.10, the use of a higher threshold value (317 K) in the wet season on average gives (42.05-38.35)/42.05=8.8% lower FHS number from the detected FHS number with the recommended threshold value. On the other hand, the use of a lower threshold value (316 K) in the dry season gives an average of (54.88-49.58)/49.58=10.7% higher on the detected FHS number compared to the detected FHS number by using the recommended threshold value

As described in Chapter 2, the fire detection algorithm for the T_4 threshold, which is used for examining potential fire pixels in the MOD14 algorithm, is 310 K and the threshold in the IndoFire algorithm is 316 K. Drawing on the previous results, we can justify that the threshold value applied to the IndoFire algorithm appears to be more appropriate for MODIS data over Indonesia. The data show that the average number of FHS from MODIS datasets for August 2009 decreases steeply within the threshold range 310 K to 325 K. The data were assessed using the MOD14 algorithm with various T_4 threshold values in the potential fire pixels test. The MOD14 and IndoFire threshold values are linked to the average values of FHS numbers using solid black lines in Figure 3.32.

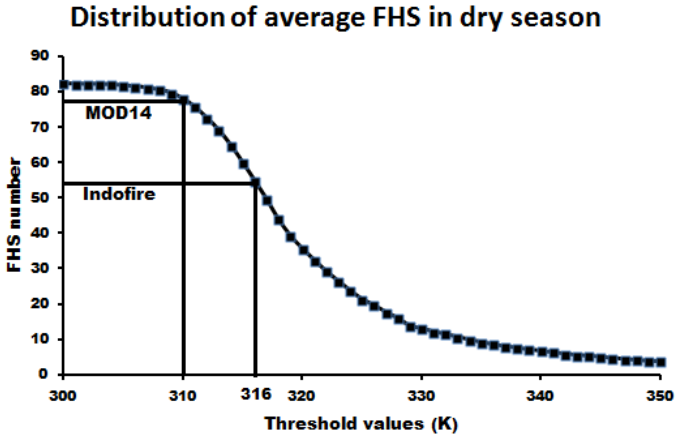

Figure 3.32. Distribution of average detected FHS numbers in the dry season during August 2009 using various T_4 threshold values in the potential fire pixels test for the MOD14 algorithm.

The maximum number of the average detected FHS as shown in Figure 3.32, which occurs at a 300 K threshold value, is 82.26 pixels; the minimum FHS number, which takes place at a 350 K threshold, is 3.60 fire pixels. The number of detected FHS at the MOD14 threshold (310 K) is 77.96 fire pixels and the detected number of FHS at the IndoFire threshold (316 K) is 54.88 fire pixels. There are 23.08 different FHS, or about 23.08/82.26=28.06% of the detected FHS, between the MOD14 and the IndoFire threshold applications. By applying the same calculation as given in the example, the percentage difference of the average of FHS differences in the wet season is about 23.71%. Thus on average, the application of the genuine MOD14 algorithm to MODIS datasets over Indonesia will overestimate by 28.06% the detected FHS number for dry season datasets and by 23.71% for wet season datasets. This result is based on the dry and wet season MODIS datasets, which were acquired in August 2009 and February 2010 respectively.

These findings give evidence that the MOD14 algorithm needs some adjustment with respect to the threshold value when the algorithm is applied to MODIS data over Indonesia. This research suggests utilizing the threshold value of 316 K for the wet season and 317 K for the dry season. These threshold values are slightly higher than those applied for fire detection in Alaska (314 K to 315 K) by Seielstad et al. (2002). Moreover, they are largely different from threshold values applied to South-Eastern United States, i.e. 293 K.

There are a number of possible reasons underlying the larger threshold values for the fire detection algorithm using MODIS data over Indonesia. In the land degradation area (that is, low vegetation cover) the average atmospheric temperature near the Earth's surface will increase (Jarraud, 2005). As introduced in Chapter 1, massive transmigration, logging, and mega rice projects left a large forest area degraded (Roach et al., 2004; Riley, 2006) which led to a reduction of the cooling effect of evapotranspiration. Decreasing vegetation cover will increase open land area, which may lead to increasing the surface reflectance of solar radiation. Thermal solar energy will be emitted to the atmosphere and thus the temperature above the surface increases.

As reported by Nicholson, Davenport, and Malo (1990), rainfall has a strong relationship with seasonal NDVI. This indicates that the wet season, which has a lot of rainfall, leads to vegetation growth; the cooling effect of water vapour in the air as a result of evapotranspiration by vegetation increases and the average temperature decreases. The likelihood is that fire occurring in the wet season will also have a lower temperature compared to fire in the dry season

It is also possible that vegetation cover changing in peat land forest degradation causes an increasing environmental temperature. Riau and Kalteng provinces, regarded as the most fire prone, are mostly comprised of peat land forests which have been converted to oil palm plantations (Miettinen et. al., 2012) and rice fields as a part of the mega rice project (Riley, 2006). The land use changes can produce green-house gases (CO_2) as a result of vegetation changing (Strack, 2008). Miettinen et al. (2012) estimate that peat land forests in Kalimantan will decrease by 0.5 million hectares a year by 2020.

The proportions of vegetation cover types in 2009 for Kalteng and Riau are shown in Table 3.3. The table shows that primary forest types represent nearly 27% of the vegetation cover in Kalteng and Plantation nearly 27% in Riau. Non-burning or non-vegetated areas (clear land, water, fishponds, swamp, settlement, mining, and airport/harbour) represent approximately 4% of the whole Kalteng province area. As described in Section 3.2, primary forest (including swamp forest and dry land forest) experiences very few fires compared to secondary forest and other vegetation cover types, especially bush and swamp bush. All other vegetation cover types may undergo seasonal changes due to either wet or dry season, as shown in Table 3.5 for Kalteng province and Table 3.6 for Riau province.

Sensitivity of the fire detection algorithm is seasonally affected. Hence, some adjustments of the applied threshold values are needed for different seasons. The finding of this study reveals that the appropriate threshold values are 316 K for the wet season and 317 K for the dry season, based on each being the most sensitive threshold to changes in threshold.

3.6 Validation of the MOD14 and IndoFire Algorithms

Methods for the validation of the MOD14 algorithm using SPOT imagery have been reported by Liew et al (2003). The validation research was performed on the FHS detected by the MOD14 algorithm and SPOT imagery data over Sumatra and Borneo. This section discusses the fire detection results of the MOD14 and IndoFire algorithms validated by high resolution SPOT images. This section also discusses validation using ground truth data provided by the local forestry agency in Kalteng province. The discussion consists of two sections: i) validation using SPOT data (Section 3.6.1); and ii) validation using ground truth data (Section 3.6.2).

3.6.1 Validation Using SPOT Data

It has been described in the previous chapter, Section 2.6.1 that the SPOT sensor does not have a thermal infra red channel which is very essential in the fire detection work. The only relevant channel that SPOT has is a short wave infra red at about 1.6 μm wavelength (Anonymous, 2010b), but this is typically dominated by solar radiation which must be rejected in fire pixels classification (Giglio et al., 2003). This is the basic reason why Liew et al. (2003) utilized SPOT data to detect fire visually.

This section discusses a visual validation method using a SPOT high-resolution image, which was compared to the FHS data detected by the MODIS sensor closest in observation time to the SPOT data.. The FHS data were collected from the results of the MOD14 and IndoFire algorithms. The FHS locations both from the MOD14 and IndoFire algorithms are overlaid on the associated SPOT images as shown in Figure 3.33 to Figure 3.38. The high resolution SPOT images constitute the SPOT quick look data accessed from either the CRISP[10] or LAPAN[11] websites. The images are selected only for the data that have cloud coverage less than 25%. This value is regarded as the best value to choose among the provided cloud coverage values on the CRISP website, i.e. 0%, 10%, 25%, and 75%. The

[10] http://www.crisp.nus.edu.sg/crisp_cat.html
[11] http://222.124.178.110/html/katalog.php?id=spot

lower cloud fraction in images will make the visual analysis easy to be administered.

As stated previously in Section 2.2, the SPOT satellite has temporal resolution of 26 days. This long repeat time for the SPOT satellite leads to difficulties in finding coincident SPOT and MODIS data. Good SPOT images with a small fraction of cloud cover, less than 25%, are also difficult to find. In this section we validate FHS detected using the MOD14 and IndoFire algorithms with two SPOT images. The MODIS data were acquired on 22 January 2009 at 03.40 UTC (10.40 AM local time) and the SPOT images were acquired two minutes earlier on 22 January 2009 at 03.38 UTC.

Figure 3.33 and Figure 3.34 show the SPOT images overlaid with FHS detected by the MOD14 and IndoFire algorithms respectively. The detected FHS resulted from the most overlaps with MODIS data acquired 2 minutes later. For these two figures, the two algorithms (MOD14 and IndoFire) have the same ability to detect the occurrence of fire. The number and places of FHS are exactly the same as those shown in the two figures. However, the omission error arises at the area within the drawn black circle because both fire detection algorithms cannot identify the existing active fire. We can confidently judge that the circled area contains active fires as we can see a thin smoke plume origination in that area.

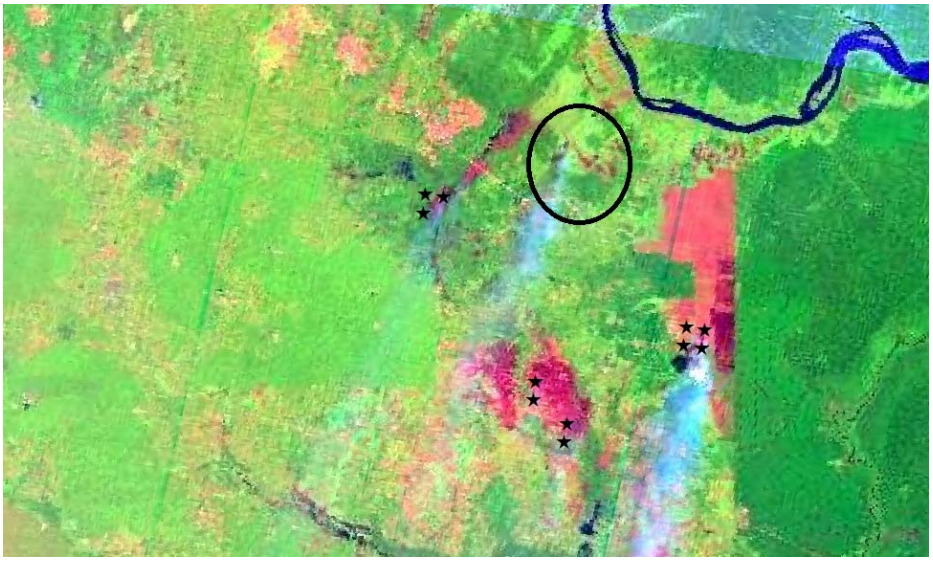

Figure 3.33. Detected FHS from MOD14 on 22 Jan 2009 at 03:40 UTC overlaid on a SPOT image for 22 Jan 2009 at 03:38 UTC; image block number K-J=272350

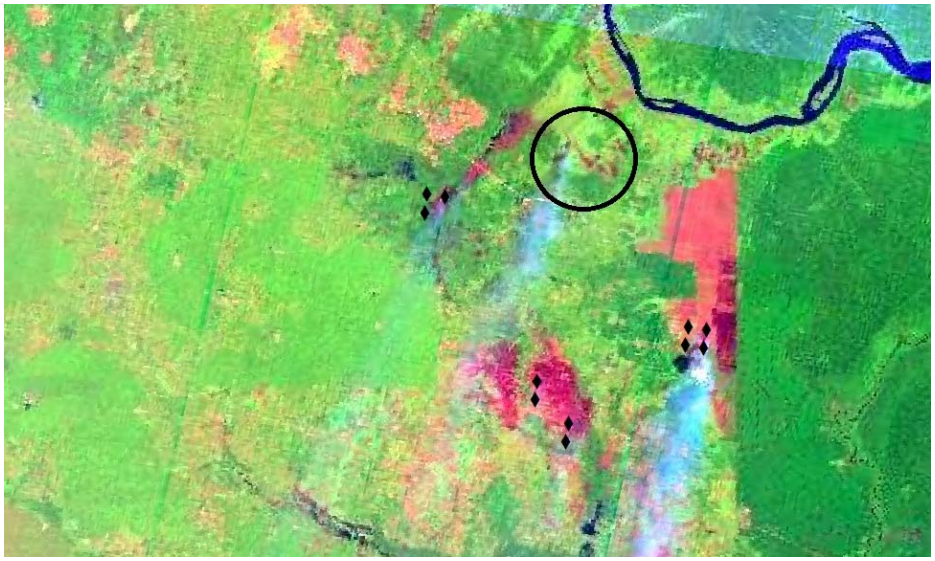

Figure 3.34. Detected FHS from IndoFire on 22 Jan 2009 at 03:40 UTC overlaid on a SPOT image for 22 Jan 2009 at 03:38 UTC; image block number K-J=272350

The possible reason for the undetected fire by either the MOD14 or IndoFire algorithms is that the pixel temperature of the occurring fire is lower than the threshold values applied on those two algorithms. Therefore, the low pixel temperature cannot pass the preliminary test and is not detected as a fire pixel. We have retrieved two pixel temperatures within the circled area with a red dark colour from where the smoke plumes come. The two pixel temperatures were measured at 303.5 K and 308.5 K (see Table 3.11 for pixel temperatures with no FHS detected). Pixel temperatures below 310 K are not possible to be flagged as fire by either the MOD14 or IndoFire algorithms. The conditions of fire existence with detected temperature below the threshold value, 310 K, may result in omission error.

Table 3.11. The statistics data properties of selected pixels referred to Figure 3.33 and Figure 3.34. This data properties is derived from MODIS data 22 January 2009 (MOD14.A2009022.0340.hdf)

No	Fire Position		L1B manual data reading			
	Lat	Lon	Row	Col	DN	T4
Pixels temperatures with no FHS detected						
1	0.186	102.303	600	677	2994	303.5
2	0.188	102.306	1501	989	3050	308.5
Pixels temperatures with shown FHS detected						
1	0.133	102.597	601	711	3169	317.2

No	Fire Position		L1B manual data reading			
	Lat	Lon	Row	Col	DN	T4
2	0.169	102.230	603	670	3212	319.8
3	0.178	102.232	602	670	3363	327.8
4	0.066	102.300	613	680	3167	317.0
5	0.068	102.292	613	679	3152	316.1
6	0.078	102.284	612	678	3543	335.4
7	0.087	102.285	611	678	3442	331.3
8	0.094	102.365	609	686	3175	317.5
9	0.103	102.366	608	686	5038	371.6
10	0.112	102.367	607	686	3351	327.2
11	0.121	102.369	606	686	3164	316.8
12	-0.119	102.307	633	685	3273	323.2

As a comparison, the temperatures of the other 12 pixels identified as fires in Figure 3.33 and Figure 3.34 are investigated. We found that the 12 pixel temperatures range from 316.1 K to 371.6 K; all of them are above the 316 K threshold. The detail of the data is shown in Table 3.11. Since the threshold values of the IndoFire algorithm and MOD14 algorithms are 316 K and 310 K respectively, all the 12 pixels can be classified as fire pixels by both the MOD14 and IndoFire algorithms.

In addition, different results are shown in different locations of detected FHS by the MOD14 algorithm using the same MODIS dataset (22 Jan 2009 at 03:40 UTC) as shown in Figure 3.35. In the locations of detected FHS, no smoke plumes were detected, as shown in the SPOT high resolution image in Figure 3.35. There are 6 FHS locations detected from the MOD14 algorithm over the areas shown in Figure 3.35, but smoke plumes did not appear from any of the areas.

Figure 3.35. Detected FHS from MOD14 for 22 Jan 2009 at 03:40 UTC overlaid on a SPOT image for 22 Jan 2009 at 03:38 UTC; image block number K-J=272348

Extracting pixel temperature may potentially explain the reason that the MOD14 algorithm detected fire in the areas without smoke plumes. The pixel temperature data of circled areas for numbers 2 and 3 in Figure 3.35 can be seen in the row numbers 7 and 8 in Table 3.12. The data show that the temperature of the red dark pixel in the circled area for number 2 is 293.9 K, while the temperature of the red dark pixel in the circled area number 3 is 302 K. These results give evidence that the MOD14 algorithm cannot flag the two pixels as fire because the pixel temperatures are below the MOD14 threshold value, 310 K.

Furthermore, the other pixel temperatures, which represent the FHS data points within circled areas numbered 1, 4, 5, 6, and 7, are presented in rows 1 to 6 of Table 3.12. All of the pixels have temperatures above the MOD14 threshold, 310 K, and therefore they have the possibility to be determined as fires by the MOD14 algorithm. The pixel temperature value above the threshold is an essential requirement for fire pixel classification. The next requirement of the pixels is that they should pass the contextual test, as described in Section 2.3.1.3.

Table 3.12. Details of selected pixels referred to in Figure 3.35. These data properties are derived from MODIS data for 22 January 2009 (MOD14.A2009022.0340.hdf)

No	Circle number	Fire Position		L1B manual data reading			
		Lat	Lon	Row	Col	DN	T4
Pixels temperatures with shown FHS detected							
1	1	1.024	102.182	511	645	3089	311.6
2		1.022	102.191	511	646	3128	314.4
3	4	1.059	102.256	506	652	3079	310.9
4	5	1.032	102.380	507	666	3073	310.4
5	6	0.852	102.350	527	667	3081	311.0
6	7	0.791	102.263	535	659	3099	312.4
Pixels temperatures with no FHS detected							
7	2	1.085	102.269	503	653	2909	293.9
8	3	1.046	102.282	507	655	2979	302.0

In a specific case, the pixels with a temperature more than the threshold value might not be classified as fire by the fire detection algorithm. This might occur because the contextual algorithm applied in the MOD14 algorithm compares the suspected pixel temperature with the surrounding pixel temperatures. The slight difference of temperature between the pixel suspected to be fire and the surrounding pixels may cause the potential fire pixel to not be classified as a fire pixel. To support this argument, we have found out that the MOD14 algorithm did not consider a pixel with temperature more than 310 K as a fire pixel. We took two pixels with temperatures that are close together but with different fire status. The first pixel was taken from data in row number 2 of Tale 3.12 with temperature of 314.4 K. This pixel is classified as a fire pixel. The second pixel was taken from the neighbouring pixel at latitude 1.03 and longitude 102.19 with a temperature of 313.0 K and it was classified as a non-fire clear land pixel.

In the MOD14 algorithm, one requirement for the pixel to be flagged as fire is that a pixel has $T_4 > \overline{T_4} + 3\,\delta_4$. The complete requirements have been described previously in Section 2.7.2 under the contextual test heading. In the case of a pixel with a temperature of 314.4 K, by taking a 5x5 pixel window size, we found that

the value of $\overline{T_4} + 3\,\delta_4$ is equal to 314.1 K. This means that the pixel with a temperature of 314.4 K meets this requirement and it is flagged as a fire pixel. On the other hand, we have assessed the second example of a pixel, 313.0 K, by taking also a 5x5 pixel window size surrounding the pixel. We found that the calculated value of $\overline{T_4} + 3\,\delta_4$ is equal to 313.8 K. Therefore the assessed pixel is not determined to be a fire pixel. Figure 3.36 shows the scatter plot of pixels temperatures surrounding the assessed pixel, with temperatures of 314.4 K (upper plot) and 313.0 K (lower plot). The detail of pixel temperatures for both scatter plots can be seen in Appendix 11.

(a)

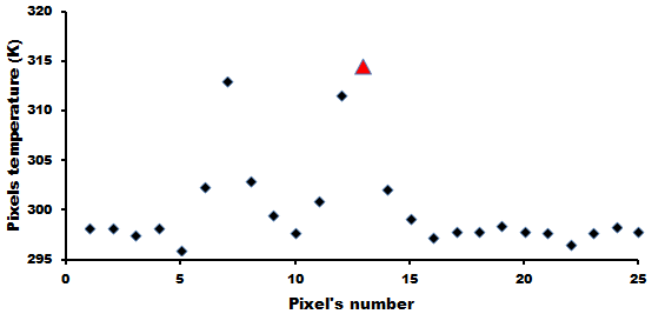

(b)

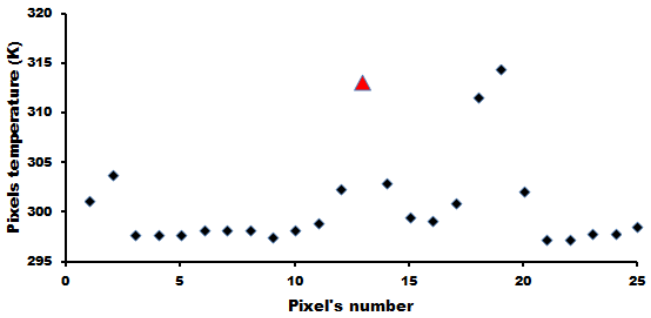

Figure 3.36. Scatter plots of pixels' temperatures within a 5x5 pixel window size surrounding the assessed pixel with a temperature of (a) 314.4K detected as fire by MOD14 and (b) 313.0K not detected as fire by MOD14. The temperature values are extracted from the MODIS dataset for 22 Jan 2009 at 03:40 UTC.

The horizontal axis of the two charts represents the pixel's number in a matrix order as displayed in Figure 3.37 (a). The centre pixel in the 5x5 window is indicated by red triangles in the plots of Figure 3.36. In each of the plots, and in grids (b) and (c) displayed in Figure 3.37, there are two pixels (other than the central pixel) with temperatures above 310 K.

1	2	3	4	5
6	7	8	9	10
11	12	13	14	15
16	17	18	19	20
21	22	23	24	25

(a)

298.2	298.2	297.5	298.2	296.1
302.4	313.0	303.0	299.6	297.8
301.0	311.6	314.4	302.1	299.3
297.3	297.9	297.9	298.5	297.9
297.8	296.6	297.8	298.3	297.8

(b)

301.2	303.8	297.8	297.8	297.8
298.2	298.2	298.2	297.5	298.2
299.0	302.4	313.0	303.0	299.6
299.3	301.0	311.6	314.4	302.1
297.3	297.3	297.9	297.9	298.5

(c)

Figure 3.37. The matrix of (a) the order of pixel's number which represents 5x5 window size and pixels temperature surrounding suspected fire pixel with temperature (b) 314.4K which is classified as a fire pixel and (c) 313K which is classified as a non-fire pixel

The three pixels with temperatures above 310 K are adjacent pixels as illustrated in Figure 3.37 (b) and (c). The MOD14 algorithm failed to detect the 313 K pixel as fire due to the high average temperature of the surrounding pixels. This pixel failed detection because the suspected fire pixel temperature is lower than the temperature mean (average) value of surrounding pixels plus 3 standard deviations (see the mean and standard deviation values in the last row of the second table of Appendix 11).

Referring to the previous discussion, we can learn that validation of detected FHS using SPOT imagery data cannot only be done by visual analysis but it needs another supporting method, such as pixel temperature measurement. Figure 3.33 and Figure 3.34 have shown false detection of the fire algorithms (MOD14 and IndoFire) due to low pixel temperatures measured, even though the burning area (within circled area) obviously produces smoke plumes. Conversely, Figure 3.35 shows the occurring FHS detected in the areas which did not produce smoke plumes, and the measured pixel temperatures (Table 3.12) show values which are higher than the threshold value of the fire algorithm (MOD14).

When we look at Figure 3.35 carefully, the same land colour (dark red) can be seen on the SPOT image within circled areas; numbers 2, 3, 4, and 5 even though the areas do not represent the same fire status. The MOD14 algorithm only detects fire in the area within circles 4 and 5 but it does not detect fires within the circle areas 2 and 3. We cannot simply justify that the areas within circles 2 and 3 are fires because they have the same colour as those within circles 4 and 5. Thus, we do not necessarily make a statement that the MOD14 algorithm has an omission error for the two circled areas (numbers 2 and 4).

In the true colour satellite images (that is, SPOT images) the areas which have been burned in the last few days potentially show the same colour as those which are burned recently. We have investigated the occurrence of FHS detected from MODIS time series data. Five-day time series data acquired from 18 to 22 January 2009 were examined. We have detected FHS from MODIS data captured on 20 January 2009 at 03:50 UTC (two days earlier than the acquired SPOT image) in the circled area number 3 of Figure 3.35. The locations of the detected FHS on 20 January 2009 are displayed in Figure 3.38.

Figure 3.38. Detected FHS from the MODIS dataset of 20 Jan 2009 at 03:50 UTC using the MOD14 algorithm overlaid on the SPOT image for 22 Jan 2009 at 03:38 UTC (two days later); image block number K-J =272348

The fire pixel temperatures for all detected FHS shown in Figure 3.38 have been retrieved and shown in Table 3.13. With respect to the temperature data, we

observe that the pixel temperatures of the dark red land location identified in the circled area number 3 of Figure 3.35 was 310.1 K on 20 Jan 2009 at 03:50 UTC and 302 K on 22 Jan 2009 at 03:40 UTC. This data provides evidence that the fire had recently occurred in the circled area number 3 of Figure 3.35 on 20 Jan 2009 at 03:50 UTC and it had extinguished by the time the satellite overpassed two days later on 22 Jan 2009 at 03:40 UTC.

The SPOT true colour image shows the burning land areas as appearing a dark red colour. The other areas that have been burned recently also appear as a dark red colour when visually observed from the SPOT true colour image. Therefore, the true colour image analysis cannot obviously distinguish the occurrence of active fire. Other methods such as pixel temperature retrieval and time series analysis have supported the reliable analysis results.

Table 3.13. Data properties of fire pixels highlighted in Figure 3.38. These data properties are derived from MODIS data for 20 January 2009 (MOD14.A2009020.0350.hdf).

Fire No	Fire Position		L1B manual data reading			
	Lat	Lon	Row	Col	DN	T4
1	0.924	102.167	1423	963	3129	314.5
2	0.914	102.165	1424	963	3689	340.7
3	1.050	102.286	1407	971	3069	310.1
4	1.035	102.386	1407	980	3076	310.6
5	0.855	102.359	1427	981	3126	314.3

The above descriptions suggest that in the application stage, it is difficult to employ SPOT images as a visual validation of MODIS fire detection results. The difficult method is related to the validation of fires with faint smoke or even no smoke plumes produced. It appears that the visual area being burned and that was burned a few days ago cannot be distinguished clearly from the recent burned areas simply by land colour detection.

However, it is easy to validate fires which produce smoke plumes because using SPOT images with the high spatial resolution can obviously show the occurring smoke plumes. Liew et al. (2003) reported that generally smoke plumes were produced by biomass burning in the tropical area. In contrast, this research

data shows that a SPOT image as shown in Figure 3.35 does not necessarily exhibit the occurrence of smoke plumes. However, the MOD14 algorithm, which was applied to the MODIS dataset of 22 January 2009 at 03.40 UTC over Riau province, detected FHS in the areas associated with the SPOT image, as displayed in Figure 3.35. This means that the findings of this study partly disagree with those of Liew et al. (2003).

In conclusion, validation of the fire detection algorithm results using SPOT images is possible to be conducted through visual analysis only for fire burning areas which produce smoke plumes. The validation cannot be performed reliably by visual analysis of the fire areas that do not produce smoke plumes. The validation process in the non-smoke areas needs a further method such as pixel temperatures and time series data analysis to classify fire and non-fire pixels, instead of visual smoke plume observation only. Finally, validation of the MOD14 and IndoFire algorithms using SPOT data cannot work simply using a single method (visually) but it needs some quantitative methods to distinguish fire and non-fire pixels to gain reliable conclusions of accuracy detection.

3.6.2 Validation Using Ground Data

The perfect data for validation of satellite detected FHS are in-situ (ground) observational data because ground observation data confirm exactly that the fires are in a particular location at a specific time. In Indonesia, field data collection of fire occurrences is tasked to the Natural Resources Conservation Agency (BKSDA) officers as a local agency of the Indonesian Forestry Ministry. The ground data collection activities are typically conducted close to the suspected location of fire as indicated by the satellite data. Some fire location data are also recorded from public information or the district officer who passes through the fire locations. Given the varied data sources and no standard form of reports, the structure of the data records usually differ from any different sources and times. Some data even do not provide latitude and longitude coordinates but simply block and district locations which lead to difficulties in compiling comprehensive data.

Generally, the ground data collection is only performed in easily accessible areas and other areas able to be reached by the officers. The isolated and un-

touched areas are only able to be reached by helicopter or other aerial observation methods. However, fire observation using a helicopter is considered expensive and hence practically this method is rarely used. Another method, satellite observation, provides a much better choice in terms of costing.

Furthermore, the data of the field observations are not generally archived properly and are typically formed in a single activity report which might be presented in a variety of different ways. There is no integrated information system which accommodates the ground observation data that can be easily accessed by researchers and other stakeholders, e.g. an environment conservator acting as an official reference.

BKSDA staff in Kalteng province have collected fire ground data in the period of January to September in 2011. They attempted to provide data with a consistent format, as can be seen in Appendix 10. There are 202 recorded fire spots with various areas ranging from 0.5 to 116 hectares. The monthly distributed FHS ground data for Kalteng province are shown in Table 3.14. The data were collected from LAPAN and the copyright belongs to BKSDA of Kalteng.

Table 3.14. FHS number recorded from ground checked observation compared to its number detected by the IndoFire system in Kalteng province during 2011.

Month	FHS number		Ground/IndoFire (%)
	Ground data	IndoFire	
January	2	23	8.7
February	2	23	8.7
May	2	44	4.5
June	16	410	3.9
July	72	462	15.6
August	106	3152	3.4
September	2	2591	0.1
	202	**6705**	**6.4**

The recorded ground data for 2011 were only available for 7 months, while the remaining 5 months (March, April, October, November, and December) data were not available. The percentages of ground data number divided by the number

of FHS detected from IndoFire are shown in the last column of Table 3.14. The percentage data ranged from 0.1% to 15.6% with an average value of 6.4%. The lowest percentage value was achieved in September 2011 and the highest percentage value was recorded in July 2011. The 6.4% ground data available is considered insufficient to do validation for all detected FHS by IndoFire. In the case that all ground data are 100% in agreement with FHS detected, the validation result only represents less than 10% of fire activity characteristics.

In addition to the lack of sufficient data availability, the existing ground data often do not match the FHS data detected from satellite images (Cardoso et al., 2005) due to the small size of burned areas (Vetrita et al., 2012). Tansey et al. (2008) related the number of detected FHS to burned areas. They reported that each detected FHS by MODIS estimated a burned area of 15 to 16 hectares (ha) or 15% to 16% of a MODIS pixel area (100 ha). Burned areas observed on the ground by BKSDA Kalteng officers in 2011 are mostly less than 15 ha. Therefore, most ground data recorded (less than 15 ha) cannot be detected as fire by the MOD14 algorithm and thus the data are not reliable to validate the results of the fire detection algorithm, which is applied on the MODIS data.

Hence, we sorted the ground data to obtain only data with an area of at least 15 ha. There are only 11 of 202 ground data points available with areas of more than or equal to 15 ha in Kalteng in the year of 2011. Based on the findings of Tansey et al. (2008), these 11 fire data points collected within three months (June, August, and September 2011) are likely to be detected as fire from MODIS data. The detail of the eleven data points can be seen in Appendix 8. The locations of the eleven fire ground data points are represented by black stars as shown in Figure 3.39.

Figure 3.39. The locations of recorded ground observation data (black stars) in Kalteng province with areas more than or equal to 15 hectares. None of the FHS detected by the MOD14 and IndoFire algorithms are associated with these ground data displayed.

In this thesis, we define the ground data validation method as aligning the FHS data detected from the fire detection algorithm, such as MOD14 and IndoFire, with the observed ground data. By aligning and overlaying the 11 ground data points with the nearest and coincident FHS detected data, we find out that none of the FHS detected by either the MOD14 or IndoFire algorithms can be associated with the record of the ground data locations.

Some possible reasons can be addressed to this research finding. Low brightness temperature of pixels would lead to exclusion of the pixels by the preliminary test of the MOD14 and IndofFire algorithms. To assess this, pixel temperature retrieval has been conducted for all 11 ground data points. The temperature data for those 11 ground data points are shown in Appendix 9. The attributes of the ground data indicate that pixels temperatures range from 255.5 K to 306.3 K. These values, all below 310 K, will cause both the MOD14 and IndoFire algorithms to not detect the occurrence of fires in the positions indicated for the ground data.

Further, the MOD14 algorithm considered the 11 pixels associated with the ground data point locations as either cloud or non-fire clear land pixels. Cloud and

clear land pixels are notated by digital number 4 and 5 respectively. There are 5 pixels identified as cloud and 6 pixels are classified as clear land. When the MOD14 algorithm masked pixels as cloud, this means that the areas of potentially occurring fire were covered by cloud and therefore satellite sensors were not able to sense the fire radiance energy.

The result of this study disagrees with the findings of Tansey et al. (2008) . That is, all ground data areas are greater than 15 ha and in fact there is even one ground data area of 116 ha which is actually larger than one MODIS pixel i.e. 1x1 km = 100 ha. With reference to the findings of Tansey et al. (2008), this research result is interesting because all ground data cannot be recognized as fire even though the burning areas range from 15 ha to 116 ha. However, this result is in line with those of Giglio et al. (2009). According to Giglio et al. (2009) the minimum detectable burned size area for the MOD14 algorithm is 120 ha.

Furthermore, investigation of fire detection by the MOD14 algorithm within 5 days time of the observed fire supports the previous study of Vetrita, Haryani, and Komaruddin (2012). They report that fire pixels are regarded as valid if the fire pixels occur within 2 or 3 days around the date of ground data observation. Based on our investigated time series data for all 11 ground data locations, remote sensing data do not detect the fire pixels at any time in the series data, as shown in Appendix 12. This finding is consistent with the previous discussion, that is, no ground data match the FHS detected by IndoFire.

Drawing on the spatial buffering method as applied by Vetrita et al. (2012), we assess the the pixel data in a 3x3 window size around the ground data locations (see Appendix 13). The 3x3 window size represent a radius of approximately 2 km as a buffering area in the Vetrita ground validation method. As can be seen in Appendix 13, the data suggest that no pixels within a 2 km radius from the ground data points can be classified as fires as all pixel temperatures are below the 310 K threshold.

The failure to show a positive match up of the collected ground data with the detected FHS by the fire detection algorithms could be caused by the time difference of acquiring ground data and the satellite overpassing times (Prins et al., 1998; Cardoso et al., 2005; Giglio, 2007). In this case we cannot confirm that un-

detected ground-observed fires is because of the time differences. The ground data obtained by BKSDA officers did not include observation time (see data in Appendix 8). In terms of fire with a short life time, the time difference of observation will contribute a significant impact on the validation method using ground data. The active fire observed on the ground might be extinguished or dying by the time of the satellite overpasses. But again, lack of time data associated with the ground observations cannot give a conclusive outcome on this matter.

To summarize, we have attempted to use the ground data which were collected by BKSDA Kalteng officers for 7 months in 2011 for validating FHS detected from MODIS data. The findings suggest that no record of ground data matched the FHS detected from MODIS data generated by both the MOD14 and IndoFire algorithms. Based on the ground data area, our findings support those of Giglio et al. (2009). That is, fire cannot be detected by fire detection algorithms if the burnt/burning area is less than 120 ha. Thus, our finding disagrees with Tansey et al. (2008) who report that a minimum of 15 ha is able to be detected as fire by the MOD14 algorithm. Investigation of pixels' temperature at the identified locations of ground data shows low temperatures (less than the 310 K MOD14 threshold value). These low temperatures lead to exclusion by the MOD14 and IndoFire algorithms. The similarly low values of pixels' temperatures are also found around ground data points within 3x3 pixel windows centred on the ground data pixels. We also found low temperature pixels within 5 day time series data for every ground data point, with temperature values ranging from 225.7 K to 305.9 K.

3.7 Summary

In summary, this chapter provides descriptions of cloud coverage which affects the accuracy of detecting fire occurence in Indonesia for the decade 2001-2010. The average of yearly cloud cover over Indonesia in a decade was 80.4% ± 9%. This cloud fraction caused low numbers of detected FHS by the IndoFire system. The cloud existence obstructs the fire detection from satellite remote sensing and so the actual number of occurring fires may not be detected exactly. There was only 19.6% of FHS detected by IndoFire compared to the estimated number of occurring FHS for the decade in Indonesia.

Further analysis of cloud cover impact has been performed using monthly cloud coverage data. The estimation of FHS numbers with respect to the cloud coverage has been carried out using monthly and yearly FHS IndoFire data. The results show that the estimated number of FHS from yearly data is higher than those estimated from monthly data. The estimation of FHS numbers derived from yearly data is shown to over estimate by 10.9 % compared to the estimation of FHS numbers derived from monthly data. We consider that the estimation which is based on the narrower range of time is better, so the estimation from yearly data leads to an over-estimate of extrapolated FHS number.

Additionally, analysis of the impact of vegetation cover types on the fire detection shows that the area under low vegetation cover suffered more fire compared to the area under high vegetation cover. In Kalteng province, the fire density under low vegetation was 588 ha per fire and the fire density under high vegetation was 4162 ha per fire. On the other side in Riau province, fire density data showed 529 ha per fire for low vegetation and areas under high vegetation cover had a fire density of 2333 ha per fire. This data indicates that Kalteng province potentially has a higher risk of fire compared to Riau province. Focusing the investigation at low vegetation categories, we found that the swamp bush classification is identified as the category with the highest risk of fire. Thus, the extra awareness of fire risk should be given in this type of vegetation cover area. The fire risk of swamp bush area in Riau province is estimated to be 1.3 times higher compared to the risk in the same type of area in Kalteng province, based on fire density.

The relationship between FHS number and climate parameters has been determined by calculating the correlation coefficients of the relationships. Time series data for a decade (2001-2010) were analysed to determine the coefficient relationship values for different time lags and then select the extreme value as the closest relationship between the two assessed parameters. The results show that the precipitation and FHS coefficient relationship in Riau province have an extreme value (-0.336) at the lag+2 which means that precipitation has a delayed effect on the fire activity in Riau, while in Kalteng province the extreme of coefficient

relationship (-0.344) has a lag of 0, or, the precipitation has no delay effect on the fire activity.

Moreover, the effect of dry versus wet seasons showed significant impacts to the detection sensitivity. Dry and wet season analysis suggested that different threshold values needed to be applied for MODIS datasets over Indonesia. Dry season results indicated the need for a higher threshold value compared to the wet season threshold value. The result of analysing the change in number of detected FHS with change in threshold suggested a threshold application of 317 K for the dry season and 316 K for the wet season. Inappropriate usage of those suggested thresholds for each season (by exchanging the threshold of dry and wet season with each other) leads to an increase in the commission or omission error of about 10% for the detected FHS number.

Finally, validation assessment has been conducted by comparing MODIS data to SPOT high spatial resolution images and ground data. Visual validation using SPOT imagery cannot distinguish clearly occurring active fires. This is due to the similarities in the colour of land areas which are burning and the areas which have been burned in the last few days. To support visual analysis using SPOT data, pixel temperature investigation and time series analysis is needed to confidently assess fire pixel locations. Furthermore, ground data validation methods are expected to overcome these issues, however, unsynchronized ground data collection methods with respect to the FHS detected by satellite makes the problem difficult to resolve. Our analysis using ground data from BKSDA Kalteng province indicated that the collected ground data were insufficient for accurate and robust validation. The available ground check data comprised 202 data points. These data were recorded by BKSDA officers in the Kalteng province for 7 months in 2011. All these ground data represent only 6.4% of the number of detected FHS by IndoFire. There are only 11 data points of those 202 ground data which have an area more than or equal to 15 ha, which potentially have an effect on the ability of the satellite sensors to detect the thermal radiance from such small fires. Not all those 11 data points can be associated with occurring FHS detected by the IndoFire algorithm in the associated date and positions of ground data. The reason is because 5 pixels were covered by cloud and the other 6 pixels had low temperature and

were thus classified as non-fire clear land. The ground data fire area analysis indicated that, in Indonesia, the finding of Giglio et al. (2009) appears to be appropriate for the Kalteng province, that is, the minimum area able to be detected as fire is 120 ha.

CHAPTER 4

CONCLUSIONS

Fire monitoring is an important task for the Indonesian government as this country often deals with big fires which impact regionally on people and the environment. Providing accurate information of fire occurrence and fire activities represents significant contributions in controlling some of the negative effects of fire. Thus this research investigated and monitored the fire activity over Indonesia using freely accessible MODIS data.

4.1 Review of Aims

The investigation included the study of the form and sensitivity of the fire algorithms and some parameters that impacted the detection and monitoring of fire patterns. With respect to the statement in the first chapter of this thesis, the aims of this research are:

- Analyse the impact of cloud cover on the reported FHS number, and design an approach to predict the actual number of FHS for the whole area of interest.
- Investigate and analyse the impact of vegetation cover types on the fire activity based on the reported FHS number in various land cover classifications.
- Determine the sensitivity of the MOD14 algorithm applied to MODIS data over Indonesia.
- Analyse the relationship of detected FHS number and the seasonal factors, precipitation and Southern Oscillation Index (SOI), for a decadal time series.

In brief, the following sections describe the outcomes and conclusions of this thesis with respect to the research aims stated above, including the effects of cloud coverage, vegetation cover types, and climate parameters (SOI and precipitation) and also the results of the sensitivity analysis.

4.1.1 Cloud Coverage Impact on The Reported FHS Number

Cloud cover existence obscures fire monitoring because it blocks the viewing of land surfaces from space. The increasing cloud coverage leads to the decreasing possibility of observing clear land where fires may occur. Chapter 3 shows that, based on the Giovanni-GES DISC cloud fraction data, Indonesia has high cloud coverage, between 70% and 90% over a decade (2001-2010). This leads to reducing the number of FHS detected using the IndoFire system by 80.4% from the number of extrapolated FHS estimated as fire. From the investigated data, Riau was on average covered by cloud on average by about 33% during July 2009 while Kalteng was covered by cloud on average by about 24% for September 2009. From these cloud coverage values, the visible clear land in Kalteng was on average about 71% and Riau land visibility was about 44%, smaller than Kalteng because Riau province has a water area of about 22% while Kalteng has only about 5% water area.

4.1.2 The Impact of Vegetation Cover Types on The Reported FHS Number

Fire activity in 15 various types of vegetation cover over two province areas of Indonesia was investigated. Vegetation cover type classifications refer to the data from the Forestry Ministry of Indonesia which was provided for the year 2009. The analysis was carried out by studying the intersection of detected FHS from IndoFire and the vegetation cover type classifications. The results show that the vegetation types which are most prone to be burned are the low vegetation category. In contrast, the areas which are covered by higher vegetation types (categorized as tree) or the areas which are not commonly accessed by people, termed as primary vegetation areas, are found to have low fire activity.

This work showed that the swamp bush classification exhibited the highest fire density, and the highest proportion of vegetation cover area and fire, compared to other vegetation cover types. Swamp bush fires in Riau province have a risk of fire 1.3 times higher compared to the same type of area in Kalteng province. Furthermore, seasonal analysis shows that dry season fires in Kalteng province account for almost 99% of recorded FHS of this province during 2009. In addition,

dry season fire activity in Riau represents 2/3 of all detected FHS in this province for the whole year of 2009.

4.1.3 Sensitivity of The Fire Algorithm

Application of various values of thresholds in the MOD14 algorithm shows the highest response of detected FHS number occurs between 310K and 325K. This temperature range is then considered with respect to the sensitivity to threshold values. Seasons are considered as one of the factors affecting the operation of the algorithm in fire detection. Analysis of sensitivity in dry and wet seasons in Indonesia was carried out by analyzing data for the dry season in 2009 and the wet season in 2010. Separate assessments on dry and wet season datasets were performed to investigate seasonal effects on the detection sensitivity. The results showed that the FHS numbers from the wet season data decreased more rapidly in response to changes in the threshold compared to the dry season data. This indicates that changing the threshold value in the wet season displays a bigger effect on the number of detected FHS. The change in FHS values data analysis gives the most sensitive threshold for the dry season at 317 K while its value for the wet season is 316 K. The application of the threshold at 316 K in the dry season will lead to a 10.7% higher detected FHS number, and on the other side, the utilization of 317 K in the wet season gives 8.8% less of the number of detected FHS. These results suggest the need to adopt different thresholds values between dry and wet season data in which the wet season threshold value is lower than the dry season threshold value.

4.1.4 The Effect of Precipitation and SOI on Fire Activity

The relationship of precipitation, related to a season's indicator, and Southern Oscillation Index (SOI) which can affect the wet and dry seasons patterns and thus impact the occurrence of fires has been investigated. This relationship is examined by a correlation coefficient test. The peak point, that is the time at which the correlation is highest, of FHS and SOI occurs at the lag of 2 months in both Riau and Kalteng provinces. It suggests the effect of SOI on the occurrence of fire is not

direct, but there is a two month delay. On the other hand, the peak of correlation coefficient of precipitation and FHS in Kalteng occurs at the same month, that is it has a lag of 0, while the peak of correlation coefficient of precipitation and FHS in Riau has a lag of 2 months. Vegetation responds to the soil water content but there is a delay between the time of rain and the response of plants in terms of their growth and greenness. This leads to the delay in the effect of rainfall on the fire activity trends.

4.2 Conclusion

Four affected parameters have been discussed in relation to detecting fire using MODIS data over Indonesia. Cloud coverage, vegetation cover types, seasons (wet and dry) and climate parameters (SOI and precipitation) have shown to impact the number of occurring FHS in different manners. All those parameters described impact the reported number of FHS detected by remote sensing fire algorithms. With respect to the results of this research, reporting the trend of fire activity needs accurate data, preferably those that have been validated. In this research we attempt to analyse the validation methods based on high resolution SPOT image data and ground data. SPOT data, as high spatial resolution remote sensing imagery, have the potential to be used in the validation method of MODIS fire detection products. However, the SPOT satellite does not have a thermal infrared band so it cannot detect the heat of fire pixels from its digital data. Instead, the recognition of active fire is made by visual investigation through the manipulation of image composition. Liew et al. (2003) validated MOD14 results using SPOT data over Sumatra and Borneo based on exhibited smoke plumes coming from fires. Some fire may not produce obvious smoke plumes and this matter is difficult to overcome in validation. Observing land color visually is confusing and not reliable to detect fires occurring with no smoke plumes on them.

Validation using ground data is considered as the best method to validate the results of remotely sensed fire detection activity. But often ground data checking is impractical, especially for the large areas and the difficult terrain encroached upon by people. This issue leads to limited ground data becoming available which constrains the reliability in the statistical consideration. Fire observation in-situ

data are not periodically and properly recorded by responsible agencies so when the data are needed they cannot provide them appropriately. As an example, in the year 2011 there are only 7 months of recorded ground data from the local forestry agency of Central Kalimantan province, as shown in Table 3.14. Those data only contain 202 ground data points compared to 6705 detected FHS by the IndoFire system. In other words, the availability of ground validation data is about 6.4% of the occurring FHS which we desire to be validated, and this amount is not reliable to make a reasonable justification of the accuracy of detection based on available in-situ data. We have shown that none of the collected fire ground data points were able to be matched to the FHS locations detected by both the MOD14 and IndoFire algorithms.

However, in this thesis we have undertaken several approaches to analyse and describe the fire activity characteristics. The activities which have been conducted are:

- Analysed the patterns of detected FHS and cloud cover for a decade over Indonesia for both yearly and monthly data. We developed a method to estimate the number of fires under cloud cover which are not able to be directly detected. The estimation number is calculated by extrapolation from the FHS number related to the fraction of cloud cover. We found that the extrapolation numbers of yearly FHS which are derived from yearly FHS data are higher compared to the yearly FHS which are derived from the number of monthly FHS data. So the estimation FHS numbers from the monthly data is recommended as more reliable than referring to the yearly FHS data.
- Investigated the fire activity over 16 different vegetation cover classes for the year 2009. The results show that the low vegetation types are prone to be burned more compared to the high vegetation classification; thus the awareness of fire management should be directed more at the low vegetation areas.
- Determined the detection responses of the MOD14 algorithm applied to MODIS data over Indonesia for 2009, a period considered as impacted by a moderate El-Nino effect. Seasonal investigations showed that the MOD14 algorithm applied to dry season data is more sensitive to changes in the threshold value at a higher

threshold value compared to changes in the threshold for the wet season MODIS data over Indonesia.

- Calculated the correlation coefficient relationship between FHS number and precipitation level. The calculation of the coefficient relationship between FHS and SOI was also carried out. The coefficient relationship values indicated that precipitation and SOI have delayed effects to the fire activity, with a delay period of approximately 2 months.

4.3 Further Work

The work presented in this thesis has not been considered complete due to the time and financial limitations. We have estimated the FHS number with respect to the cloud cover existence, analysed the impact of vegetation cover on fire activity, analysed the sensitivity detection of the MOD14 algorithm, and related the precipitation level to the detected FHS number. All those aspects could be continued by the suggestions of further work as listed below.

- Providing an accurate result of fire detection needs reliable and robust validation work for the accuracy of fire detection results. Improved validation will lead to a stronger justification for how reliable the reported fire activity patterns are.
- Analyse the relationship of cloud cover and precipitation level so it contributes to the estimation of the reported FHS number extrapolation. Usually, frequent thick cloud occurrence indicates the potential of high precipitation levels. Rainfall will likely decrease the existing fire and reduce the number of occurring active fires. So the cloud cover-rainfall relationship will refine the estimation of reported FHS number.
- Create a uniform and reliable information system of ground truth data of fire occurrences which will benefit a reliable fire detection validation method.
- Perform coordinated and collaborated research between research agencies such as LAPAN and local forestry agencies to provide reliable data related to the fire monitoring and management (prevention and suppression).

- Integrate the information of a fire danger rating system (FDRS) with vegetation cover information and climate parameters (precipitation, cloud cover, and wind direction) to give people warning of possible fire hazards.

REFERENCES

ADB, and BAPPENAS. 1999. Causes, Extent, Impact and Costs of 1997/98 Fires and Drought. In *Final Report*.

Adiningsih, Erna Sri. 2003. Model Prediksi Dampak El-Nino / La-Nina untuk Mitigasi Bencana Kebakaran Hutan. In *RUT X 2003*: Pusbangja LAPAN.

Aldhous, P. 2004. Borneo is Burning. *Nature* 432, 144-146.

Anonymous. 2010a. Klasifikasi penutup lahan. edited by B. S. Nasional. Jakarta - Indonesia: BSN.

Anonymous. 2010b. *SPOT satellite technical data*. http://www2.astrium-geo.com/files/pmedia/public/r329_9_spotsatellitetechnicaldata_en_sept2010.pdf. Accessed: 15-01-2013.

As-syakur, Abd. Rahman. 2008. Pola spasial pengaruh kejadian La-Nina terhadap curah hujan di indonesia tahun 1998/1999; observasi menggunakan data TRMM multisatellite precipitation analysis(TMPA) 3B43, Conference Proceedings of *Pertemuan Ilmiah Tahunan MAPIN XVII "Teknologi Geospasial Untuk Ketahanan Pangan dan Pembangunan Berkelanjutan"* December 10, at Aula Timur ITB, Jalan Ganesa 10 Bandung.

Australian-Government, Department of the Environment of. 2013. *Kyoto protocol*. http://www.climatechange.gov.au/international/negotiations/history-negotiations/kyoto-protocol. Accessed: 20-01-2014.

Ballhorn, Uwe, Florian Siegert, Mike Mason, and Suwido Limin. 2009. Derivation of burn scar depths and estimation of carbon emissions with LIDAR in Indonesian peatlands. *PNAS (Proceedings of the National Academy of Science) of the United States of America* 106 (50), 21213–21218.

BAPLAN, (Forestry Planning Agency). 2006. Forest Resources Monitoring in Indonesia. In *FRMA Document Serial*.

Bucini, Gabriela, and Eric F. Lambin. 2002. Fire impacts on vegetation in Central Africa: a remote-sensing-based statistical analysis. *Applied geography* 22, 27-48.

Cahoon, Donald DR, Brian J Stocks, Joel S. Levine, Wesley R. Cofer, and Katherine P. O'neil. 1992. Seasonal distribution of African savanna fires. *Nature* 359, 812 - 815.

Cahyono, Bowo E., Peter Fearns, and Brendon McAtee. 2013. Application of MODIS Data to A Decadal Study of Fire Hotspots and Climate Relationships Over Riau Province Indonesia. *Asian Journal of Applied Science* 1 (1), 31-37.

Campbell, James B. 2002. *Introduction to Remote Sensing*. 3 rd ed. The Guildford Press, New York.

Cardoso, Manoel F., George C. Hurtt, Berrien Moore, Carlos A. Nobre, and Heather Bain. 2005. Field work and statistical analyses for enhanced interpretation of satellite fire data. *Remote Sensing of Environment* 96, 212 - 227.

Christopher, Justice, Giglio Louis, Boschetti Luigi, Roy David, Csiszar Ivan, Morisette Jeffrey, and Kaufman Yoram. 2006. Algorithm Technical Background Document: MODIS fire products. *ATBD-MOD14* Version 2.3 (EOS ID# 2741), 1-34.

Chuvieco, Emilio. 1999. *Remote Sensing of Large Wildfires in the European Mediterranean Basin*. Springer, Berlin-Heidelberg.

Chuvieco, Emilo, and Alfredo Huete. 2010. *Fundamentals of Satellite Remote Sensing*. CRC Press, New York.

Codata. 2010. *Fundamental Physical Constants*. http://physics.nist.gov/cgi-bin/cuu/Value?bwien|search_for=wien+displacement+constant. Accessed: 15-06-2013.

CRISP. 2001. *Fire Monitoring using MODIS*, CRISP-NUS. http://www.crisp.nus.edu.sg/~research/modis_fire/modis_fire.htm. Accessed: 14-05-2013.

Crutzen, PJ, and MO Andreae. 1990. Biomass burning in the tropics - impact on atmospheric chemistry and biogeochemical cycles. *Science* 250 (4988), 1669-1678.

Dayamba, Sidzabda Djibril, Patrice Savadogo, Didier Zida, Louis Sawadogo, Daniel Tiveau, and Per Christer Oden. 2010. Fire temperature and residence time during dry season burning in a Sudanian savanna-woodland of West

Africa with implication for seed germination. *Journal of Forestry Research* 21 (4), 445−450.

Devineau, Jean-Louis, Anne Fournier, and Saibou Nignan. 2010. Savanna fire regimes assessment with MODIS fire data: Their relationship to land cover and plant species distribution in western Burkina Faso (West Africa). *Journal of Arid Environments* 74, 1092-1101.

Dwiyono, A, and Rachman. 1996. Management and conservation of the tropical peat forest of Indonesia. In: Maltby, E., Immirzi, C.P. and Safford, R.J. (eds). Tropical lowland peatlands of southeast Asia. *Proceedings of a workshop on integrated planning and management of tropical lowland peatlands held at Cisarua, Indonesia* 3-8 July 1992. IUCN, Gland, Switzerland.

FAO. 2001. Global Forest Resources Assessment 2000. In *Main Report. FAO Forestry Paper - 140*

Flannigan, M.D., and T.H. Vonder Haar. 1986. Forest fire monitoring using NOAA satellite AVHRR. *Canadian Journal for Forest Resources* 16, 975-982.

Flasse, S. P., and P. Ceccato. 1996. A contextual algorithm for AVHRR fire detection. *International Journal of Remote Sensing* 17 (2), 419-424.

Fuller, D. O., and M. Fulk. 2001. Burned area in Kalimantan, Indonesia mapped with NOAA-AVHRR and Landsat TM imagery. *International Journal of Remote Sensing* 22 (4), 691-697.

Giglio, L., J. D. Kendall, and C. O. Justice. 1999. Evaluation of global fire detection algorithms using simulated AVHRR infrared data. *International Journal of Remote Sensing* 20 (10), 1947-1985.

Giglio, L., J. D. Kendall, and C. J. Tucker. 2000. Remote sensing of fires with the TRMM VIRS. *International Journal of Remote Sensing* 21 (1), 203-207.

Giglio, Louis. 2005. MODIS Collection 4 Active Fire Product User's Guide Version 2.2. *Science Systems and Applications, Inc.*, 1-42.

Giglio, Louis. 2007. Characterization of the tropical diurnal fire cycle using VIRS and MODIS observations. *Remote Sensing of Environment* 108 (4), 407-421.

Giglio, Louis, I. Csiszar, and C. O. Justice. 2006. Global distribution and seasonality of active fires as observed with the Terra and Aqua Moderate Resolution Imaging Spectroradiometer (MODIS) sensors. *Journal of geophysical research: Biogeosciences* 111 (G02016), 1-12.

Giglio, Louis, Jacques Descloitres, Christoper O. Justice, and Yoram J. Kaufman. 2003. An Enhanced Contextual Fire Detection Algorithm for MODIS. *Remote Sensing of Environment* 87, 273-282.

Giglio, Louis, Tatiana Loboda, David P. Roy, Brad Quayle, and Christopher O. Justice. 2009. An active-fire based burned area mapping algorithm for the MODIS sensor. *Remote Sensing of Environment* 113 (2), 408-420.

Goessmann, Florian. 2007. *Improved Spatial Resolution of Bushfire Detection with MODIS*. MSc. thesis, Department ofApplied Physics, Curtin University, Perth.

Harris, Nancy L, Silvia Petrova, Fred Stolle, and Sandra Brown. 2008. Identifying optimal areas for REDD intervention: East Kalimantan, Indonesia as a case study. *Environmental Research Letters* 3 (3), 1-11.

Hawbaker, Todd J., Volker C. Radeloff, Alexandra D. Syphard, Zhiliang Zhu, and Susan I. Stewart. 2008. Detection rates of the MODIS active fire product in the United States. *Remote Sensing of Environment* 112 (5), 2656-2664.

Hoffmann, Anja A., Alexander Hinrichs, and Florian Siegert. 1999. Fire Damage in East Kalimantan in 1997/98 Related to Land Use and Vegetation Classes: Satellite RADAR Inventory Results and Proposal for Further Actions. In *Technical Cooperation between Indonesia and Germany*.

Indofire. 2007. *IndoFire Map Service*, Landgate, WA. http://indofire.landgate.wa.gov.au/indofire.asp. Accessed: 11-04-2011.

Irianto, Gatot. 2003. Implikasi Penyimpangan Iklim Terhadap Tataguna Lahan. In *Makalah pada Seminar Nasional Ilmu Tanah dengan tema Menggagas Strategi Alternatif dalam Menyiasati Penyimpangan Iklim serta Implikasinya pada Tataguna Lahan dan Ketahanan Pangan Nasional*. Universitas Gajah Mada, Yogyakarta.

Jaenicke, J., J.O. Rieley, C. Mott, P. Kimman, and F. Siegert. 2008. Determination of the amount of carbon stored in Indonesian peatlands. *Geoderma* 147, 151–158.

Jaenicke, Julia, Henk Wösten, Arif Budiman, and Florian Siegert. 2010. Planning hydrological restoration of peatlands in Indonesia to mitigate carbon dioxide emissions. *Mitig Adapt Strateg Glob Change* 15, 223–239.

Jarraud, M. 2005. *Climate and land degradation*. Vol. 989. World Meteorological Organization (WMO) United Nation, Switzerland.

Johnson, Joel T. 2002. Brightness Temperature of a Flat Water Surface.

Justice, C., and P. Dowty. 1994. Technical Report of the IGBP-DIS Satellite Fire Detection. *Paris: IGBP-DIS*.

Justice, C.O., L. Giglio, S. Korontzi, J. Owens, J.T. Morisette, D. Roy, J. Descloitres, S. Alleaume, F. Petitcolin, and Y. Kaufman. 2002. The MODIS fire products. *Remote Sensing of Environment* 83, 244–262.

Kant, Yogesh, V. Krishna Prasad, and K.V.S. Badarinath. 2000. Algorithm for detection of active fire zones using NOAA-AVHRR data. *Infrared Physics & Technology* 41, 29-34.

Kauffman, J. B., and C. Uhl. 1990. Interactions of Anthropogenic Activities, Fire, and Rain Forests in the Amazon Basin: Springer Berlin Heidelberg.

Kaufman, Yoram J., Christopher O . Justice, Luke P. Flynn, Jackie D. Kendall, Elaine M. Prins, Louis Giglio, Darold E. Ward, W. Paul Menzel, and Alberto W. Setzer. 1998. Potential global fire monitoring from EOS-MODIS. *Journal of Geophysical Research* 103 (D24), 32215-32238.

Kaufman, Yoram J., Richard G. Kleidman, and Michael D. King. 1998. SCAR-B fires in the tropics: Properties and remote sensing from EOS-MODIS. *Journal of Geophysical Research* 103 (D24), 31955-31968.

Kaufman, Yoram J., Compton J. Tucker, and Inez Fung. 1990. Remote Sensing of Biomass Burning in the Tropics. *Journal of Geophysical Research* 96 (D7), 9927-9939.

Kishore, Kamal, A.R. Subbiah, Tien Sribimawati, Sri Diharto, Sutarto Alimoeso, Peter Rogers, and Adang Setiana. 2000. Indonesia Country Study. http://archive.unu.edu/env/govern/ElNIno/CountryReports/pdf/indonesia.pdf.

Landgate. 2007. *Indofire*. http://indofire.landgate.wa.gov.au/. Accessed: 11-04-2011.

Langaas, Sindre. 1992. Temporal and Spatial Distribution of Savanna Fires in Senegal and The Gambia, West Africa, 1989-90, Derived from Multi-temporal AVHRR Night Images. *International Journal of Wildland Fire* 2 (1), 21-36.

Langner, Andreas , and Florian Siegert. 1996. Number of fire hotspots in Borneo (detected by NOAA, ATSR & MODIS) 1997-2006. http://www.restorpeat.alterra.wur.nl/download/Fires%20in%20Indonesia%201997-2006%20Hotspots%20RSS.pdf. Accessed: 30-06-2010.

Langner, Andreas Johanes. 2009. *Monitoring Tropical Forest Degradation and Deforestation in Borneo, Southeast Asia*.

Langner, Andreas, Jukka Miettinen, and Florian Siegert. 2007. Land cover change 2002-2005 in Borneo and the role of fire derived from MODIS imagery. *Global Change Biology* 13 (11), 2329.

Langner, Andreas, and Florian Siegert. 2006. Fires in Kalimantan and Sumatra 2006. http://www.restorpeat.alterra.wur.nl/download/Fires%20in%20Indonesia%202006%20RSS.pdf. Accessed: 29-06-2010.

Langner, Andreas, and Florian Siegert. 2009. Spatiotemporal fire occurrence in Borneo over a period of 10 years. *Global Change Biology* 15, 48-62.

Levin, Noam. 1999. *Fundamentals of Remote Sensing*. International Maritime Academy, Trieste, Italy.

Levine, Joel S., ed. 1995. *Introduction* Edited by J. S. Levine. Vol. 1, *Biomass Burning and Global Change*. MIT Press, London.

Li, Z., Y. J. Kaufman, C. Ichoku, R. Fraser, A. Trishchenko, L. Giglio, J. Jin, and X. Yu. 2000. A Review of AVHRR-based Active Fire Detection Algorithms: Principles, Limitations, and Recommendations. Ottawa, Canada.

Li, Z., S. Nadon, J. Cihlar, and B. Stocks. 2000. Satellite-based mapping of Canadian boreal forest fires: evaluation and comparison of algorithms. *International Journal of Remote Sensing* 21 (16), 3071-3082.

Liew, Soo Chin, Chaomin Shen, John Low, Agnes Lim, and Leong Keong Kwoh. 2003. Validation of MODIS fire product over Sumatra and Borneo using High Resolution SPOT Imagery. *Proc. 24th Asian Conference on Remote Sensing & 2003 International Symposium on Remote Sensing* 1, 671-673.

Lillesand, Thomas M., and Ralph W. Keifer. 2004. *Remote Sensing and Image Interpretation*. 4th ed. John Wiley & Sons, Inc, New York.

Lillesand, Thomas M., and Ralph W. Kiefer. 2000. *Remote Sensing and Image Interpretation*. 4 th ed. John Wiley & Sons, New York.

Lindsey, John. 2013. *What time of day do local temperatures peak?* , The Tribune. http://www.sanluisobispo.com/2013/06/08/2539340/what-time-of-day-do-local-temperatures.html. Accessed: 12-12-2013.

Matson, Michael, and Jeff Dozier. 1981. Identification of subresolution high temperature sources using a thermal IR sensor. *Photogrammetric Engineering and Remote Sensing* 47 (9), 1311-1318.

Menzel, W. P., and Elaine Prins. 1996. Monitoring biomass burning with the new geostationary satellites. In *Biomass burning and global change: Remote sensing, modeling and inventory dvelopment, and biomass burning in Africa*, edited by J. S. Levine. Cambridge: MIT press.

Miettinen, J., and S. C. Liew. 2005. Connection between fire and land cover change in Southeast Asia: a remote sensing case study in Riau, Sumatra. *International Journal of Remote Sensing* 26 (6), 1109-1126.

Miettinen, Jukka, A. Hooijer, C. Shi, D. Tollenaar, R. Vernimmen, Soo Chin Liew, C. Malins, and S.E. Page. 2012. Extent of industrial plantations on Southeast Asian peatlands in 2010 with analysis of his-torical expansion and future projections. *Global Change Biology (GCB) Bioenergy* 4, 908-918.

Miettinen, Jukka, and Soo Chin Liew. 2003. Connection between Fire and Land Cover Change in Riau Province, Sumatra from 1998 to 2002. *IEEE*, 2496-2498.

Mongabay. 2010a. *Rainforest: Structure and Characters*. http://rainforests.mongabay.com/0201.htm. Accessed: 01-07-2010.

Mongabay. 2010b. *Tropical Rainforest of The World*. http://rainforests.mongabay.com/0101.htm. Accessed: 20-06-2010.

Mongabay. 2010c. *Tropical Rainforest of The World (Section 1)* http://rainforests.mongabay.com/0101.htm. Accessed: 26-06-2010.

Morisette, Jeffrey T., Louis Giglio, Ivan Csiszar, and Christopher O. Justice. 2005. Validation of the MODIS active fire product over Southern Africa with ASTER data. *International Journal of Remote Sensing* 26 (19), 4239 - 4264.

Morisette, Jeffrey T., Louis Giglio, Ivan Csiszar, Alberto Setzer, Wilfrid Schroeder, Douglas Morton, and Christopher O. Justice. 2005. Validation of MODIS Active Fire Detection Products Derived from Two Algorithms. *Earth Interactions* 9 (9), 1-25.

MWH-Indonesia. 2005. Country Environmental Profile Indonesia. *Final Report*, 1-66.

Nakayama, M., M. Maki, C. D. Elvidge, and S. C. Liew. 1999. Contextual algorithm adapted for NOAA-AVHRR fire detection in Indonesia. *International Journal of Remote Sensing* 20 (17), 3415-3421.

NASA. 2013. *MS2GT: The MODIS Swath-to-Grid Toolbox*, NASA Goddard Space Flight Center. http://gcmd.nasa.gov/records/MS2GT.html. Accessed: 15-04-2014.

Nicholson, Sharon E., Michael L. Davenport, and Ada R. Malo. 1990. A comparison of the vegetation response to rainfall in the Sahel and East Africa, using Normalized Difference Vegetation Index from NOAA AVHRR. *Climate Change* 17, 209-241.

NOAA. 2014. *UV index information: Diurnal Variability* Mac Donald - USA, National Weather Service: Climate Prediction Center. http://www.cpc.ncep.noaa.gov/products/stratosphere/uv_index/uv_diurnal.shtml. Accessed: 09-10-2014.

NOVA, (Science in the News). 2010. *Carbon currency – the credits and debits of carbon emissions trading*. http://www.science.org.au/nova/054/054key.htm. Accessed: 26-06-2010.

Page, Susan E., Florian Siegert, John O. Rieley, Hans-Dieter V. Boehm, Adi Jayak, and Suwido Limin. 2002. The amount of carbon released from peat and forest fires in Indonesia during 1997. *Nature* 420, 61-65.

Page, Susan, and Jack Riley. 2004. Wise Use of Tropical Peatlands: is restoration necessary and feasible? : University of Nothingham.

Pallant, Julie. 2011. *SPSS Survival Manual*. 4th ed. Allen & Unwin, New South Wales.

Philip, Susan. 2007. *Active Fire Detection Using Remote Sensing Based Polar-Orbitingand Geostationary Observations: An Approach Towards Near Real-Time Fire Monitoring*. MSc. thesis, International Institute for Geo-information Science and Earth Observation, Enschede, The Netherlands.

Prins, Elaine M., Joleen M. Feltz, W. Paul Menzel, and Darold E. Ward. 1998. An overview of GOES-8 diurnal fire and smoke results for SCAR-B and 1995 fire season in South America. *JOURNAL OF GEOPHYSICAL RESEARCH* 103 (D24), 31,821-31,835.

Prins, Elaine M., and W. Paul Menzel. 1992. Geostationary satellite detection of bio mass burning in South America. *International Journal of Remote Sensing* 13 (15), 2783-2799.

Prins, Elaine M., and W. Paul Menzel. 1994. Trends in South American biomass burning detected with the GOES visible infrared spin scan radiometer atmospheric sounder from 1983 to 1991. *Journal of Geophysical Research* 99 (D8), 16,719-16,735.

REDD-Indonesia. 2011a. *World Bank: Environmental governance and climate change mitigation and adaptation identified as key challenges*. http://www.reddindonesia.com/?p=16. Accessed: 06-01-2011.

REDD-Indonesia. 2011b. *World Bank: Protect Forest*. http://www.reddindonesia.com/?p=17. Accessed: 06-01-2011.

Rees, William Gareth. 2001. *Physical Principles of Remote Sensing*. 2nd ed. Cambridge University Press, Cambridge.

Rice, Barry. 2012. *Atmospheric windows*. http://www.sarracenia.com/astronomy/remotesensing/physics060.html. Accessed: 07-03-2012.

Richards, John A., and Xiuping Jia. 2006. *Remote Sensing Digital Image Analysis: An Introduction*. 4th ed. Springer, Berlin - Germany.

Riley, Jack. 2006. Wise Use of Tropical Peatland: A New Approach to Old problems. In *Seminar of Restoration and Wise Use of Tropical Peatlands*. Can Tho University in Vietnam.

Roach, John, Jack Riley, and Larry Smith. 2004. *Indonesia Peat Fires May Fuel Global Warming*, National Geographic News. http://news.nationalgeographic.com.au/news/2004/11/1111_041111_indonesia_fires.html. Accessed: 04-06-2010.

Roberts, G., M. J. Wooster, and E. Lagoudakis. 2009. Annual and diurnal african biomass burning temporal dynamics. *Biogeosciences* 6, 849-866.

Robinson, Jennifer M. 1991. Fire from space: Global fire evaluation using infrared remote sensing. *International Journal of Remote Sensing* 12 (1), 3 - 24.

Ruchiat, Yayat. 2001. Penyebab dan Dampak Kebakaran Hutan dan Lahan: Studi Kasus Tumbang Titi, Kabupeten Ketapang, Kalimantan Barat. *Center for International Forestry Research (CIFOR)*, 1-8.

Sabins, Floyd F. 1987. *Remote Sensing: Principles and Interpretation*. 2nd ed. W.H. Freeman and Company, New York.

Saharjo, Bambang Hero. 2004. Forest and Land Fire Management in Peatland Areas. In *Climate Change, Forests and Peatlands in Indonesia*.

Savadogo, Patrice. 2012. *Seasonal variation in fire temperature and influence on soil CO2 efflux, root biomass, and soil water properties in a Sudanian savanna-woodland, West Africa*, CSIRO Australia. http://www.thefreelibrary.com/Seasonal+variation+in+fire+temperature+and+influence+on+soil...-a0295258407. Accessed: 28-04-2013.

Schwemlein, Doug J., and Roger A. Williams. 2006. Effects of landscape position and season of burn on fire temperature in Southern Ohio's oak forests, Conference Proceedings of *Proceedings of the 15th Central Hardwood Forest Conference*, 250-257. February 27–March 1, 2006, at Knoxville, TN.

Seielstad, C.A., J.P. Ridderlng, S.R. Brown, L.P. Queen, and W.M. Hao. 2002. Testing the Sensitivity of a MODIS-Like Daytime Active Fire Detection Model in Alaska Using NOAA/AVHRR Infrared Data. *Photogrammetric Engineering & Remote Sensing* 68 (8), 831-838.

Siegert, F., G. Ruecker, A. Hinrichs, and A. A. Hoffmann. 2001. Increased damage from fires in logged forests during droughts caused by El Nino. *Nature* 414.

Siegert, Florian. 2008. *Deforestation, Forest Degradation, Biodiversity Loss, and CO2 Emissions in Riau, Sumatra, Indonesia*. Personal.

Siegert, Florian, and Anja A. Hoffmann. 2000. *The 1998 Forest Fires in East Kalimantan (Indonesia): A Quantitative Evaluation Using High Resolution, Multitemporal ERS-2 SAR Images and NOAA-AVHRR Hotspot Data*, Remote Sensing of Environment.

Sizer, Nigel, Andrew Leach, Susan Minnemeyer, Mark Higgins, Fred Stolle, James Anderson, and Julius Lawalata. 2014. *Preventing Forest Fires in Indonesia: Focus on Riau Province, Peatland, and Illegal Burning*, World Resources Institute. http://www.wri.org/blog/2014/04/preventing-forest-fires-indonesia- focus-riau-province-peatland-and-illegal-burning. Accessed: 24-09-2014.

Steber, Mike. 2013. *Indofire System for Fire Detction in Indonesia*. Personal communication. Perth.

Strack, Maria. 2008. *Peatlands and climate change*. International Peat Society, Finland.

Tacconi, Luca. 2003. Fires in Indonesia : Causes, Costs and Policy Implications. In *Center for International Forestry Research (CIFOR) Occasional Paper No. 38*. Bogor Indonesia.

Tanpipat, Veerachai, Kiyoshi Honda, and Prayoonyong Nuchaiya. 2009. MODIS hotspot validation over Thailand. *Remote Sensing* 1 (4), 1043-1054.

Tansey, K., J. Beston, A. Hoscilo, S. E. Page, and C. U. Paredes Hernandez. 2008. Relationship between MODIS fire hotspot count and burned area in a degraded tropical peat swamp forest in Central Kalimantan, Indonesia. *Journal of Geophysical Research* 113 (D23112).

Thoha, Achmad Siddik. 2008. Penggunaan data hotspot untuk monitoring kebakaran hutan dan lahan di Indonesia. Medan - Indonesia: Departemen Kehutanan-Fakultas Pertanian Universitas Sumatera Utara

Thoumi, Gabriel. 2009. *Indonesia: Kalimantan's Lowland Peat Forests Explained*, Mongabay.com. http://news.mongabay.com/2009/1204-thoumi_kalimantan.html. Accessed: 07-06-2010.

Tomich, Thomas P., Meine van Noordwijk, Stephen A. Vosti, and Julie Witcover. 1998. Agricultural development with rainforest conservation: methods for seeking best bet alternatives to slash-and-burn, with applications to Brazil and Indonesia. *Agricultural Economics* 19, 159-174.

Tso, Brandt, and Paul L. Mather. 2009. *Classification Methods for Remotely Sensed Data*. 2nd ed. CRC Press, New York.

Tulbure, Mirela G., Michael C. Wimberly, David P. Roy, and Geoffrey M. Henebry. 2011. Spatial and temporal heterogenity of agricultural fires in the central United States in relation to land cover and land use. *Lanscape Ecology* 26, 211-224.

Vetrita, Yenni, Nanik Suryo Haryani, and M.Rokhis Komaruddin. 2012. Validasi hotspot MODIS Indofire di Propinsi Riau. *Jurnal Geomatika* 18 (1), 1-13.

Wang, Chunzai, Clara Deser, Jin-Yi Yu, Pedro DiNezio, and Amy Clement. 2012. El Niño and Southern Oscillation (ENSO): A Review. In *Coral Reefs of the Eastern Pacific*.

Wang, Wanting, John J. Qu, Xianjun Hao, Yongqiang Liu, and William T. Sommers. 2007. An improved algorithm for small and cool fire detection using MODIS data: A preliminary study in the southeastern United States. *Remote Sensing of Environment* 108 (2), 163-170.

Wooster, M.J., G.L.W. Perry, and A. Zoumas. 2012. Fire, Drought and El Nino relationship on Borneo (Southeast Asia) in the pre-MODIS era (1980-2000). *Biogeosciences* 9, 317-340.

Yasunari, Tetsuzo. 1981. Temporal and Spatial Variations of Monthly Rainfall in Java, Indonesia. *Southeast Asian Studies* 19 (2), 170-186.

APPENDICES

Appendix 1. MODIS Spacecraft Characteristics

Orbit:	705 km, 10:30 a.m. descending node (Terra) or 1:30 p.m. ascending node (Aqua), sun-synchronous, near-polar, circular
Scan Rate:	20.3 rpm, cross track
Swath Dimensions:	2330 km (cross track) by 10° of latitude (along track at nadir)
Telescope:	17.78 cm diam. off-axis, afocal (collimated), with intermediate field stop
Size:	1.0 x 1.6 x 1.0 m
Weight:	228.7 kg
Power:	162.5 W (single orbit average)
Data Rate:	10.6 Mbps (peak daytime); 6.1 Mbps (orbital average)
Quantization:	12 bits
Spatial Resolution:	250 m (bands 1-2) 500 m (bands 3-7) 1000 m (bands 8-36)
Design Life:	6 years

MODIS Sensor Characteristics

Primary Use	Band	Bandwidth1	Spectral Radiance[2]	Required SNR[3]
Land/Cloud/Aerosols Boundaries	1	620 - 670	21.8	128
	2	841 - 876	24.7	201
Land/Cloud/Aerosols Properties	3	459 - 479	35.3	243
	4	545 - 565	29.0	228
	5	1230 - 1250	5.4	74
	6	1628 - 1652	7.3	275
	7	2105 - 2155	1.0	110
Ocean Color Phytoplankton Biogeochemistry	8	405 - 420	44.9	880
	9	438 - 448	41.9	838
	10	483 - 493	32.1	802
	11	526 - 536	27.9	754
	12	546 - 556	21.0	750
	13	662 - 672	9.5	910
	14	673 - 683	8.7	1087
	15	743 - 753	10.2	586
	16	862 - 877	6.2	516
Atmospheric Water Vapor	17	890 - 920	10.0	167
	18	931 - 941	3.6	57
	19	915 - 965	15.0	250
Surface/Cloud Temperature	20	3.660 - 3.840	0.45 (300K)	0.05
	21	3.929 - 3.989	2.38 (335K)	2.00
	22	3.929 - 3.989	0.67 (300K)	0.07
	23	4.020 - 4.080	0.79 (300K)	0.07
Atmospheric Temperature	24	4.433 - 4.498	0.17 (250K)	0.25
	25	4.482 - 4.549	0.59 (275K)	0.25

Cirrus Clouds Water Vapor	26	1.360 - 1.390	6.00	150(SNR)
	27	6.535 - 6.895	1.16 (240K)	0.25
	28	7.175 - 7.475	2.18 (250K)	0.25
Cloud Properties	29	8.400 - 8.700	9.58 (300K)	0.05
Ozone	30	9.580 - 9.880	3.69 (250K)	0.25
Surface/Cloud Temperature	31	10.780 - 11.280	9.55 (300K)	0.05
	32	11.770 - 12.270	8.94 (300K)	0.05
Cloud Top Altitude	33	13.185 - 13.485	4.52 (260K)	0.25
	34	13.485 - 13.785	3.76 (250K)	0.25
	35	13.785 - 14.085	3.11 (240K)	0.25
	36	14.085 - 14.385	2.08 (220K)	0.35

** Footnotes:*

[1] Bands 1 to 19 are in nm; Bands 20 to 36 are in µm

[2] Spectral Radiance values are (W/m^2 - µm-sr)

[3] SNR = Signal-to-noise ratio

[4] NE(delta)T = Noise-equivalent temperature difference

Note: Performance goal is 30-40% better than required.

Source link: http://modis.gsfc.nasa.gov/about/specifications.php

Appendix 2. Monthly detected fire hotspots by IndoFire over Indonesia for a decade (2001-2010)

Month	FHS number in year									
	2001	2002	2003	2004	2005	2006	2007	2008	2009	2010
January	82	263	216	866	3620	1150	600	913	1430	420
February	97	1820	276	673	7919	2015	1628	1766	1395	1672
March	607	1435	1345	779	6173	2544	1402	521	746	1266
April	176	195	309	630	1160	591	667	516	1178	744
May	407	474	1775	2600	1018	1010	839	3263	2792	1076
June	124	583	4322	6128	3640	1615	1123	1750	4439	776
July	2038	1263	3141	1768	2712	7547	2255	2814	8301	1104
August	3412	5742	8902	21067	10279	22938	5318	6620	17599	2441
September	2067	6635	9563	15167	10138	27419	9394	6440	27233	2055
October	523	13181	4860	19206	4319	38187	6181	2825	6127	3138
November	219	2904	1430	4586	901	9616	1410	938	2547	558
December	130	592	236	569	322	1913	523	274	627	275

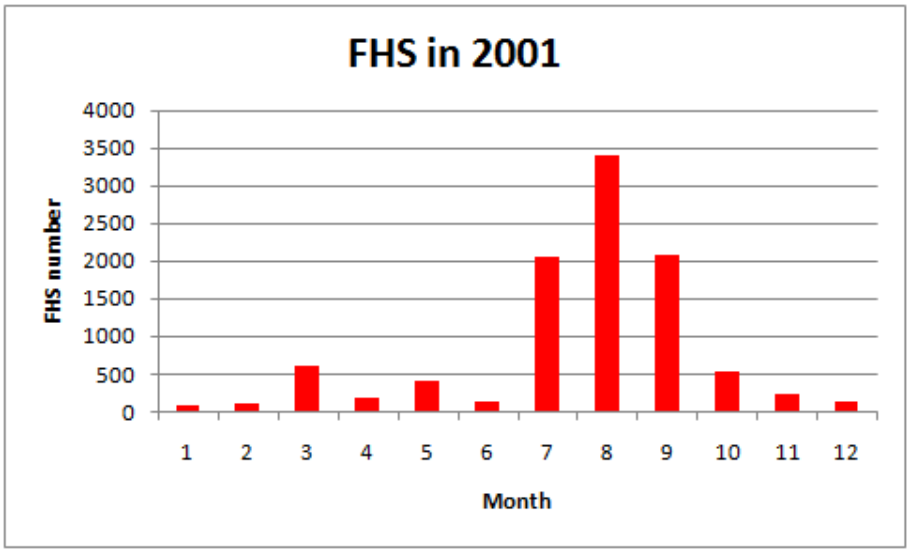

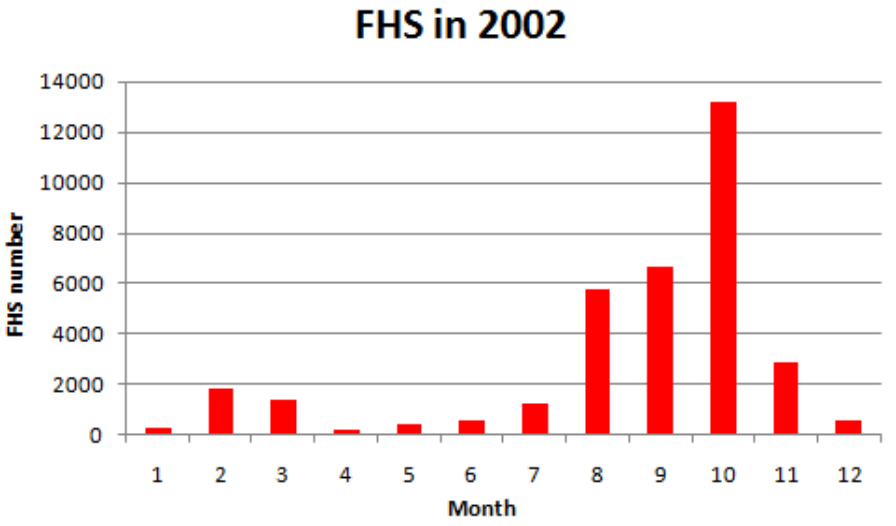
FHS in 2002
FHS number
14000
12000
10000
8000
6000
4000
2000
0
1 2 3 4 5 6 7 8 9 10 11 12
Month

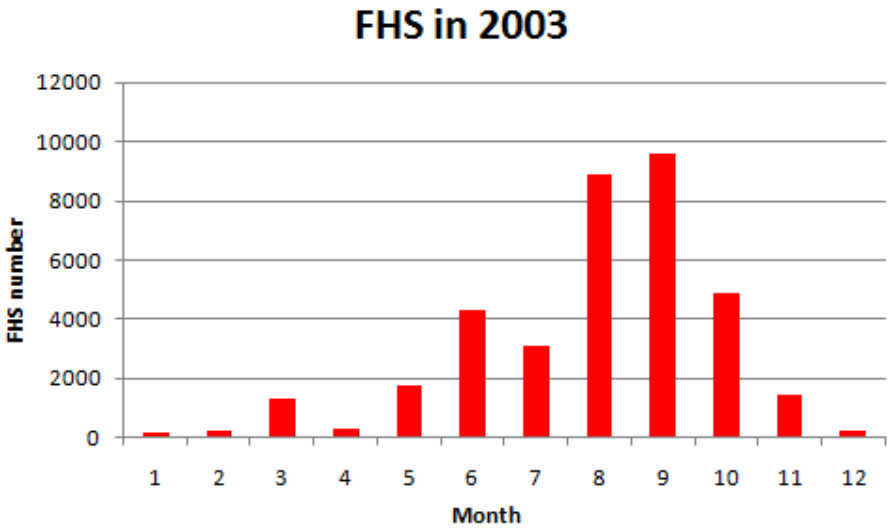
FHS in 2003
FHS number
12000
10000
8000
6000
4000
2000
0
1 2 3 4 5 6 7 8 9 10 11 12
Month

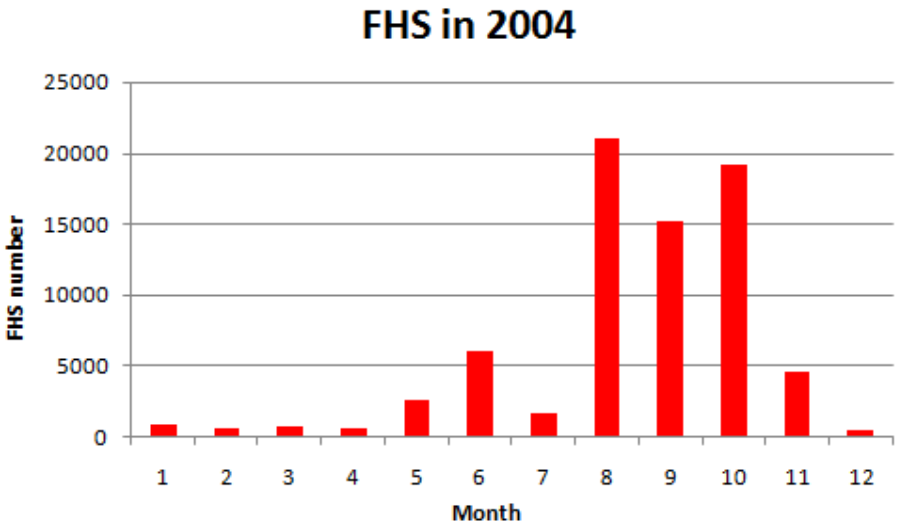
FHS in 2004
FHS number
25000
20000
15000
10000
5000
0
1 2 3 4 5 6 7 8 9 10 11 12
Month

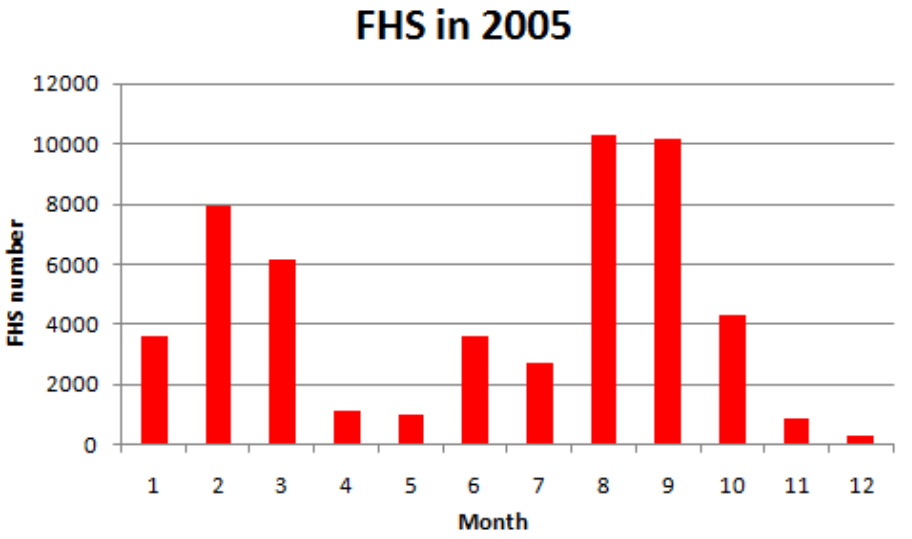
FHS in 2005
FHS number
12000
10000
8000
6000
4000
2000
0
1 2 3 4 5 6 7 8 9 10 11 12
Month

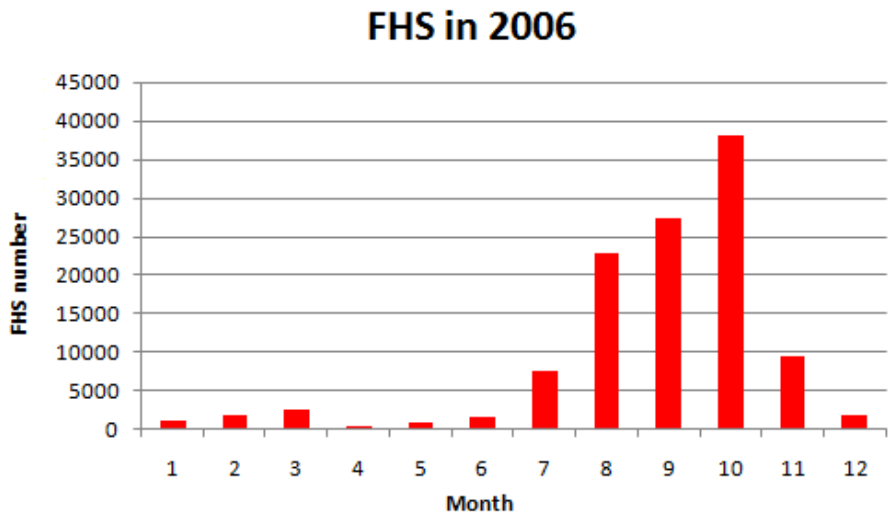
FHS in 2006
FHS number
45000
40000
35000
30000
25000
20000
15000
10000
5000
0
1 2 3 4 5 6 7 8 9 10 11 12
Month

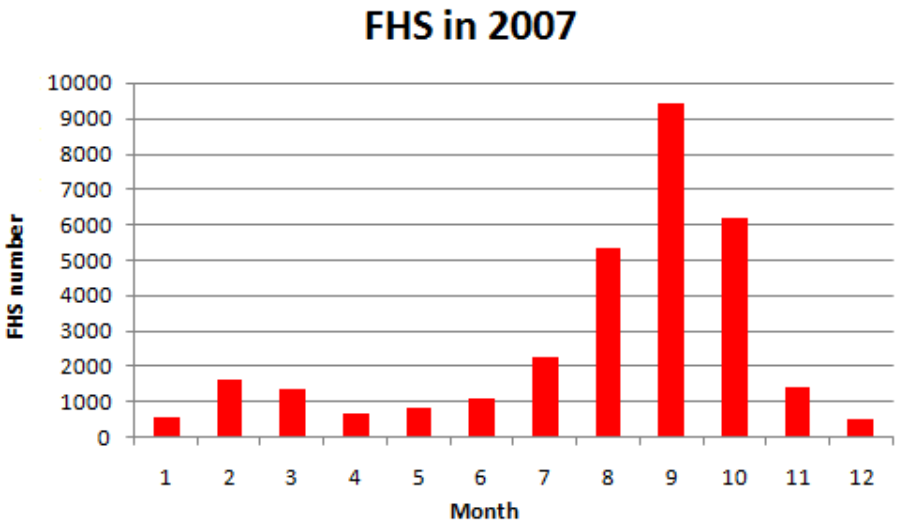
FHS in 2007
FHS number
10000
9000
8000
7000
6000
5000
4000
3000
2000
1000
0
1 2 3 4 5 6 7 8 9 10 11 12
Month

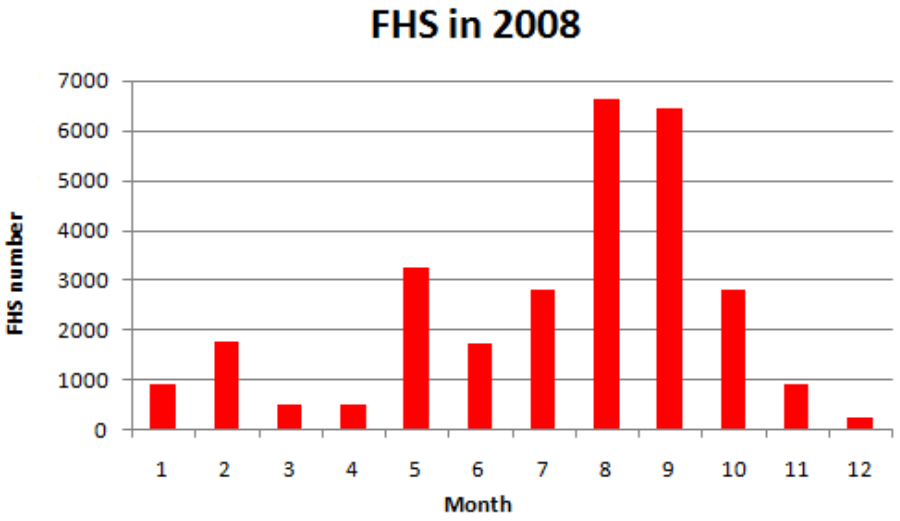
FHS in 2008
FHS number
7000
6000
5000
4000
3000
2000
1000
0
1 2 3 4 5 6 7 8 9 10 11 12
Month

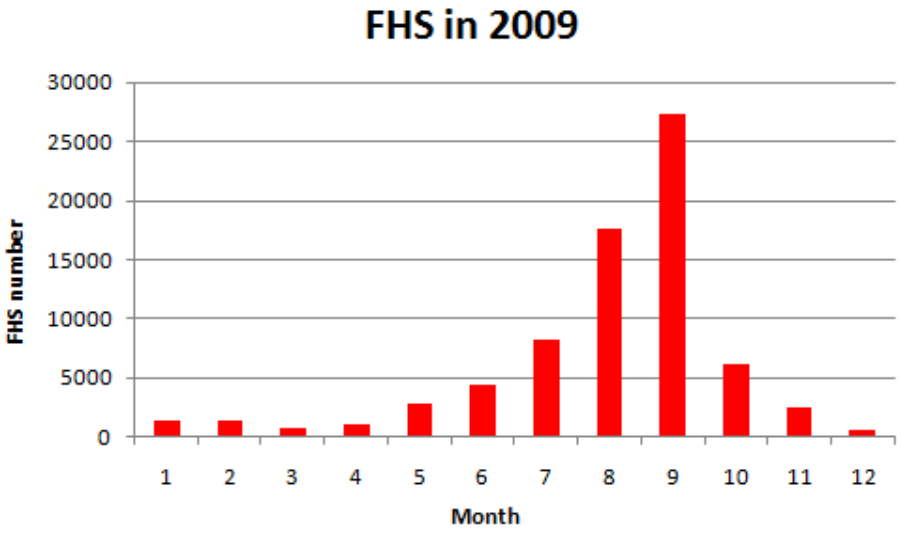
FHS in 2009
FHS number
30000
25000
20000
15000
10000
5000
0
1 2 3 4 5 6 7 8 9 10 11 12
Month

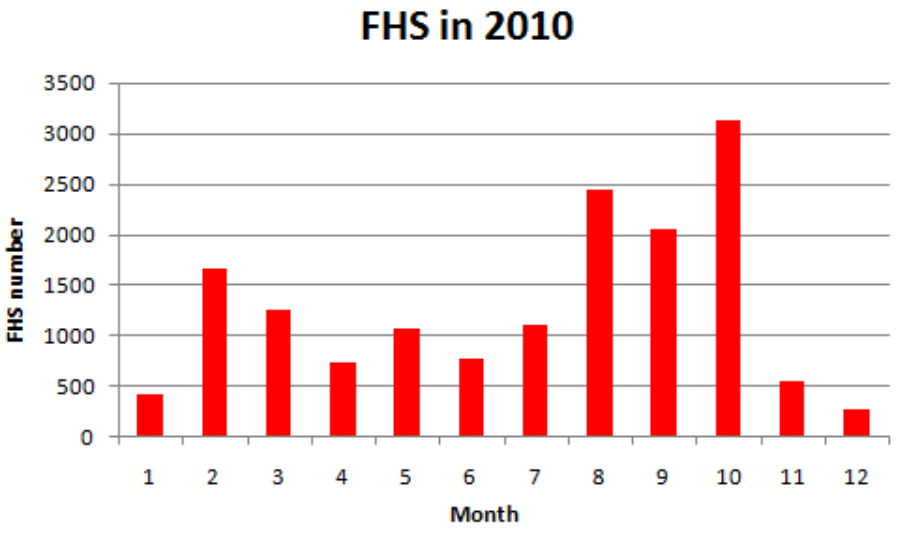
FHS in 2010
FHS number
3500
3000
2500
2000
1500
1000
500
0
1 2 3 4 5 6 7 8 9 10 11 12
Month

Appendix 3. The number of FHS in each province of Indonesia for the decade 2001-2010 detected by IndoFire system

No	Provinces	∑FHS	Area (sq.km)	FHS/Area
1	Riau	81744	87023	0.94
2	Central Kalimantan (Kalteng)	105258	153564	0.69
3	East Nusa Tenggara (NTT)	29983	48718	0.62
4	South Kalimantan (Kalsel)	21952	38744	0.57
5	South Sumatera (Sumsel)	50732	91592	0.55
6	West Nusa Tenggara (NTB)	8044	18572	0.43
7	West Kalimantan (Kalbar)	61476	147307	0.42
8	Jambi	19956	50058	0.4
9	Bangka-Belitung (Babel)	6060	16424	0.37
10	South East Sulawesi (Sultra)	11429	38067	0.3
11	Lampung	8754	34623	0.25
12	South Sulawesi (Sulsel)	10370	46717	0.22
13	North Sulawesi (Sulut)	3112	13851	0.22
14	Riau Archipelago (Kepri)	1806	8201	0.22
15	North Sumatera (Sumut)	15535	72981	0.21
16	Gorontalo	2316	11257	0.21
17	East Kalimantan (Kaltim)	27865	139462	0.2
18	East Jawa (Jatim)	9705	47799	0.2
19	Maluku	8739	46914	0.19
20	West Jawa (Jabar)	6701	35377	0.19
21	DKI Jakarta	114	664	0.17
22	West Sumatera (Sumbar)	6580	42012	0.16
23	Bengkulu	3024	19919	0.15
24	Banten	1432	9662	0.15
25	Central Sulawesi (Sulteng)	8433	61841	0.14
26	West Sulawesi (Sulbar)	2308	16787	0.14
27	DI Yogyakarta (DIY)	305	3133	0.1
28	Aceh	5301	57956	0.09
29	North Maluku (Malut)	2817	31982	0.09
30	Papua	24750	319036	0.08
31	Central Jawa (Jateng)	3310	40800	0.08
32	West Papua (Irian Barat)	1485	97024	0.02
33	Bali	120	5780	0.02

Appendix 4. Monthly detected FHS by province for the decade 2001-2010

(i)

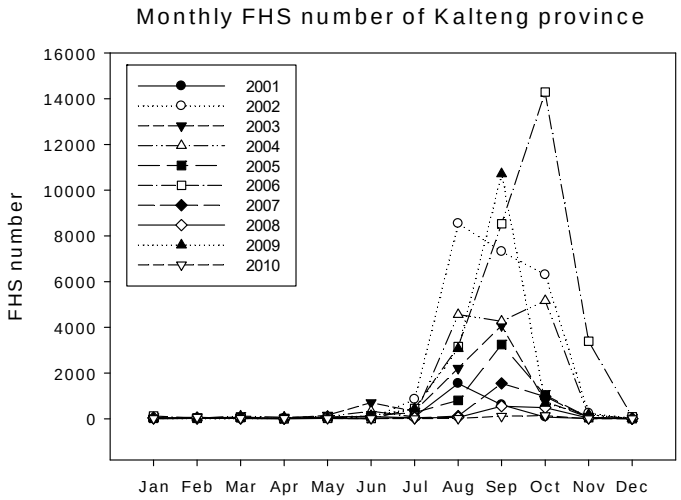

(ii)

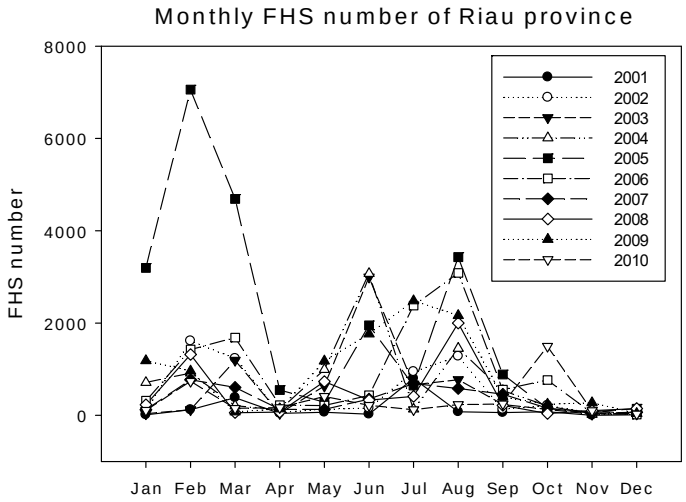

(iii)

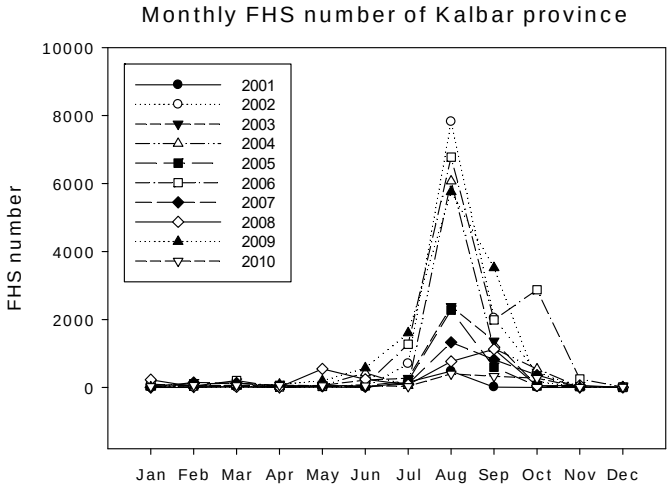

(iv)

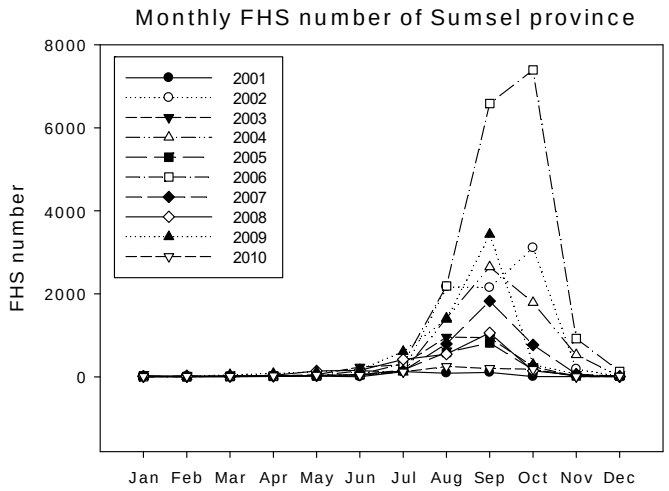
Monthly FHS number of Sumsel province
FHS number
8000
6000
4000
2000
0
2001
2002
2003
2004
2005
2006
2007
2008
2009
2010
Jan Feb Mar Apr May Jun Jul Aug Sep Oct Nov Dec

(v)

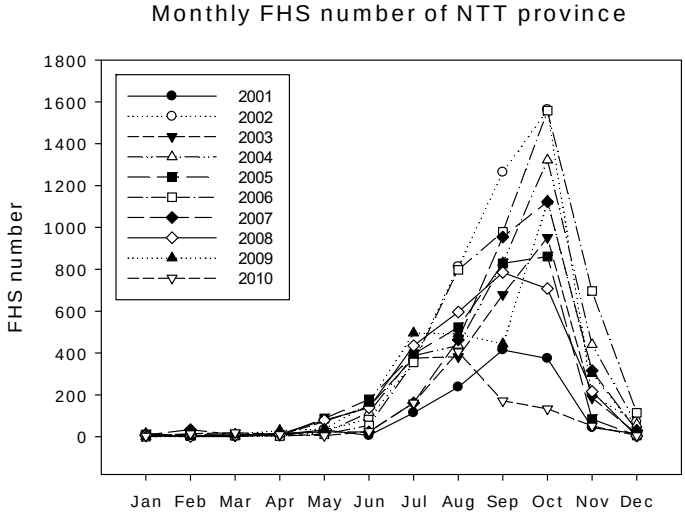
Monthly FHS number of NTT province
FHS number
1800
1600
1400
1200
1000
800
600
400
200
0
2001
2002
2003
2004
2005
2006
2007
2008
2009
2010
Jan Feb Mar Apr May Jun Jul Aug Sep Oct Nov Dec

(vi)

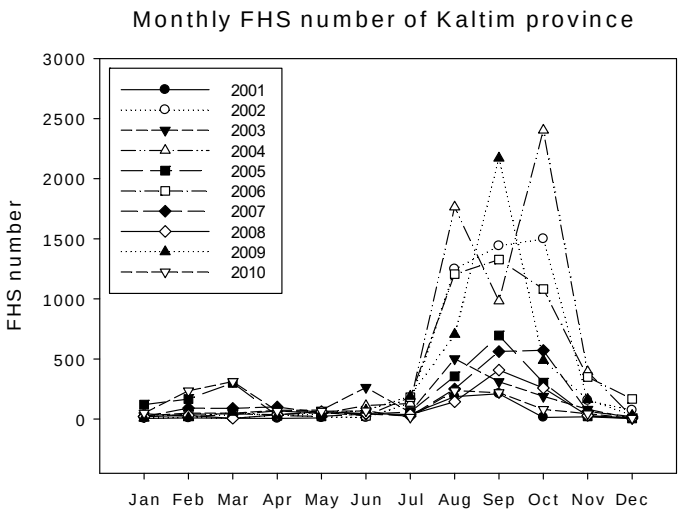
Monthly FHS number of Kaltim province
FHS number
3000
2500
2000
1500
1000
500
0
2001
2002
2003
2004
2005
2006
2007
2008
2009
2010
Jan Feb Mar Apr May Jun Jul Aug Sep Oct Nov Dec

(vii)

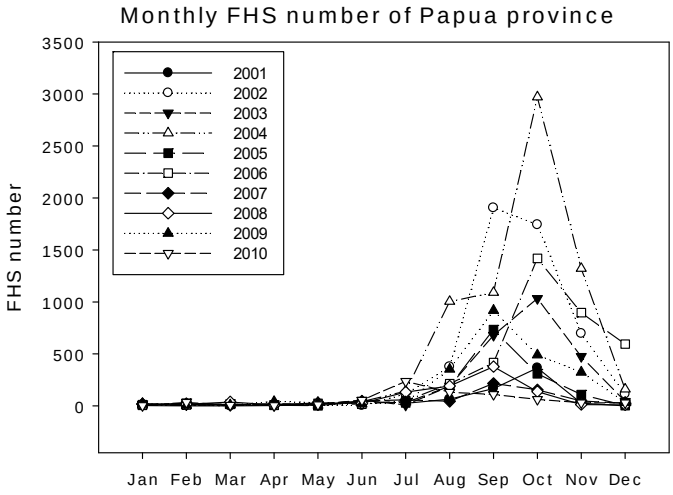
Monthly FHS number of Papua province
FHS number
3500
3000
2500
2000
1500
1000
500
0
2001
2002
2003
2004
2005
2006
2007
2008
2009
2010
Jan Feb Mar Apr May Jun Jul Aug Sep Oct Nov Dec

(viii)

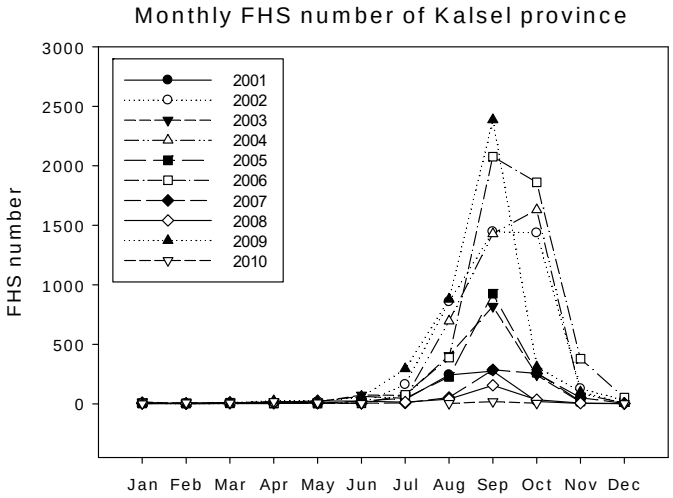
Monthly FHS number of Kalsel province
FHS number
3000
2500
2000
1500
1000
500
0
2001
2002
2003
2004
2005
2006
2007
2008
2009
2010
Jan Feb Mar Apr May Jun Jul Aug Sep Oct Nov Dec

(ix)

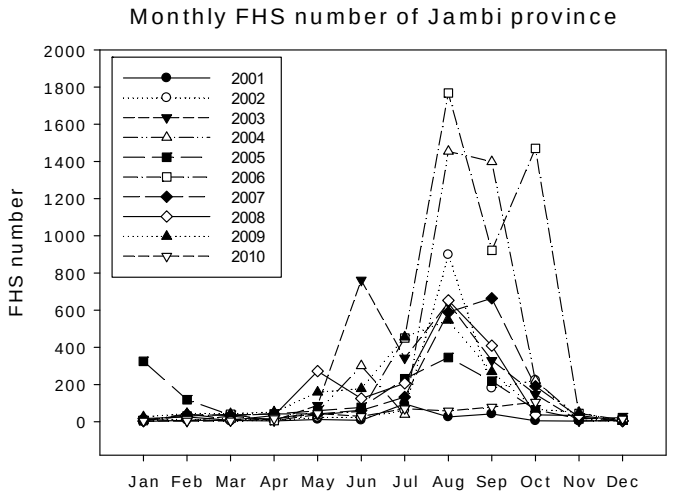
Monthly FHS number of Jambi province
FHS number
2000
1800
1600
1400
1200
1000
800
600
400
200
0
2001
2002
2003
2004
2005
2006
2007
2008
2009
2010
Jan Feb Mar Apr May Jun Jul Aug Sep Oct Nov Dec

(x)

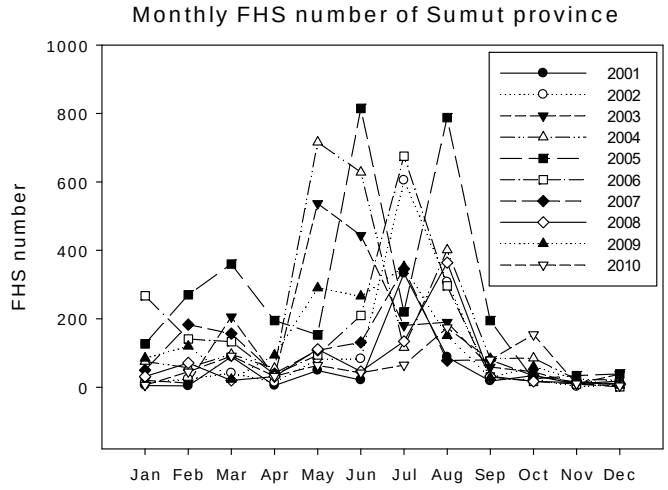
Monthly FHS number of Sumut province
FHS number
1000
800
600
400
200
0
Jan Feb Mar Apr May Jun Jul Aug Sep Oct Nov Dec
2001
2002
2003
2004
2005
2006
2007
2008
2009
2010

(xi)

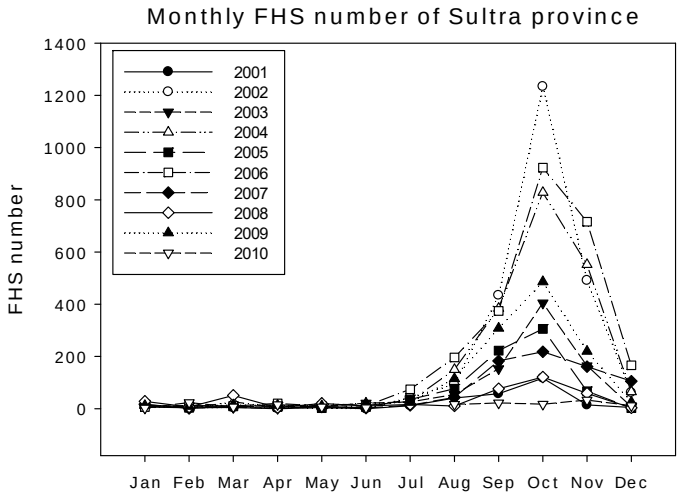
Monthly FHS number of Sultra province
FHS number
1400
1200
1000
800
600
400
200
0
Jan Feb Mar Apr May Jun Jul Aug Sep Oct Nov Dec
2001
2002
2003
2004
2005
2006
2007
2008
2009
2010

(xii)

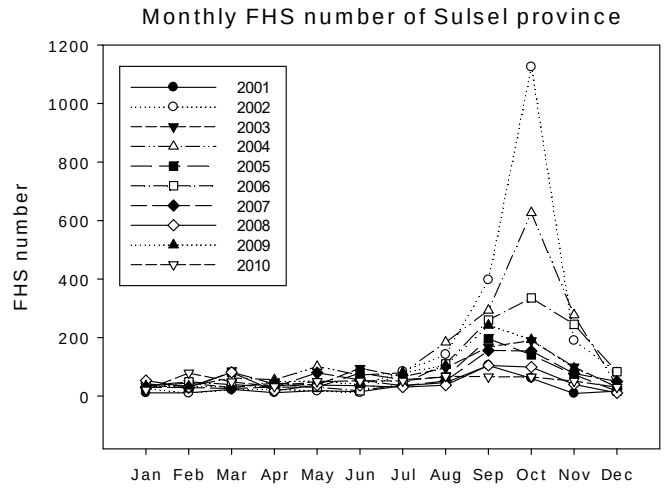
Monthly FHS number of Sulsel province
FHS number
1200
1000
800
600
400
200
0
Jan Feb Mar Apr May Jun Jul Aug Sep Oct Nov Dec
2001
2002
2003
2004
2005
2006
2007
2008
2009
2010

(xiii)

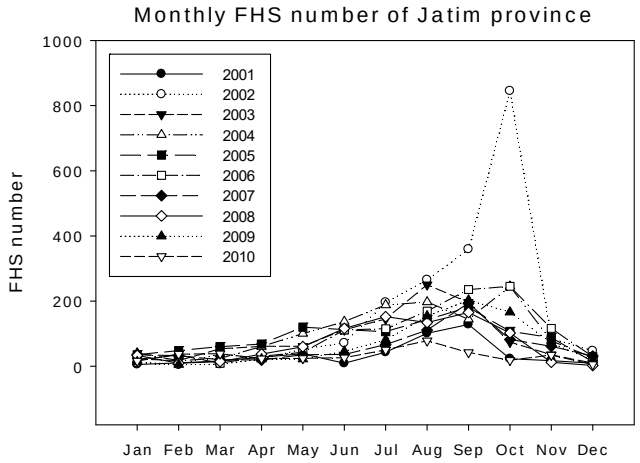
Monthly FHS number of Jatim province
FHS number
1000
800
600
400
200
0
2001
2002
2003
2004
2005
2006
2007
2008
2009
2010
Jan Feb Mar Apr May Jun Jul Aug Sep Oct Nov Dec

(xiv)

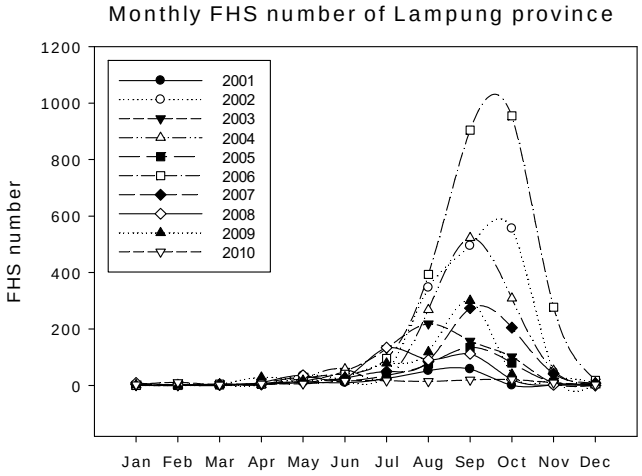
Monthly FHS number of Lampung province
FHS number
1200
1000
800
600
400
200
0
2001
2002
2003
2004
2005
2006
2007
2008
2009
2010
Jan Feb Mar Apr May Jun Jul Aug Sep Oct Nov Dec

(xv)

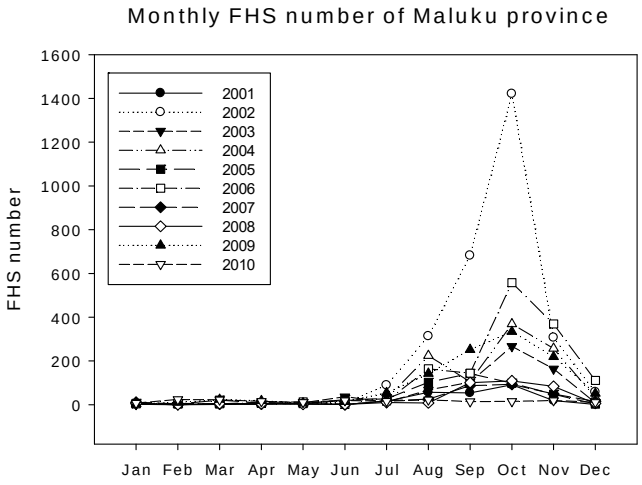
Monthly FHS number of Maluku province
FHS number
1600
1400
1200
1000
800
600
400
200
0
2001
2002
2003
2004
2005
2006
2007
2008
2009
2010
Jan Feb Mar Apr May Jun Jul Aug Sep Oct Nov Dec

(xvi)

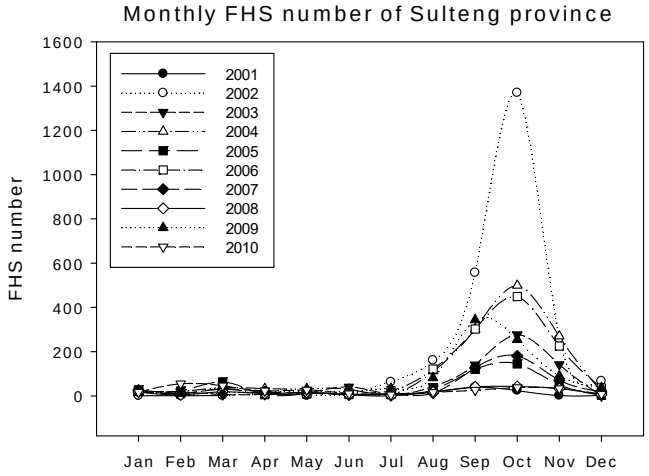

(xvii)

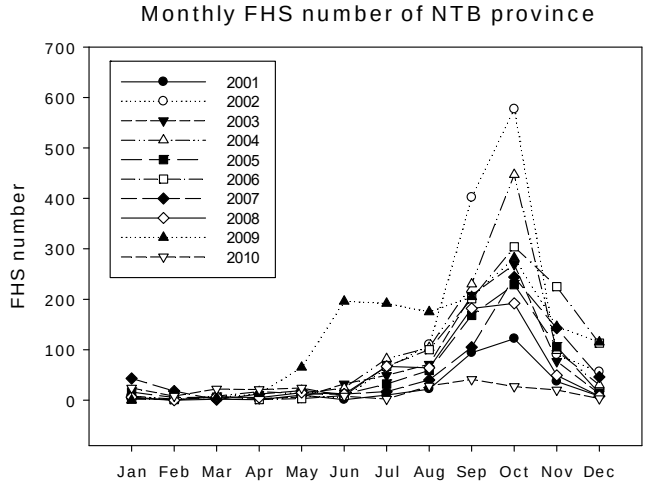

(xviii)

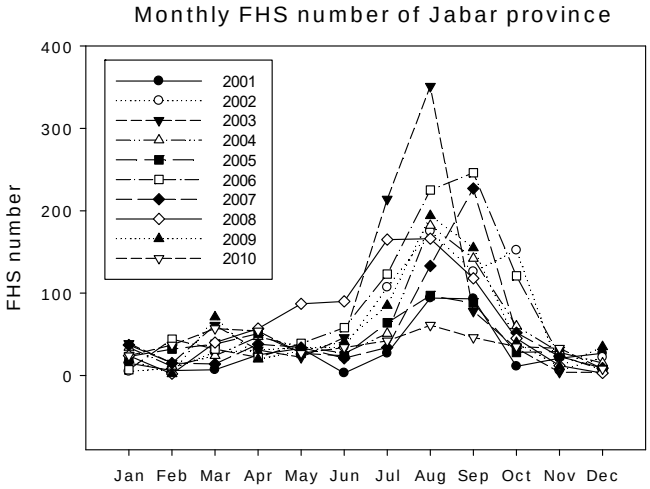

(xix)

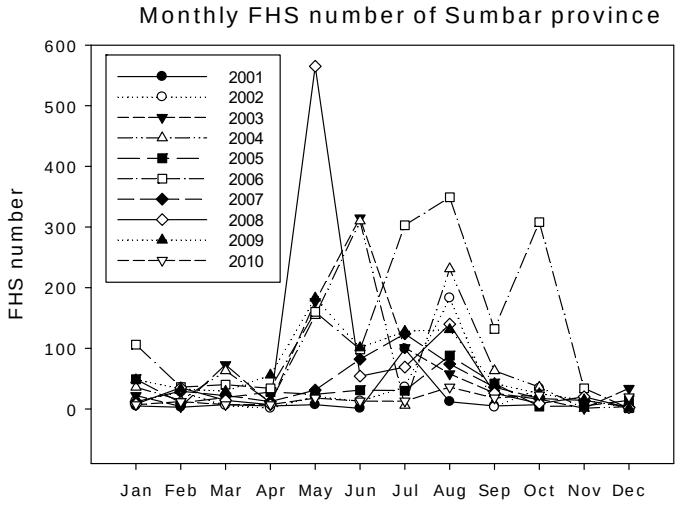
Monthly FHS number of Sumbar province
FHS number
600
500
400
300
200
100
0
2001
2002
2003
2004
2005
2006
2007
2008
2009
2010
Jan Feb Mar Apr May Jun Jul Aug Sep Oct Nov Dec

(xx)

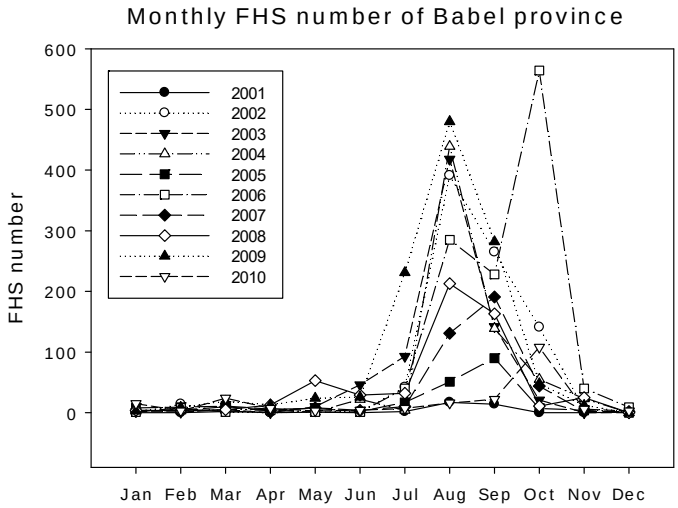
Monthly FHS number of Babel province
FHS number
600
500
400
300
200
100
0
2001
2002
2003
2004
2005
2006
2007
2008
2009
2010
Jan Feb Mar Apr May Jun Jul Aug Sep Oct Nov Dec

(xxi)

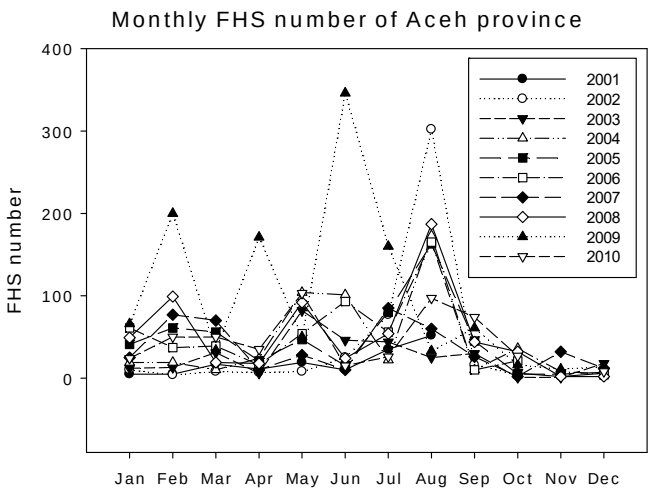
Monthly FHS number of Aceh province
FHS number
400
300
200
100
0
2001
2002
2003
2004
2005
2006
2007
2008
2009
2010
Jan Feb Mar Apr May Jun Jul Aug Sep Oct Nov Dec

(xxii)

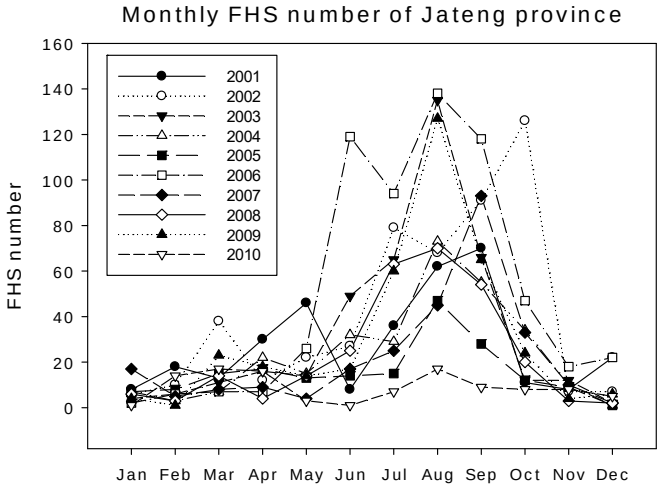

(xxiii)

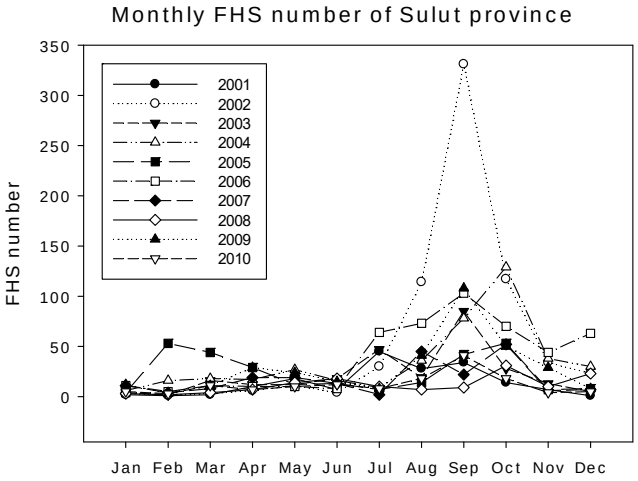

(xxiv)

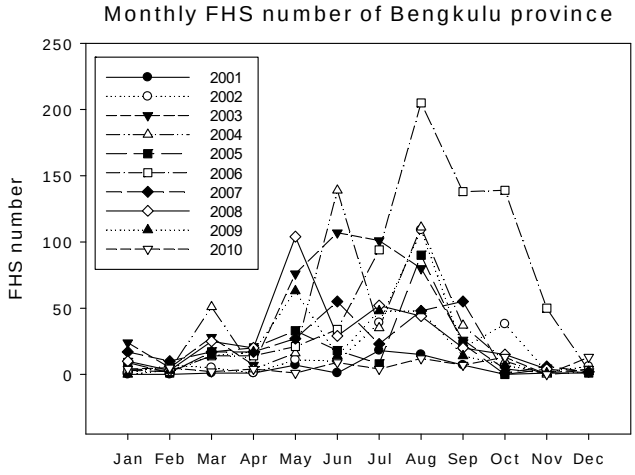

(xxv)

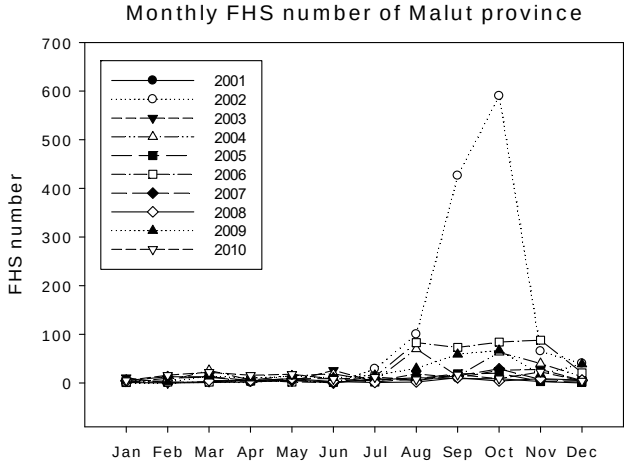

(xxvi)

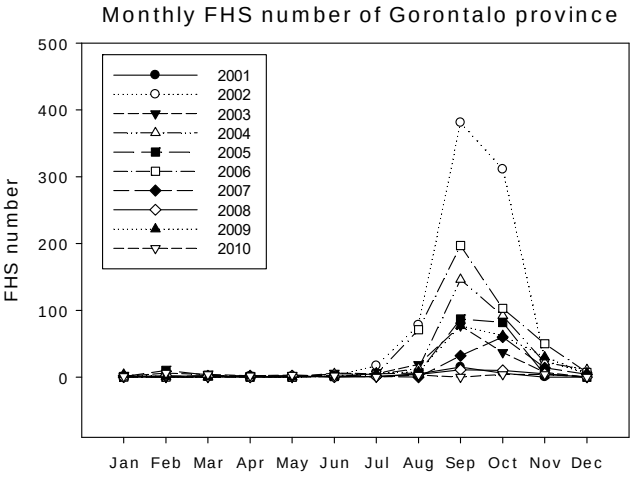

(xxvii)

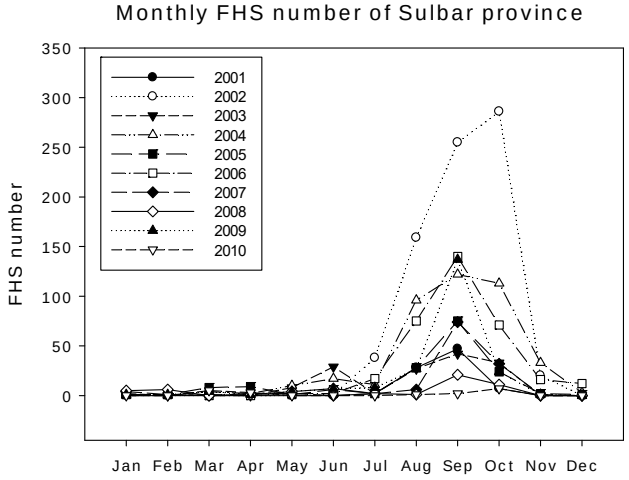

(xxviii)

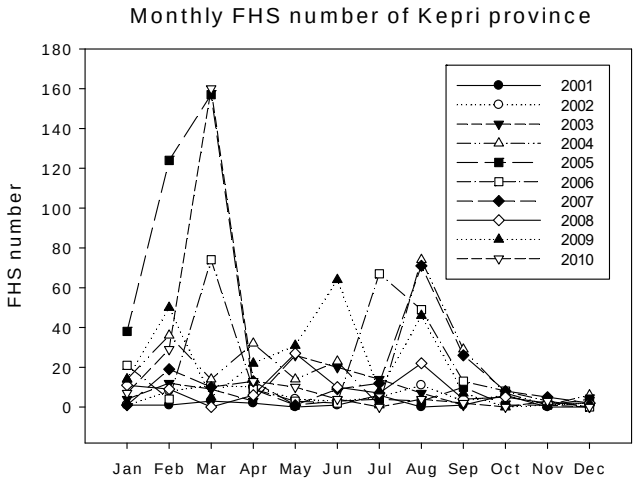

(xxix)

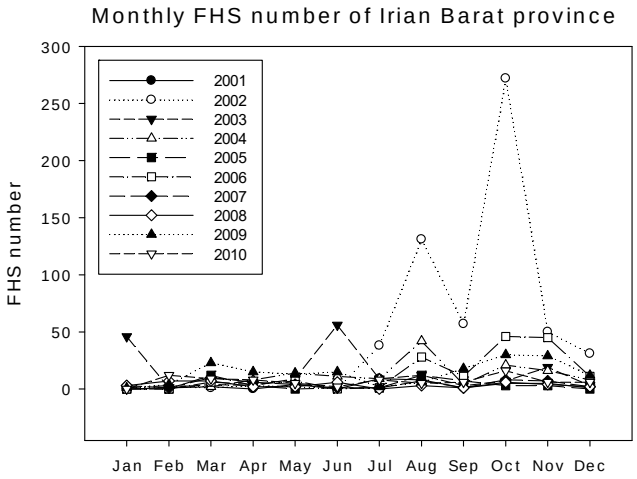

(xxx)

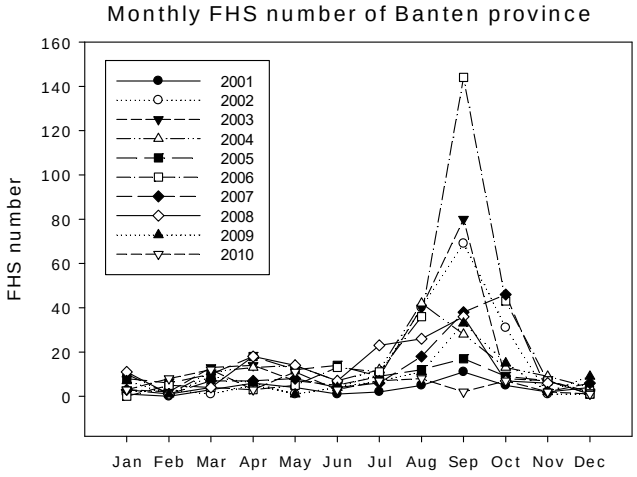

(xxxi)

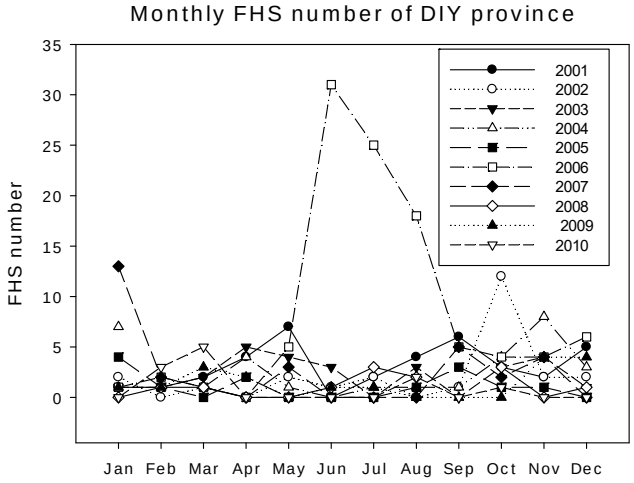

(xxxii)

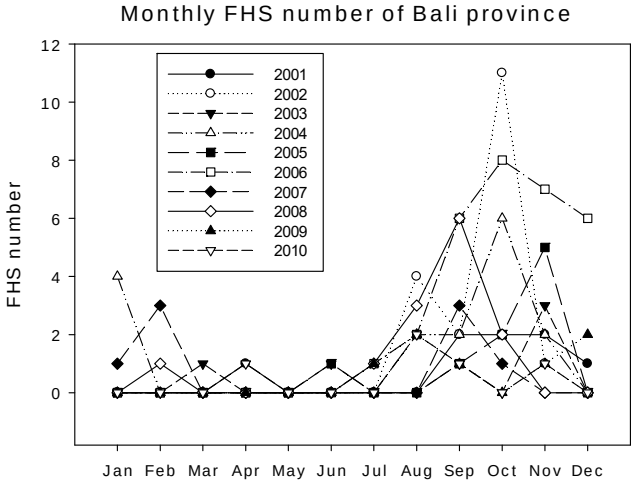

(xxxiii)

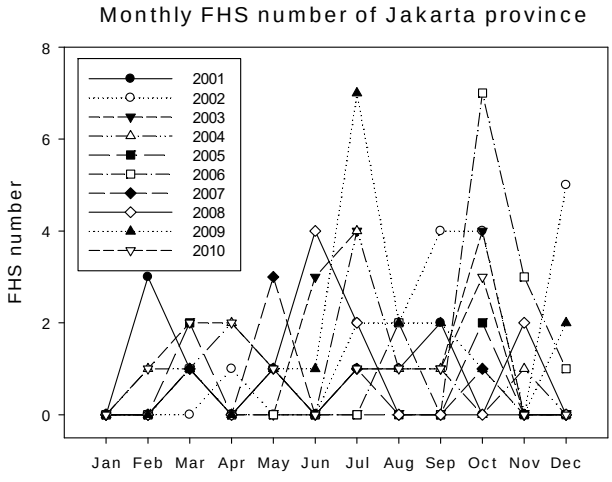

Appendix 5. Fire detection algorithm flowchart for NOAA AVHRR data (Kant et. al., 2000)

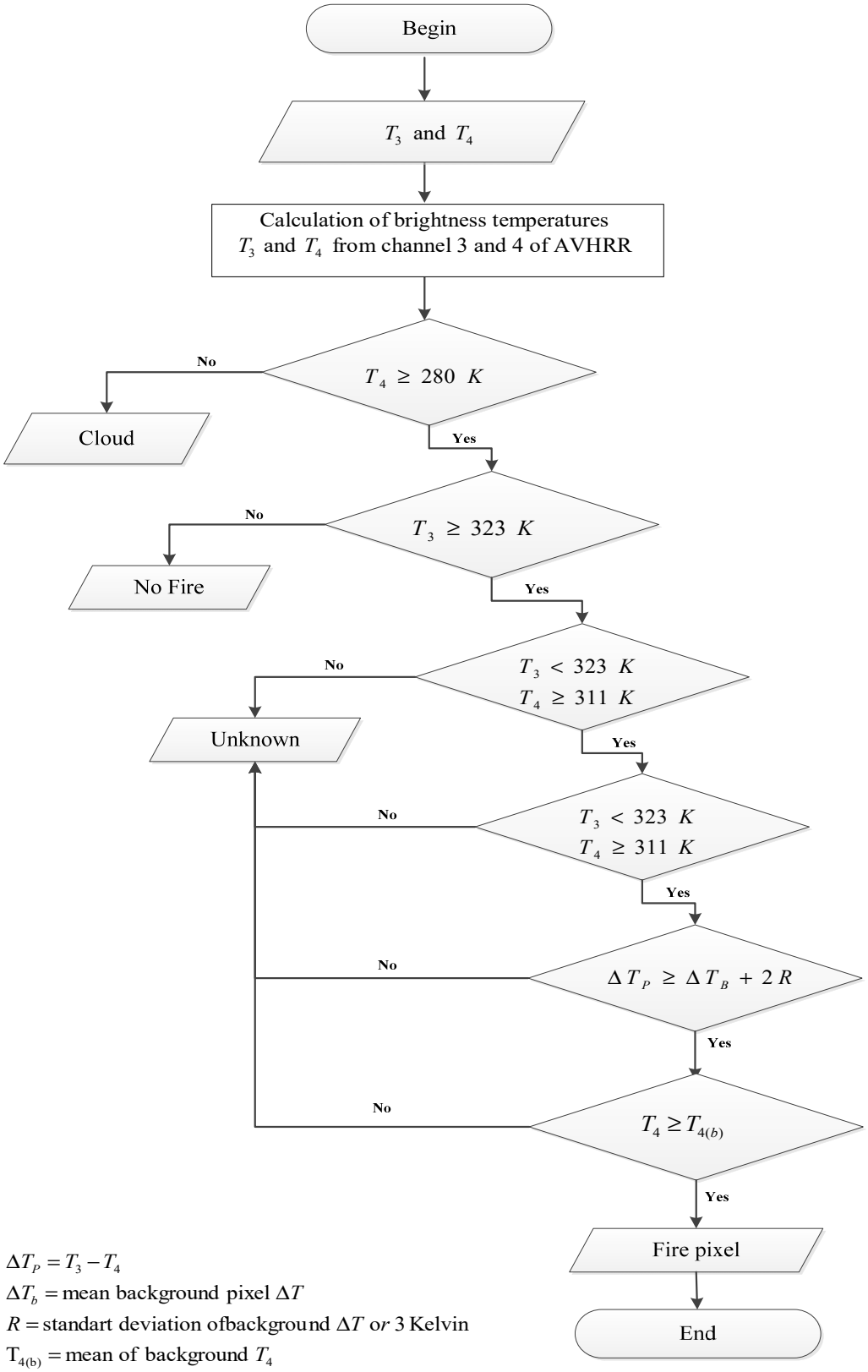

$\Delta T_P = T_3 - T_4$

ΔT_b = mean background pixel ΔT

R = standart deviation ofbackground ΔT *or* 3 Kelvin

$T_{4(b)}$ = mean of background T_4

Appendix 6. Perl script to process MODIS L1B datasets to MOD14 products and fire hotspots (FHS) shape files

```
#!/usr/bin/perl

print "It is Batch Processing script in Perl......!\n";
print "This script proccess L!A into Geolocation, L1B, MOD14
   and FHS shape file \n";

@files = </media/MODIS3/mixed/DATA/M*D021KM*>;
 foreach $file (@files) {

$sat=substr($file, 25, 3);
$day = substr($file, 35, 7);
$time = substr($file, 43, 4);
$ID = substr($file, 34, 13);
$lev="14";
$lgeo="03";


@geo = </media/MODIS3/mixed/DATA/$sat$lgeo.$ID.*>;
@MOD14 = </media/MODIS3/mixed/MOD14/$sat$lev.$ID.hdf>;
@lat = <$sat$lev.lat.$ID.txt>;
@lon = <$sat$lev.lon.$ID.txt>;
@conf = <$sat$lev.conf.$ID.txt>;
@pwr = <$sat$lev.pwr.$ID.txt>;
@mrg = <$sat$lev.mrg.$ID.txt>;

system("./mod14 -tv $file @geo @MOD14");
system("hdp dumpsds -n FP_latitude -d -o
   /media/MODIS3/mixed/MOD14/@lat @MOD14");
system("hdp dumpsds -n FP_longitude -d -o
   /media/MODIS3/mixed/MOD14/@lon @MOD14");
system("hdp dumpsds -n FP_confidence -d -o
   /media/MODIS3/mixed/MOD14/@conf @MOD14");
system("hdp dumpsds -n FP_power -d -o
   /media/MODIS3/mixed/MOD14/@pwr @MOD14");

system("mergeasc /media/MODIS3/mixed/MOD14/@lon
   /media/MODIS3/mixed/MOD14/@lat
   /media/MODIS3/mixed/MOD14/@conf
   /media/MODIS3/mixed/MOD14/@pwr >
   /media/MODIS3/mixed/MOD14/@mrg");

system("txt2shp_fhs Terra $ID $time $day Goddard 3
   /media/MODIS3/mixed/shp/$sat$lev.$ID  <
   /media/MODIS3/mixed/MOD14/@mrg");
system("rm /media/MODIS3/mixed/MOD14/*.txt");

 }
```

Appendix 7. MATLAB script to pick up classified pixels from MOD14 products

```
%clean-up mathwork==========
close all;
clear all;
clc;
disp('Progress is running....');

%=======file identification && Variable Definition ================
geofile=dir('M*D03*.hdf');
fileName = 'Kalteng_Cloud_Land_fire_pixels_number.txt';
delete(fileName);
fid = fopen(fileName,'w');       %Create and open txt file ========

%=========write header in the file text ==============
fprintf(fid,'%s\t','No');
fprintf(fid,'%s\t','Orbit');
fprintf(fid,'%s\t','Missing');
fprintf(fid,'%s\t','No-Proc');
fprintf(fid,'%s\t','Water');
fprintf(fid,'%s\t','cloud');
fprintf(fid,'%s\t','land');
fprintf(fid,'%s\t','Unknown');
fprintf(fid,'%s\t','fire-7');
fprintf(fid,'%s\t','fire-8');
fprintf(fid,'%s\t','fire-9');
fprintf(fid,'%s\r\n','Max pixels');

%############## INITIALIZE GEOFILE & L1BFILE ########################
for k=1:length(geofile)
    geoname=geofile(k).name;
    geoinfo=hdfinfo(geoname);
    AT=geoname(1:3);
    ID=geoname(8:19);

mod14name=strcat('E:\mixed\KaltengAT_Sept2009\MOD14\',AT,'14.A',ID,
     '.hdf');
info=hdfinfo(mod14name);
mod14=hdfread(info.SDS(1,1));

%################  START READING GEOFILE  ########################
%This step reads Row/Col of Geofile base on lat/lon value of MOD14

lat=hdfread(geoinfo.Vgroup.Vgroup(1,1).SDS(1,1));
lon=hdfread(geoinfo.Vgroup.Vgroup(1,1).SDS(1,2));
[a,b]=find(lat>=-3.5 & lat<=1 & lon>=110.5 & lon<=116);

%variable definition of row and colomn of pixels classifications ##
[P0r,P0c]=find(mod14==0);       %Missing input class
       q=length(P0r);
       pix0=0;
[P2r,P2c]=find(mod14==2);       %Not processed class
       r=length(P2r);
       pix2=0;
```

```
[P3r,P3c]=find(mod14==3);       %Water class
       s=length(P3r);
       pix3=0;
[Cr,Cc]=find(mod14==4);         %Cloud class
       n=length(Cr);
       cloud=0;
[Lr,Lc]=find(mod14==5);         %Land class
       l=length(Lr);
       land=0;
[P6r,P6c]=find(mod14==6);       %Unknown class
       t=length(P6r);
       pix6=0;
[F7r,F7c]=find(mod14==7);       %Low confidence fires class
       m=length(F7r);
       fire7=0;
[F8r,F8c]=find(mod14==8);       %Nominal confidence fires class
       o=length(F8r);
       fire8=0;
[F9r,F9c]=find(mod14==9);       %High confidence fires class
       p=length(F9r);
       fire9=0;

%##looping process as much as geo files number in the directory ###
%Constrain is given to pick up pixels in Kalteng square border only
=====================================================================

for i=1:q  %looping in the (k) file ##########
     if lat(P0r(i),P0c(i))>=-3.5 & lat(P0r(i),P0c(i))<=1 &
         lon(P0r(i),P0c(i))>=110.5 & lon(P0r(i),P0c(i))<=116
          pix0=pix0+1;
      else
          pix0=pix0;
     end
end

for i=1:r  %looping in the (k) file ##########
     if lat(P2r(i),P2c(i))>=-3.5 & lat(P2r(i),P2c(i))<=1 &
         lon(P2r(i),P2c(i))>=110.5 & lon(P2r(i),P2c(i))<=116
          pix2=pix2+1;
      else
          pix2=pix2;
     end
end

for i=1:s  %looping in the (k) file ##########
     if lat(P3r(i),P3c(i))>=-3.5 & lat(P3r(i),P3c(i))<=1 &
         lon(P3r(i),P3c(i))>=110.5 & lon(P3r(i),P3c(i))<=116
          pix3=pix3+1;
      else
          pix3=pix3;
     end
end
```

```
for i=1:n  %looping in the (k) file ##########
     if  lat(Cr(i),Cc(i))>=-3.5 & lat(Cr(i),Cc(i))<=1 &
         lon(Cr(i),Cc(i))>=110.5 & lon(Cr(i),Cc(i))<=116
          cloud=cloud+1;
      else
          cloud=cloud;
     end
end

for i=1:l  %looping in the (k) file ##########
     if lat(Lr(i),Lc(i))>=-3.5 & lat(Lr(i),Lc(i))<=1 &
         lon(Lr(i),Lc(i))>=110.5 & lon(Lr(i),Lc(i))<=116
          land=land+1;
      else
          land=land;
     end
end

for i=1:t  %looping in the (k) file ##########
     if lat(P6r(i),P6c(i))>=-3.5 & lat(P6r(i),P6c(i))<=1 &
         lon(P6r(i),P6c(i))>=110.5 & lon(P6r(i),P6c(i))<=116
          pix6=pix6+1;
      else
          pix6=pix6;
     end
end

for i=1:m  %looping in the (k) file ##########
     if lat(F7r(i),F7c(i))>=-3.5 & lat(F7r(i),F7c(i))<=1 &
         lon(F7r(i),F7c(i))>=110.5 & lon(F7r(i),F7c(i))<=116
          fire7=fire7+1;
      else
          fire7=fire7;
     end
end

for i=1:o  %looping in the (k) file ##########
     if lat(F8r(i),F8c(i))>=-3.5 & lat(F8r(i),F8c(i))<=1 &
         lon(F8r(i),F8c(i))>=110.5 & lon(F8r(i),F8c(i))<=116
          fire8=fire8+1;
      else
          fire8=fire8;
     end
end

for i=1:p  %looping in the (k) file ##########
     if lat(F9r(i),F9c(i))>=-3.5 & lat(F9r(i),F9c(i))<=1 &
         lon(F9r(i),F9c(i))>=110.5 & lon(F9r(i),F9c(i))<=116
          fire9=fire9+1;
      else
          fire9=fire9;
     end
end
```

```
% Print variable values in the stated txt file ====================
       fprintf(fid,'%s\t',num2str(k));
       fprintf(fid,'%s\t',geoname);
       fprintf(fid,'%s\t',num2str(pix0));
       fprintf(fid,'%s\t',num2str(pix2));
       fprintf(fid,'%s\t',num2str(pix3));
       fprintf(fid,'%s\t',num2str(cloud));
       fprintf(fid,'%s\t',num2str(land));
       fprintf(fid,'%s\t',num2str(pix6));
       fprintf(fid,'%s\t',num2str(fire7));
       fprintf(fid,'%s\t',num2str(fire8));
       fprintf(fid,'%s\t',num2str(fire9));
       fprintf(fid,'%s\r\n',num2str(length(b)));
end
fclose all;
clc;
disp('Progress Completed !');
```

Appendix 8. Locations of 11 observed fires through the ground observation by BKSDA officers in Kalteng province with area more than or equal 15 hectares. Fire numbers are sorted by date of observation.

Fire number	Date	Lon	Lat	Location name	Area (ha)	Vegetation type
Fire 1	03/06/2011	111.25	-2.82	Natai Sedawak	72	Grass & Bush
Fire 2	04/06/2011	111.23	-2.79	SM.Lamandau	116	Primary forest
Fire 3	11/06/2011	111.64	-2.91	Kubu	25	Reed & bush
Fire 4	12/06/2011	111.63	-2.74	Pasir Panjang	42	Reed & bush
Fire 5	05/08/2011	111.60	-2.74	Sei Tendang	20	Primary forest
Fire 6	07/08/2011	111.59	-2.62	RAJA	15	Bush
Fire 7	08/08/2011	114.47	-3.10	Handil Marhanang	30	Plantation
Fire 8	12/08/2011	114.47	-3.10	Handil Marhanang	15	People field
Fire 9	22/08/2011	111.13	-2.86	SM.Lamandau	15	Grass
Fire 10	30/08/2011	112.74	-2.60	PT Agro Bukit	30	Peat land
Fire 11	19/09/2011	114.26	-2.99	Batuah - Basarang	30	People plantation area

Appendix 9. Attributes data of pixels associate with ground observed fires shown in Appendix 8. Refer to the Table 2.5, mask value 4 = cloud pixel and mask value 5 = non-fir clear land pixel.

Fire number	Date	Time (UTC)	Lat	Lon	Row	Col	DN	T4	Mask
Fire 1	03/06/2011	14.35	111.26	-2.82	22	1273	2916	294.8	5
Fire 2	04/06/2011	15.15	111.23	-2.79	1178	385	2781	266.4	4
Fire 3	11/06/2011	03.00	111.64	-2.91	1596	744	3006	304.7	5
Fire 4	12/06/2011	14.25	111.63	-2.73	1546	1313	2823	278.9	4
Fire 5	05/08/2011	03.10	111.60	-2.74	77	902	2921	295.4	4
Fire 6	07/08/2011	02.55	111.59	-2.62	1188	572	3023	306.2	5
Fire 7	08/08/2011	14.20	114.47	-3.10	1084	1269	2849	284.3	5
Fire 8	12/08/2011	03.15	114.47	-3.10	524	1220	3024	306.3	5
Fire 9	22/08/2011	14.35	111.13	-2.86	14	1277	2903	293.0	5
Fire 10	30/08/2011	15.20	112.74	-2.60	1597	168	2759	255.5	4
Fire 11	19/09/2011	14.55	114.26	-2.99	1621	548	2779	265.6	4

Appendix 10. Recorded ground check data by local forestry agency (BKSDA) Kalteng province in 2011

No	Lat	Lon	Date	Location	Vegetation types	Area (ha)
1	-2.79	111.23	4/06/11	SM. Lamandau	Primary forest	116
2	-2.82	111.25	3/06/11	Natai Sedawak	Grass & Bush	72
3	-2.74	111.63	12/06/11	Pasir panjang	Reed & bush	42
4	-2.99	114.26	19/09/11	Batuah kec.Basarang	People plantation	30
5	-3.10	114.47	8/08/11	Handil Marhanang	Plantation	30
6	-2.60	112.74	30/08/11	PT Agro Bukit	Peat	30
7	-2.91	111.64	11/06/11	Kubu	Reed & bush	25
8	-2.74	111.70	5/08/11	Sei Tendang	Primary forest	20
9	-3.10	114.47	12/08/11	Handil Marhanang	People land	15
10	-2.86	111.13	22/08/11	SM.Lamandau	Grass	15
11	-2.62	111.59	7/08/11	Raja	Bush	15
12	-2.66	111.83	5/08/11	Kumai hulu	Reed	13
13	-2.86	111.66	10/08/11	Kubu	Primary forest	13
14	-2.55	112.83	6/08/11	PT Agro Bukit	Reed	11
15	-2.77	111.55	7/08/11	Kumpai batu atas	Reed and bush	10
16	-2.62	111.60	7/08/11	Raja	Reed	10
17	-2.54	112.92	5/07/11	Baamang Hilir	Bush	10
18	-1.96	111.49	15/08/11	Nanga palikodan	Reed	9
19	-1.92	111.49	15/08/11	Nanga palikodan	Reed	9
20	-2.32	111.11	8/07/11	Jihing	Reed	8
21	-2.47	112.98	3/08/11	Baamang hulu	Reed	8
22	-2.54	111.69	6/08/11	Baru	Bush	8
23	-2.64	111.67	23/06/11	Baru	Reed & bush	7
24	-3.15	112.31	8/07/11	Tanjung Rengas	Reed	6
25	-2.30	111.37	8/07/11	Makarti Jaya	Reed	6
26	-2.65	111.73	7/08/11	Pasir panjang	Reed and bush	6
27	-1.90	111.07	16/08/11	Tanjung beringin	Reed	6
28	-2.74	111.62	16/06/11	Pasir panjang	Peat	5
29	-2.70	111.70	9/07/11	Sei Tendang	Peat	5
30	-2.67	111.18	9/07/11	Mendawai	Reed	5
31	-2.03	111.85	9/07/11	Pangkut	Reed	5
32	-2.85	111.63	18/07/11	Kubu	Bush	5
33	-1.79	111.51	30/07/11	Toka	Bush	5
34	-2.78	111.58	4/08/11	Kumpai batu atas	Reed	5
35	-2.65	111.73	5/08/11	Pasir panjang	Reed	5
36	-2.89	111.35	7/08/11	Tanjung putri	Reed	5
37	-2.74	111.70	7/08/11	Candi	Bush	5

No	Lat	Lon	Date	Location	Vegetation types	Area (ha)
38	-2.73	111.71	7/08/11	Candi	Bush	5
39	-2.73	111.70	7/08/11	Candi	Bush	5
40	-2.50	111.53	7/08/11	Kota waringin hilir	Reed	5
41	-1.75	111.17	16/08/11	Kinipan	Reed	5
42	-1.73	111.18	18/08/11	Ginih	Bush	5
43	-2.75	111.64	15/06/11	Pasir panjang	Reed, Bush, field	4
44	-2.74	111.63	18/06/11	Pasir panjang	Reed & bush	4
45	-2.71	111.63	18/06/11	Madurejo	Bush, field	4
46	-2.87	111.63	1/07/11	Kubu	Peat	4
47	-2.01	111.92	2/07/11	Pangkut	Peat	4
48	-2.87	111.54	6/07/11	Sebuai	Reed	4
49	-1.99	111.44	7/07/11	Nanga Bulik	Peat	4
50	-2.46	112.93	8/07/11	Batuah	Bush	4
51	-2.91	111.09	26/07/11	Sungai Damar	Reed	4
52	-2.25	111.39	26/07/11	Makarti Jaya	Bush	4
53	-2.76	111.53	27/07/11	Kumpai batu atas	Reed	4
54	-1.92	111.58	28/07/11	Mukti Manunggal	Bush	4
55	-0.98	111.73	28/07/11	Buntut Sapau	Bush	4
56	-2.67	111.70	29/07/11	Pasir panjang	Bush	4
57	-2.34	112.90	29/07/11	Simpur	Bush	4
58	-1.93	111.59	29/07/11	Malata	Bush	4
59	-3.05	112.90	30/07/11	Lampuyang	Reed	4
60	-2.91	112.90	30/07/11	Basirih Hilir	Bush	4
61	-3.33	112.51	31/07/11	Kuala Pembuang Satu	Peat	4
62	-2.63	111.63	5/08/11	Raja	Peat	4
63	-2.63	111.62	5/08/11	Raja	Peat	4
64	-2.87	111.66	6/08/11	Kubu	Bush	4
65	-2.88	111.35	7/08/11	Tanjung putri	Reed	4
66	-2.88	111.35	7/08/11	Tanjung putri	Bush	4
67	-2.85	111.49	7/08/11	Kumpai batu bawah	Reed	4
68	-2.51	111.54	7/08/11	Raja seberang	Peat	4
69	-2.24	111.42	7/08/11	Suka makmur	Reed	4
70	-2.23	111.42	7/08/11	Kondang	Reed	4
71	-1.96	111.48	15/08/11	Nanga palikodan	Bush	4
72	-1.94	111.17	16/08/11	Panopa	Bush	4
73	-1.61	111.40	16/08/11	Batu tunggal	Bush	4
74	-2.85	111.50	30/08/11	Kumpai batu bawah	Reed	4
75	-2.85	111.49	30/08/11	Kumpai batu bawah	Reed	4
76	-2.35	112.86	2/07/11	Simpur	Reed	3.5
77	-2.31	111.34	7/07/11	Suka Mulya	Reed	3.5

No	Lat	Lon	Date	Location	Vegetation types	Area (ha)
78	-2.55	111.17	8/07/11	Padang	Reed	3.5
79	-2.51	111.91	11/07/11	Pangkalan Banteng	Reed	3.5
80	-2.01	111.67	28/07/11	Pangkut	Bush	3.5
81	-2.73	111.64	21/01/11	Pasir panjang	Bush	3
82	-2.74	111.65	28/02/11	Pasir panjang	Bush	3
83	-3.17	112.90	3/07/11	Ujung Pandaran	Reed	3
84	-2.75	111.68	7/07/11	Sungai kapitan	Bush	3
85	-2.24	111.54	7/07/11	Kondang	Bush	3
86	-2.69	111.75	8/07/11	Candi	Peat	3
87	-2.67	112.88	8/07/11	Sumber Makmur	Peat	3
88	-2.63	111.62	8/07/11	Kampung Raja	Peat	3
89	-2.38	111.29	8/07/11	Suka Raja	Peat	3
90	-2.18	111.36	8/07/11	Makarti Jaya	Bush	3
91	-2.85	111.49	9/07/11	Kumpai batu bawah	Bush	3
92	-2.73	111.70	9/07/11	Candi	Peat	3
93	-2.72	111.16	9/07/11	Mendawai	Reed	3
94	-2.48	112.96	9/07/11	Baamang hulu	Reed	3
95	-2.13	112.45	9/07/11	Baampah	Reed	3
96	-2.48	111.92	11/07/11	Pangkalan Banteng	Reed	3
97	-1.63	111.65	11/07/11	Pandau	Peat	3
98	-2.39	112.10	12/07/11	Asam Baru	Reed	3
99	-2.82	111.45	26/07/11	Tanjung putri	Bush	3
100	-2.60	112.67	27/07/11	Pondok Damar	Peat	3
101	-2.65	111.13	28/07/11	Mendawai	Bush	3
102	-2.46	112.98	28/07/11	Baamang hulu	Bush	3
103	-2.37	111.71	28/07/11	Baru	Reed	3
104	-2.15	111.50	28/07/11	Kondang	Bush	3
105	-2.78	112.86	29/07/11	Bagendang Hilir	Peat	3
106	-2.66	111.86	29/07/11	Bumi Harjo	Bush	3
107	-2.60	111.92	29/07/11	Kumai Hulu	Peat	3
108	-2.02	111.61	29/07/11	Umpang	Reed	3
109	-2.02	112.83	29/07/11	Damar Makmur	Peat	3
110	-2.79	111.62	2/08/11	Sungai kapitan	Peat	3
111	-2.79	111.62	2/08/11	Sungai kapitan	Peat	3
112	-2.59	111.69	5/08/11	Baru	Bush	3
113	-2.59	111.68	5/08/11	Baru	Peat	3
114	-2.59	111.69	5/08/11	Baru	Bush	3
115	-2.92	111.48	6/08/11	Sebuai	Peat	3
116	-2.93	111.49	7/08/11	Sebuai	Bush	3
117	-2.91	111.49	7/08/11	Sebuai	Bush	3

No	Lat	Lon	Date	Location	Vegetation types	Area (ha)
118	-2.88	111.36	7/08/11	Tanjung putri	Reed	3
119	-2.85	111.49	7/08/11	Kumpai batu bawah	Reed	3
120	-2.74	111.63	7/08/11	Batu belaman	Bush	3
121	-2.73	111.68	7/08/11	Candi	Peat	3
122	-2.65	111.68	7/08/11	Madurejo	Reed	3
123	-2.35	111.70	7/08/11	Raja seberang	Peat	3
124	-2.32	111.42	7/08/11	Sukamulya	Reed	3
125	-2.27	111.51	7/08/11	Rungun	Bush	3
126	-2.25	111.44	7/08/11	Suka makmur	Bush	3
127	-2.23	111.44	7/08/11	Kondang	Reed	3
128	-2.23	111.42	7/08/11	Kondang	Bush	3
129	-1.71	111.11	18/08/11	Sepoyu	Reed	3
130	-2.91	111.48	24/08/11	Sebuai	Bush	3
131	-2.74	111.70	25/08/11	Candi	Bush	3
132	-2.72	111.70	25/08/11	Candi	Peat	3
133	-2.50	111.41	30/08/11	Kel.Sidorejo	Peat	3
134	-2.42	111.91	7/07/11	Pandu Sanjaya	Reed	2.5
135	-2.23	111.87	9/07/11	Sidomulyo	Bush	2.5
136	-2.14	111.40	9/07/11	Kenawan	Reed	2.5
137	-2.21	111.88	12/07/11	Sidomulyo	Bush	2.5
138	-2.77	111.63	27/07/11	Batu belaman	Bush	2.5
139	-2.39	112.87	27/07/11	Simpur	Bush	2.5
140	-2.73	111.18	28/07/11	Mendawai	Reed	2.5
141	-2.40	112.89	28/07/11	Simpur	Reed	2.5
142	-2.34	111.72	28/07/11	Raja seberang	Bush	2.5
143	-2.02	111.67	29/07/11	Pangkut	Reed	2.5
144	-1.96	111.60	29/07/11	Malata	Reed	2.5
145	-1.91	111.54	29/07/11	Sungkup	Reed	2.5
146	-1.01	111.82	31/07/11	Tumbang Sepan	Bush	2.5
147	-2.91	111.49	5/08/11	Sebuai	Peat	2.5
148	-2.24	111.43	7/08/11	Suka makmur	Reed	2.5
149	-2.78	111.23	23/01/11	Natai Sedawak	Reed	2
150	-2.75	111.64	20/05/11	Pasir panjang	Reed & bush	2
151	-2.74	111.63	25/05/11	Pasir panjang	Reed	2
152	-2.74	111.63	11/06/11	Pasir panjang	Bush	2
153	-2.75	111.64	14/06/11	Pasir panjang	Bush, field	2
154	-1.90	111.45	26/07/11	Tamiang	Reed	2
155	-2.92	111.48	5/08/11	Sebuai	Bush	2
156	-2.91	111.48	5/08/11	Sebuai	Reed	2
157	-2.85	111.50	5/08/11	Kumpai batu bawah	Bush	2

No	Lat	Lon	Date	Location	Vegetation types	Area (ha)
158	-2.74	111.67	5/08/11	Sungai kapitan	Peat	2
159	-2.74	111.69	5/08/11	Candi	Peat	2
160	-2.74	111.70	5/08/11	Candi	Peat	2
161	-2.93	111.49	6/08/11	Sebuai	Peat	2
162	-2.92	111.49	6/08/11	Sebuai	Bush	2
163	-2.77	111.55	6/08/11	Kampar batu atas	Reed	2
164	-2.67	111.59	6/08/11	Mendawai	Peat	2
165	-2.54	111.70	6/08/11	Baru	Bush	2
166	-2.54	111.70	6/08/11	Baru	Peat	2
167	-2.91	111.49	7/08/11	Sebuai	Bush	2
168	-2.88	111.55	7/08/11	Sebuai	Peat	2
169	-2.67	111.59	7/08/11	Mendawai	Peat	2
170	-2.59	111.70	7/08/11	Baru	Peat	2
171	-2.51	111.52	7/08/11	Kota waringin hilir	Reed	2
172	-2.25	111.44	7/08/11	Suka makmur	Reed	2
173	-2.25	111.44	7/08/11	Suka makmur	Peat	2
174	-2.25	111.44	7/08/11	Suka makmur	Peat	2
175	-2.24	111.44	7/08/11	Kondang	Reed	2
176	-2.23	111.45	7/08/11	Kondang	Peat	2
177	-2.23	111.45	7/08/11	Kondang	Peat	2
178	-2.23	111.43	7/08/11	Kondang	Bush	2
179	-2.07	111.45	15/08/11	Kujan	Peat	2
180	-1.88	111.11	15/08/11	Tanjung beringin	Peat	2
181	-2.74	111.70	24/08/11	Candi	Bush	2
182	-2.83	111.56	25/08/11	Sebuai	Bush	2
183	-2.74	111.70	25/08/11	Candi	Peat	2
184	-2.74	111.71	25/08/11	Candi	Bush	2
185	-2.74	111.62	17/06/11	Pasir panjang	Peat	1.5
186	-2.75	111.64	18/06/11	Pasir panjang	Bush, field	1.5
187	-2.71	111.63	22/06/11	Madurejo	Bush, field	1.5
188	-2.97	111.59	5/08/11	Teluk bogam	Reed	1.5
189	-2.73	111.70	5/08/11	Candi	Bush	1.5
190	-2.88	111.55	6/08/11	Sebuai	Peat	1.5
191	-2.92	111.50	7/08/11	Sebuai	Peat	1.5
192	-2.92	111.49	7/08/11	Sebuai	Peat	1.5
193	-2.50	111.54	7/08/11	Kota waringin hilir	Peat	1.5
194	-2.66	111.48	11/02/11	SM. lamandau	Bush	1.2
195	-2.71	111.64	17/06/11	Madurejo,	Bush	1
196	-2.55	112.97	6/07/11	Ketapang	Reed	1
197	-2.44	111.38	14/08/11	Pasir panjang	Bush	1

No	Lat	Lon	Date	Location	Vegetation types	Area (ha)
198	-2.41	111.38	26/08/11	KP.Panggung	Peat	1
199	-2.98	114.39	9/09/11	Pulau Telo	People land	1
200	-2.74	111.71	5/08/11	Sei Tendang	Reed	1
201	-2.75	111.62	20/06/11	Pasir panjang	Reed & bush	0.5
202	-2.95	114.33	25/08/11	Tambun Raya	People land	0.5

Appendix 11. Data of scatter plots of pixels' temperature from MODIS dataset on 22 Jan 2009 at 03:40 UTC with 5x5 window size surrounding the assessed pixel with 314.4K and 313.0K.

Note: Mask values 3 = water pixel, 4 = cloud pixel, 5 = non-fire clear land pixel, and 8 = fire pixel

No	Lat	Lon	Row	Col	DN	T4	Mask
Pixels' temperature surrounding central pixel 314.4K							
1	1.04	102.18	509	644	2944	298.2	5
2	1.04	102.19	509	645	2944	298.2	5
3	1.04	102.20	509	646	2938	297.5	5
4	1.04	102.21	509	647	2944	298.2	5
5	1.04	102.22	509	648	2926	296.1	3
6	1.03	102.18	510	644	2983	302.4	5
7	1.03	102.19	510	645	3108	313.0	5
8	1.03	102.20	510	646	2989	303.0	5
9	1.03	102.21	510	647	2956	299.6	5
10	1.03	102.22	510	648	2940	297.8	3
11	1.02	102.17	511	644	2969	301.0	5
12	1.02	102.18	511	645	3089	311.6	8
13	1.02	102.19	511	646	3128	314.4	8
14	1.02	102.20	511	647	2980	302.1	5
15	1.02	102.21	511	648	2953	299.3	3
16	1.02	102.17	512	644	2936	297.3	5
17	1.01	102.18	512	645	2941	297.9	5
18	1.01	102.19	512	646	2941	297.9	5
19	1.01	102.20	512	647	2946	298.5	5
20	1.01	102.21	512	648	2941	297.9	5
21	1.01	102.17	513	644	2940	297.8	5
22	1.01	102.18	513	645	2930	296.6	5
23	1.00	102.19	513	646	2940	297.8	5
24	1.00	102.20	513	647	2945	298.3	5
25	1.00	102.21	513	648	2940	297.8	5
Mean = 300.3				**Stdev = 4.6**		**mean+3 stdev = 314.1**	

No	Lat	Lon	Row	Col	DN	T4	Mask
Pixels' temperature surrounding central pixel 313.0K							
1	1.05	102.17	508	643	2971	301.2	5
2	1.05	102.18	508	644	2997	303.8	5
3	1.05	102.19	508	645	2940	297.8	5
4	1.05	102.20	508	646	2940	297.8	5
5	1.05	102.21	508	647	2940	297.8	3

No	Lat	Lon	Row	Col	DN	T4	Mask
6	1.04	102.17	509	643	2944	298.2	5
7	1.04	102.18	509	644	2944	298.2	5
8	1.04	102.19	509	645	2944	298.2	5
9	1.04	102.20	509	646	2938	297.5	5
10	1.04	102.21	509	647	2944	298.2	5
11	1.04	102.17	510	643	2951	299.0	5
12	1.03	102.18	510	644	2983	302.4	5
13	1.03	102.19	510	645	3108	313.0	5
14	1.03	102.20	510	646	2989	303.0	5
15	1.03	102.21	510	647	2956	299.6	5
16	1.03	102.16	511	643	2953	299.3	5
17	1.02	102.17	511	644	2969	301.0	5
18	1.02	102.18	511	645	3089	311.6	8
19	1.02	102.19	511	646	3128	314.4	8
20	1.02	102.20	511	647	2980	302.1	5
21	1.02	102.16	512	643	2936	297.3	5
22	1.02	102.17	512	644	2936	297.3	5
23	1.01	102.18	512	645	2941	297.9	5
24	1.01	102.19	512	646	2941	297.9	5
25	1.01	102.20	512	647	2946	298.5	5
Mean = 300.9				**Stdev = 4.3**		**mean+3 stdev = 313.8**	

Appendix 12. Five day time series of pixel temperatures of ground data locations described in Appendix 8 (from 2 days before until 2 days after the reported acquisition date of the ground data, shown by shaded rows).

Note: Time in UTC, Mask values 4 = cloud pixel and 5 = non-fire clear land pixel

No	Date	Time	Lat	Lon	Row	Col	DN	T4	Mask
Fire data number 1									
1	1/6/2011	02.25	-2.82	111.24	953	45	2826	279.6	4
2	1/6/2011	14.45	-2.82	111.25	935	1118	2859	286.2	5
3	2/6/2011	03.1	-2.82	111.25	65	866	2735	225.7	4
4	2/6/2011	15.3	-2.82	111.25	57	168	2808	275.1	5
5	3/6/2011	14.35	-2.82	111.26	22	1273	2916	294.8	5
6	4/6/2011	02.55	-2.82	111.25	1182	537	2907	293.6	4
7	4/6/2011	15.15	-2.82	111.25	1174	384	2760	256.1	4
8	5/6/2011	03.4	-2.82	111.26	294	1325	2950	298.9	5
Fire data number 2									
1	2/6/2011	03.1	-2.79	111.23	62	864	2736	228.6	4
2	2/6/2011	15.3	-2.79	111.23	60	169	2821	278.4	4
3	3/6/2011	14.35	-2.79	111.23	24	1274	2907	293.6	5
4	4/6/2011	02.55	-2.79	111.23	1179	534	3019	305.9	5
5	4/6/2011	15.15	-2.79	111.23	1178	385	2781	266.4	4
6	5/6/2011	03.4	-2.79	111.23	288	1324	2966	300.7	5
7	6/6/2011	02.45	-2.79	111.23	255	263	2982	302.3	5
8	6/6/2011	15.05	-2.79	111.23	252	700	2888	290.9	5
Fire data number 3									
1	9/6/2011	03.15	-2.91	111.64	483	1039	2960	300.0	5
2	9/6/2011	15.35	-2.92	111.64	450	84	2932	296.8	5
3	10/6/2011	02.2	-2.90	111.64	450	13	2772	262.5	5
4	10/6/2011	14.4	-2.91	111.64	416	1189	2955	299.5	5
5	11/6/2011	03.	-2.91	111.64	1596	744	2785	267.9	5
6	11/6/2011	15.2	-2.90	111.64	1568	239	2931	296.7	5
7	12/6/2011	14.25	-2.92	111.64	1526	1314	2895	291.9	5
8	13/6/2011	02.5	-2.91	111.64	669	421	2976	301.7	5
1	13/6/2011	15.1	-2.91	111.64	641	498	2893	291.6	5
Fire data number 4									
1	10/6/2011	02.2	-2.74	111.63	436	12	2883	290.1	5
2	10/6/2011	14.4	-2.74	111.63	435	1188	2915	294.7	5
3	11/6/2011	03.	-2.74	111.63	1578	739	2832	280.9	5
4	11/6/2011	15.2	-2.73	111.63	1587	237	2931	296.7	4
5	12/6/2011	14.25	-2.73	111.63	1546	1313	2751	249.7	4
6	13/6/2011	02.5	-2.74	111.63	651	417	2944	298.2	5

No	Date	Time	Lat	Lon	Row	Col	DN	T4	Mask
7	13/6/2011	15.1	-2.74	111.63	659	495	2947	298.6	5
8	14/6/2011	03.3	-2.74	111.63	1802	1287	2766	259.6	5
Fire data number 5									
1	3/8/2011	03.2	-2.73	111.60	994	1145	2949	298.8	4
2	3/8/2011	15.4	-2.74	111.60	1004	32	2753	251.3	4
3	4/8/2011	02.25	-2.74	111.59	958	56	2922	295.6	5
4	4/8/2011	14.45	-2.74	111.60	964	1091	2941	297.9	5
5	5/8/2011	03.1	-2.74	111.60	77	902	2763	257.9	4
6	5/8/2011	15.3	-2.74	111.60	88	148	2951	299.0	5
7	6/8/2011	14.35	-2.75	111.59	55	1258	2755	252.8	5
8	7/8/2011	02.55	-2.74	111.60	1201	576	2974	301.5	5
9	7/8/2011	15.15	-2.74	111.60	1214	349	2735	225.7	5
Fire data number 6									
1	5/8/2011	03.1	-2.62	111.59	65	899	2929	296.4	4
2	5/8/2011	15.3	-2.63	111.59	100	147	2748	246.9	5
3	6/8/2011	14.35	-2.62	111.58	71	1257	2942	298.0	5
4	7/8/2011	02.55	-2.62	111.59	1188	572	2938	297.5	5
5	7/8/2011	15.15	-2.63	111.59	1226	348	2803	273.7	5
6	8/8/2011	03.4	-2.62	111.58	310	1334	2740	236.9	5
7	8/8/2011	14.2	-2.61	111.60	1183	1352	2907	293.6	5
8	9/8/2011	02.45	-2.62	111.59	273	289	2873	288.6	5
9	9/8/2011	15.05	-2.62	111.59	309	652	2935	297.2	4
Fire data number 7									
1	6/8/2011	02.15	-3.10	114.47	51	52	2868	287.7	5
2	6/8/2011	14.3	-3.10	114.47	2003	1111	2982	302.3	5
3	7/8/2011	02.55	-3.10	114.47	1195	888	2933	296.9	5
4	7/8/2011	15.15	-3.10	114.47	1127	163	2940	297.8	5
5	8/8/2011	14.2	-3.10	114.47	1084	1269	2908	293.7	5
6	9/8/2011	02.45	-3.10	114.47	278	560	2963	300.4	5
7	9/8/2011	15.05	-3.10	114.47	212	374	2959	299.9	5
8	10/8/2011	03.25	-3.11	114.46	1430	1331	2773	263.0	5
Fire data number 8									
1	10/8/2011	03.25	-3.11	114.46	1430	1331	2949	298.8	5
2	11/8/2011	02.3	-3.10	114.47	1400	281	2931	296.7	5
3	11/8/2011	14.5	-3.10	114.47	1333	686	2905	293.3	5
4	12/8/2011	03.15	-3.10	114.47	524	1220	2727	285.6	5
5	12/8/2011	15.35	-3.10	114.47	448	1	2934	297.1	5
6	13/8/2011	02.2	-3.09	114.47	485	108	2943	298.1	5
7	13/8/2011	14.4	-3.10	114.48	413	994	2933	296.9	5
8	14/8/2011	03.	-3.10	114.47	1634	1026	2940	297.8	5
9	14/8/2011	15.2	-3.10	114.48	1566	93	2754	252.1	5

No	Date	Time	Lat	Lon	Row	Col	DN	T4	Mask
Fire data number 9									
1	20/8/2011	02.25	-2.86	111.12	957	42	2889	291.0	5
2	20/8/2011	14.45	-2.87	111.13	935	1125	2906	293.5	5
3	21/8/2011	03.1	-2.86	111.13	64	857	2740	236.9	5
4	21/8/2011	15.3	-2.86	111.13	49	174	2779	265.6	5
5	22/8/2011	14.35	-2.86	111.13	14	1277	2914	294.5	5
6	23/8/2011	02.55	-2.86	111.13	1184	528	2996	303.7	5
7	23/8/2011	15.15	-2.86	111.13	1170	393	2771	262.1	5
8	24/8/2011	03.4	-2.86	111.14	311	1323	2884	290.3	5
Fire data number 10									
1	28/8/2011	03.15	-2.60	112.74	448	1116	2855	285.5	5
2	28/8/2011	15.35	-2.60	112.75	487	43	2880	289.7	4
3	29/8/2011	02.2	-2.60	112.74	409	42	2948	298.7	5
4	29/8/2011	14.4	-2.60	112.74	445	1118	2838	282.2	5
5	30/8/2011	03.	-2.60	112.74	1556	857	2837	282.0	5
6	30/8/2011	15.2	-2.60	112.74	1597	168	2930	296.6	4
7	31/8/2011	14.25	-2.60	112.74	1562	1273	2910	294.0	4
8	1/9/2011	02.50	-2.60	112.74	644	528	3090	311.7	5
9	1/9/2011	15.50	-2.60	112.74	685	383	2899	292.5	5
Fire data number 11									
1	17/9/2011	02.5	-2.99	114.26	567	695	2970	301.1	5
2	17/9/2011	15.1	-2.98	114.26	523	272	2937	297.4	5
3	18/9/2011	14.15	-2.99	114.26	467	1328	2933	296.9	5
4	19/9/2011	02.35	-2.98	114.26	1667	380	2737	231.1	4
5	19/9/2011	14.55	-2.99	114.26	1621	548	2849	284.3	4
6	20/9/2011	03.2	-3.00	114.26	785	1272	2937	297.4	5
7	21/9/2011	02.25	-2.99	114.26	747	166	2920	295.3	5
8	21/9/2011	14.45	-2.99	114.26	697	877	2853	285.1	5

Appendix 13. Pixels temperature in 3x3 window size which are centred on every ground data locations which are referred to Appendix 8.

Note: Time in UTC, Mask values 4 = cloud pixel and 5 = non-fire clear land pixel

No	Date	Time	Lat	Lon	Row	Col	DN	T4	Mask
Fire number 1									
1	03/06/2011	14.35	-2.83	111.29	21	1272	2771	262.1	5
2	03/06/2011	14.35	-2.83	111.26	21	1273	2763	257.9	5
3	03/06/2011	14.35	-2.84	111.23	21	1274	2763	257.9	5
4	03/06/2011	14.35	-2.81	111.28	22	1272	2765	259.0	5
5	03/06/2011	14.35	-2.82	111.26	22	1273	2760	256.1	5
6	03/06/2011	14.35	-2.82	111.23	22	1274	2755	252.8	5
7	03/06/2011	14.35	-2.80	111.28	23	1272	2764	258.5	5
8	03/06/2011	14.35	-2.80	111.26	23	1273	2759	255.5	5
9	03/06/2011	14.35	-2.81	111.23	23	1274	2754	252.1	5
Fire number 2.									
1	04/06/2011	15.15	-2.79	111.24	1177	384	2959	299.9	4
2	04/06/2011	15.15	-2.80	111.23	1177	385	2953	299.3	4
3	04/06/2011	15.15	-2.80	111.22	1177	386	2959	299.9	4
4	04/06/2011	15.15	-2.78	111.24	1178	384	2952	299.1	4
5	04/06/2011	15.15	-2.79	111.23	1178	385	2958	299.8	4
6	04/06/2011	15.15	-2.79	111.22	1178	386	2952	299.1	4
7	04/06/2011	15.15	-2.77	111.24	1179	384	2957	299.7	4
8	04/06/2011	15.15	-2.78	111.23	1179	385	2964	300.5	4
9	04/06/2011	15.15	-2.78	111.22	1179	386	2964	300.5	4
Fire number 3.									
1	11/06/2011	03.00	-2.90	111.63	1595	743	2889	291.0	5
2	11/06/2011	03.00	-2.90	111.64	1595	744	2869	287.9	5
3	11/06/2011	03.00	-2.90	111.65	1595	745	2858	286.0	5
4	11/06/2011	03.00	-2.91	111.63	1596	743	2872	288.4	5
5	11/06/2011	03.00	-2.91	111.64	1596	744	2851	284.7	5
6	11/06/2011	03.00	-2.91	111.65	1596	745	2856	285.6	5
7	11/06/2011	03.00	-2.92	111.63	1597	743	2865	287.2	5
8	11/06/2011	03.00	-2.92	111.64	1597	744	2854	285.3	5
9	11/06/2011	03.00	-2.92	111.65	1597	745	2844	283.4	5
Fire number 4									
1	12/06/2011	14.25	-2.75	111.67	1545	1312	2910	294.0	4
2	12/06/2011	14.25	-2.75	111.64	1545	1313	2915	294.7	4
3	12/06/2011	14.25	-2.75	111.60	1545	1314	2920	295.3	5
4	12/06/2011	14.25	-2.73	111.67	1546	1312	2914	294.5	4
5	12/06/2011	14.25	-2.73	111.63	1546	1313	2919	295.2	4
6	12/06/2011	14.25	-2.74	111.60	1546	1314	2919	295.2	5
7	12/06/2011	14.25	-2.71	111.66	1547	1312	2912	294.3	4
8	12/06/2011	14.25	-2.72	111.63	1547	1313	2918	295.1	4

No	Date	Time	Lat	Lon	Row	Col	DN	T4	Mask
9	12/06/2011	14.25	-2.72	111.60	1547	1314	2918	295.1	5
Fire number 5									
1	05/08/2011	03.1	-2.72	111.59	76	901	2909	293.9	4
2	05/08/2011	03.1	-2.73	111.60	76	902	2920	295.3	4
3	05/08/2011	03.1	-2.73	111.61	76	903	2914	294.5	5
4	05/08/2011	03.1	-2.73	111.59	77	901	2914	294.5	4
5	05/08/2011	03.1	-2.74	111.60	77	902	2920	295.3	4
6	05/08/2011	03.1	-2.74	111.61	77	903	2909	293.9	4
7	05/08/2011	03.1	-2.74	111.59	78	901	2919	295.2	4
8	05/08/2011	03.1	-2.75	111.60	78	902	2919	295.2	4
9	05/08/2011	03.1	-2.75	111.61	78	903	2914	294.5	4
Fire number 6									
1	07/08/2011	02.55	-2.61	111.59	1187	571	2922	295.6	5
2	07/08/2011	02.55	-2.61	111.59	1187	572	2927	296.2	5
3	07/08/2011	02.55	-2.61	111.60	1187	573	2916	294.8	5
4	07/08/2011	02.55	-2.61	111.58	1188	571	2926	296.1	5
5	07/08/2011	02.55	-2.62	111.59	1188	572	2921	295.4	5
6	07/08/2011	02.55	-2.62	111.60	1188	573	2921	295.4	5
7	07/08/2011	02.55	-2.62	111.58	1189	571	2944	298.2	5
8	07/08/2011	02.55	-2.63	111.59	1189	572	2937	297.4	5
9	07/08/2011	02.55	-2.63	111.60	1189	573	2931	296.7	5
Fire number 7									
1	08/08/2011	14.2	-3.11	114.50	1083	1268	2751	249.7	5
2	08/08/2011	14.2	-3.11	114.47	1083	1269	2746	244.9	5
3	08/08/2011	14.2	-3.12	114.45	1083	1270	2741	238.5	5
4	08/08/2011	14.2	-3.10	114.50	1084	1268	2749	247.9	5
5	08/08/2011	14.2	-3.10	114.47	1084	1269	2739	235.2	5
6	08/08/2011	14.2	-3.10	114.44	1084	1270	2749	247.9	5
7	08/08/2011	14.2	-3.08	114.49	1085	1268	2740	236.9	5
8	08/08/2011	14.2	-3.08	114.47	1085	1269	2745	243.8	5
9	08/08/2011	14.2	-3.09	114.44	1085	1270	2745	243.8	5
Fire number 8									
1	12/08/2011	03.15	-3.08	114.45	523	1219	2932	296.8	5
2	12/08/2011	03.15	-3.09	114.47	523	1220	2927	296.2	5
3	12/08/2011	03.15	-3.09	114.49	523	1221	2932	296.8	5
4	12/08/2011	03.15	-3.10	114.45	524	1219	2936	297.3	5
5	12/08/2011	03.15	-3.10	114.47	524	1220	2936	297.3	5
6	12/08/2011	03.15	-3.10	114.49	524	1221	2931	296.7	5
7	12/08/2011	03.15	-3.11	114.45	525	1219	2931	296.7	5
8	12/08/2011	03.15	-3.11	114.47	525	1220	2931	296.7	5
9	12/08/2011	03.15	-3.12	114.49	525	1221	2931	296.7	5

No	Date	Time	Lat	Lon	Row	Col	DN	T4	Mask
Fire number 9									
1	22/08/2011	14.35	-2.87	111.16	13	1276	2783	267.1	5
2	22/08/2011	14.35	-2.88	111.13	13	1277	2772	262.5	5
3	22/08/2011	14.35	-2.88	111.10	13	1278	2767	260.1	5
4	22/08/2011	14.35	-2.86	111.16	14	1276	2779	265.6	5
5	22/08/2011	14.35	-2.86	111.13	14	1277	2774	263.5	5
6	22/08/2011	14.35	-2.86	111.10	14	1278	2774	263.5	5
7	22/08/2011	14.35	-2.84	111.15	15	1276	2780	266.0	5
8	22/08/2011	14.35	-2.85	111.13	15	1277	2780	266.0	5
9	22/08/2011	14.35	-2.85	111.10	15	1278	2775	263.9	5
Fire number 10									
1	30/08/2011	15.2	-2.61	112.76	1596	167	2801	273.1	4
2	30/08/2011	15.2	-2.62	112.74	1596	168	2796	271.6	4
3	30/08/2011	15.2	-2.62	112.72	1596	169	2796	271.6	4
4	30/08/2011	15.2	-2.60	112.76	1597	167	2816	277.2	4
5	30/08/2011	15.2	-2.60	112.74	1597	168	2789	269.3	4
6	30/08/2011	15.2	-2.61	112.72	1597	169	2789	269.3	4
7	30/08/2011	15.2	-2.59	112.75	1598	167	2811	275.9	4
8	30/08/2011	15.2	-2.59	112.74	1598	168	2800	272.8	4
9	30/08/2011	15.2	-2.59	112.72	1598	169	2784	267.5	4
Fire number 11									
1	19/11/2013	14.55	-3.00	114.27	1620	547	2952	299.1	4
2	19/11/2013	14.55	-3.00	114.26	1620	548	2957	299.7	4
3	19/11/2013	14.55	-3.00	114.26	1620	549	2957	299.7	4
4	19/11/2013	14.55	-2.99	114.27	1621	547	2950	298.9	4
5	19/11/2013	14.55	-2.99	114.26	1621	548	2950	298.9	4
6	19/11/2013	14.55	-2.99	114.25	1621	549	2958	299.8	4
7	19/11/2013	14.55	-2.98	114.27	1622	547	2948	298.7	4
8	19/11/2013	14.55	-2.98	114.26	1622	548	2958	299.8	4
9	19/11/2013	14.55	-2.98	114.25	1622	549	2953	299.3	4